

# Minimal models of invasion and clonal selection in cancer

Chay Paterson



Doctor of Philosophy  
The University of Edinburgh  
2017

# Declaration

I declare that:

1. This thesis has been composed by myself and that the work has not been submitted for any other degree or professional qualification. I confirm that the work submitted is my own, except where work which has formed part of jointly-authored publications has been included. My contribution and those of the other authors to this work have been explicitly indicated below. I confirm that appropriate credit has been given within this thesis where reference has been made to the work of others.
2. The work presented in chapter 3 was previously published in Nature - Scientific Reports as “An exactly solvable, spatial model of mutation accumulation in cancer” by myself (Chay Paterson, primary author), Prof. Martin A. Nowak and Dr. Bartek Waclaw (corresponding author). The model therein was conceived by all the authors. I derived the analytical results, and Bartek Waclaw and I produced the figures. All authors wrote the manuscript, which I edited and restructured to make appropriate for inclusion as a chapter in this thesis.
3. The data presented and analysed in chapter 4 was obtained in a clinical study carried out by Dr. Luis Diaz and his research group at the Johns Hopkins Kimmel Cancer Center in Baltimore, USA. The data analysis and interpretation detailed in chapter 4 and the text of chapter 4 are entirely my own work. Other contributions from colleagues are explicitly referenced in the text.

*(Chay Paterson, October 16, 2017)*

# Acknowledgements

In addition to my supervisor Dr. Bartek Waclaw and my co-supervisor Prof. Martin Evans for their direction and generosity with their time, I would also like to thank Prof. Martin Nowak for his interest and support, and Prof. M. E. Cates for several illuminating conversations.

I would like to thank both my parents for nurturing my interest in science from an early age, and my sisters for encouraging me to continue in difficult times, and for their unwavering belief in me. I would also like to thank my late grandmother for her enthusiastic support of my decision to pursue this particular area of study.

So many of my friends here in Edinburgh have contributed with stimulating questions or their help in learning new skills that it would be impossible to list them all individually without omitting someone: I owe my thanks to them all.

But in particular, I would like to dedicate the following to my wife Philippa, without whom this would not have been possible.

## Abstract

One of the defining features of cancer is cell migration: the tendency of malignant cells to become motile and move significant distances through intervening tissue. This is a necessary precondition for metastasis, the ability of cancers to spread, which once underway permits more rapid growth and complicates effective treatment. In addition, the emergence and development of cancer is currently believed to be an evolutionary process, in which the emergence of cancerous cell lines and the subsequent appearance of resistant clones is driven by selection.

In this thesis we develop minimal models of the relationship between motility, growth, and evolution of cancer cells. These should be simple enough to be easily understood and analysed, but remain realistic in their biologically relevant assumptions. We utilise simple simulations of a population of individual cells in space to examine how changes in mechanical properties of invasive cells and their surroundings can affect the speed of cell migration. We similarly examine how differences in the speed of migration can affect the growth of tumours. From this we conclude that cells with a higher elastic stiffness experience stronger resistance to their movement through tissue, but this resistance is limited by the elasticity of the surrounding tissue. We also find that the growth rate of large lesions depends weakly on the migration speed of escaping cells, and has stronger and more complex dependencies on the rates of other stochastic processes in the model, namely the rate at which cells transition to being motile and the reverse rate at which cells cease to be motile.

To examine how the rates of growth and evolution of an ensemble of cancerous lesions depends on their geometry and underlying fitness landscape, we develop an analytical framework in which the spatial structure is coarse grained and the cancer treated as a continuously growing system with stochastic migration events. Both the fully stochastic realisations of the system and deterministic population transport approaches are studied. Both approaches conclude that the whole ensemble can undergo migration-driven exponential growth regardless of the dependence of size on time of individual lesions, and that the relationship between growth rate and rate of migration is determined by the geometrical constraints of individual lesions. We also find that linear fitness landscapes result in faster-than-exponential growth of the ensemble, and we can determine the expected number of driver mutations present in several important cases of the model.

Finally, we study data from a clinical study of the effectiveness of a new low-dose combined chemotherapy. This enables us to test some important hypotheses about the growth rate of pancreatic cancers and the speed with which evolution occurs in reality. We test a moderately successful simple model of the observed growth curves, and use it to infer how frequently drug resistant mutants appear in this clinical trial. We conclude that the main shortcomings of the model are the difficulty of avoiding over-interpretation in the face of noise and small datasets. Despite this, we find that the frequency of resistant mutants is far too high to be explained without resorting to novel mechanisms of cross-resistance to multiple drugs. We outline some speculative explanations and attempt to provide possible experimental tests.

# Contents

<b>1</b>	<b>Introduction</b>	<b>4</b>
1.1	Background .....	4
1.1.1	Cancer as an evolutionary process .....	5
1.1.2	Cell signalling and kinase cascades .....	7
1.1.3	Adhesion .....	8
1.1.4	Cytoskeletal stiffness and migration .....	9
1.2	Why mathematical models?.....	9
1.2.1	Basis of commonly used growth models .....	10
1.2.2	How applicable are these to invasive cancers?.....	15
1.2.3	Mathematical modelling of cancer evolution .....	16
1.2.4	Our research in context.....	18
<b>2</b>	<b>Individual-based models of local invasion</b>	<b>20</b>
2.1	Introduction.....	20
2.2	Mechanistic simulation .....	21
2.2.1	Equations of motion and algorithm.....	22
2.2.2	Results .....	31
2.3	Spatial lattice model of local migration .....	34
2.3.1	Algorithm .....	36
2.3.2	Results .....	38

2.4	Lattice model with instantaneous migration .....	45
2.4.1	Algorithm .....	47
2.4.2	Results .....	47
2.5	Concluding remarks .....	50
<b>3</b>	<b>Structured population models of clonal selection</b>	<b>51</b>
3.1	Introduction.....	51
3.2	Stochastic model.....	52
3.2.1	Basic algorithm .....	55
3.3	Analytical methods.....	57
3.3.1	Definitions and exact results .....	57
3.3.2	Only one driver .....	59
3.3.3	Multiple driver mutations .....	64
3.3.4	The generating function technique.....	72
3.4	Comparison to simulations .....	75
3.4.1	Comparison of stochastic minimal model and analytics .....	76
3.5	Discussion.....	79
3.5.1	Relevance to open questions in the field.....	81
3.5.2	Future work.....	82
<b>4</b>	<b>Resistance to low-dose combination chemotherapy</b>	<b>84</b>
4.1	Background .....	84
4.1.1	Protocol and mechanisms of action .....	85
4.2	Analysis .....	86
4.2.1	Immunological noise and over-interpretation .....	86
4.2.2	Theoretical fraction of resistant cells .....	89
4.3	Results and discussion.....	90
4.3.1	Inferred fraction of resistant cells .....	90

4.3.2	Molecular mechanisms of single-drug resistance.....	92
4.3.3	Possible mechanisms of cross-resistance .....	94
4.4	Concluding remarks .....	99
<b>5</b>	<b>Conclusion</b>	<b>102</b>

# Chapter 1

## Introduction

The impact that cancer has had on human society is difficult to exaggerate. The earliest surviving record of the disease dates from ancient Egypt [1], and with ageing populations across the developed world, most families have some familiarity with the suffering that accompanies some types. All cancers are difficult to treat in their advanced stages, and some types are difficult to diagnose due to their non-specific symptoms in early stages.

It is widely understood that cancers are overgrowths of cells, and that there are many different types. Different types have different symptoms and treatments depending on where they appear, and different degrees of survivability. But less commonly appreciated are the underlying similarities between these different types and the mechanisms at work in all cancers. Common features of all true cancers, regardless of their type or tissue of origin, are abnormalities in the growth and movement of cells [2, 3]. They also have a shared nature as evolutionary processes, which involve changes in some of the most fundamental molecular machinery of complex animal life [4].

In this thesis, we ask how quickly cancers can evolve and grow, how this may be affected by the migration of cancer cells, and how cancers' evolution might affect the effectiveness of therapy.

### 1.1 Background

Cancer cells don't just divide more often. Rather, they survive for longer periods of time without undergoing programmed cell death. A cell that divides more often but also dies more often won't result in an overgrowth as such. In fact, having a population of rapidly dividing cells, in balance with the rate at which other cells die is an essential part of the normal function of tissues. Animal cells have different degrees of specialisation, such as muscle, or bone, or nerve cells (see figure 1.1), and as a rule of thumb the more specialised a cell type's functions are, the less often it will divide. Less specialised cells divide more often, and produce more specialised cells in a hierarchical manner [4, 5]. The balance between the different division and death rates, and the rate at which incrementally more specialised (or *differentiated*) cells are produced, are what determine the long term stability of cell populations in all tissues in the body. To understand precisely how this balance is upset requires a closer look at how it is controlled in normal cells.

To get a sense for what exactly goes wrong as a cancer emerges, let us take as a simple example a population of precursor cells (less specialised cells that divide and die often), which produce another population of specialised gland cells (that secrete some substance, say, and which don't divide). If these populations are both balanced over time, this means that a typical precursor cell has to produce, on average, one new precursor cell and a few more specialised cells over the course

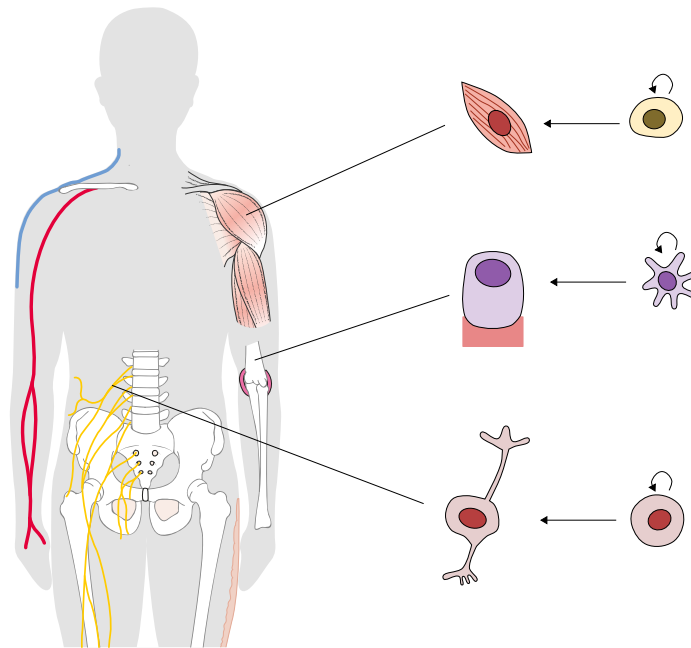


**Figure 1.1** Examples of three different normal cell types in tissues of the human body, from top to bottom: a muscle cell (myocyte), bone-producing cell (osteoblast) producing bone (reddish square), and a nerve cell (neuron). Each of these have an associated type of precursor cell that maintains their normal populations in the appropriate balance (right). Modified from [6].

of its lifetime [7–10]. There are three basic processes which determine what happens: the rate at which precursor cells divide, the rate at which they differentiate and turn into gland cells and the rate at cells of either type are removed.

There are therefore three possible points of failure here: cells can divide too quickly, they can be removed too slowly, or they can differentiate too slowly. The control of cell division, programmed cell death, and cell specialisation are critical in the normal maintenance of tissue (*homoeostasis*), and the loss of control of these is similarly critical in the development of cancer [4, 7, 11].

The type and form of a given cancer is determined by the type of cell from which it derives: that is, which sub-population of specialised cells it descended from. There are as a result approximately as many different possible cancers as there possible types of cell (including both specialised cells and their precursor cells). Despite this, all cancers have a common set of properties or “hallmarks” that distinguish cancers from similar diseases involving differentiation and growth. These six hallmarks are: the resistance to normal *controlled* cell death (“apoptosis”), sustained proliferation, replicative immortality, a muted response to growth-suppressing signals, triggering the formation of capillaries, and invasion (“metastasis”) [2, 3].

### 1.1.1 Cancer as an evolutionary process

Cancers are fundamentally evolutionary processes, in the very precise sense that some population of cells gets a replicative advantage over their neighbours [12]. The changes in cancer cells that enable them to escape the usual control of cell division and type are due to genetic mutations [12–14]. Genetic mutations are heritable, being passed down to daughter cells when a cell carrying the mutation divides [4]. What is crucial in the process of uncontrolled cell division, and what



or about one every fifty divisions. Clearly, a cancer that consists of a billion cells will have around twenty million neutral mutations, far in excess of the typical two to eight driver mutations [18].

As well as explaining the earliest stages of initiation, evolution by clonal selection is also one possible hypothesis for drug resistance in late stage metastatic cancers. Although it should be noted that the mechanism that underlies drug resistance is not as well-understood as the earlier mutations that actually get the tumour started, and establishing that evolution is responsible for resistance to chemotherapy can only be done by ruling out alternative explanations, at the time of writing this is a plausible explanation with the additional point in its favour that evolutionary processes are already known to occur [19].

Although our main areas of interest will be the relationship between invasion and evolutionary change, it is worth summarising some important discoveries of the broader underlying mechanisms that have been discovered in recent years.

### 1.1.2 Cell signalling and kinase cascades

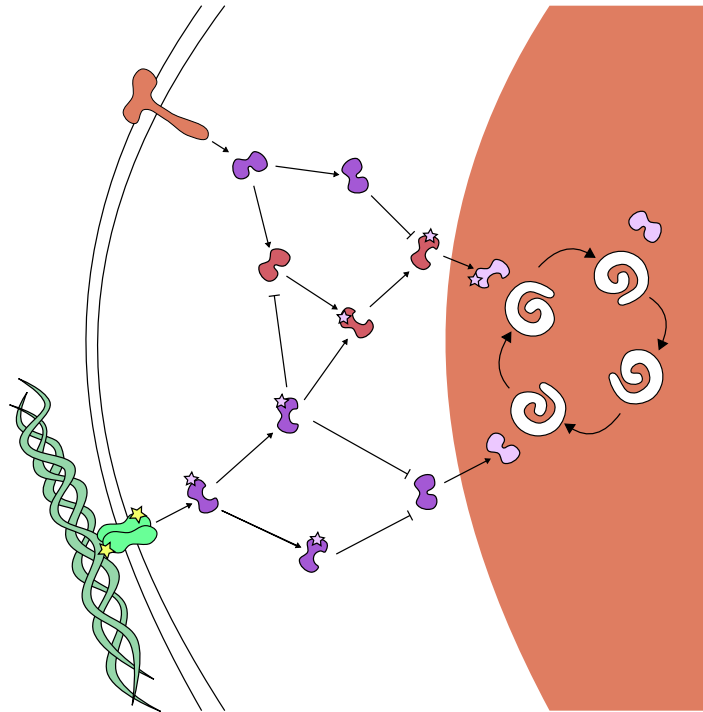


**Figure 1.3** *A cartoon of a fictitious signalling pathway, showing transmembrane proteins (green and red structures on membrane) adhering to extracellular matrix (green fibres), and triggering a kinase cascade (kinases being B-shaped red and purple blobs) that propagates into the nucleus (red oval, right). This interferes with the cell cycle through the binding of cyclin-dependent kinases (pink kinases) to cyclins (white spirals). In this example, the cell adhesion molecules function as receptors, although many other specialised receptors exist (see [4] for a comprehensive review).*

The type of a cell, that is, its form and function in terms of what it secretes and how it interacts with the cells around it, is determined by what proteins it expresses. What proteins it expresses is determined by which genes are switched on and actively “transcribed”, read by the cellular machinery that builds proteins from amino acids according to the sequence contained in the genome.

The genetic information needed to code for any protein in the body is contained in the DNA of every single cell in the body, but is only expressed and actively used when the relevant gene is switched on. Differences in cell type are thus due to differences in expression of genes found in all cells [4].

The process by which genes are activated or deactivated by stimuli is complex, but involves a network of chemical reactions between proteins inside the cell that result in the relevant gene becoming “exposed” and accessible to the transcriptional machinery. The proteins involved may be classified into transcription factors, signalling proteins and receptors. Transcription factors directly interact with the gene by sticking to it, either exposing it to transcriptional apparatus or hiding it. Signalling proteins relay information about stimuli (or signals) from receptors elsewhere in the cell to the transcription factors in the nucleus [4].

Many of the signalling proteins are kinases, enzymes which catalyse the attachment of a phosphate group to a specific target molecule. This brings about a structural change in the target molecule. The products of many of these reactions are also protein kinases, which catalyse a similar reaction for another protein kinase. This means that phosphorylation reactions between these kinases can form a long branching chain of similar reactions. If one of the kinases near the “top” of the chain is activated by a receptor, this triggers a cascade of phosphorylation reactions that cascades down the chain of kinases like a burning fuse, with the ultimate result that the transcription factors in the nucleus are activated, triggering the production of other proteins in response (see figure 1.3). Protein kinases are extremely important in development and cancer initiation, as well as a host of other functions of the cell: more than 500 different protein kinases are known, and the number of known interactions between them increases from week to week [20, 21].

Another important group of regulatory proteins are cyclins, and the protein kinases that interact with them, the cyclin-dependent kinases. In cells which have not yet fully differentiated and are still precursors or stem cells, the cell cyclically progresses through different stages of cell division. This cyclical behaviour is driven by an oscillating biochemical reaction between cyclins, and may be paused depending on the presence or absence of these other cyclin-dependent kinases, which interact with the cell’s larger signal transduction network in turn. In this way, what happens to a receptor on, for example, the surface of the cell, can trigger a cascade of events that pauses or un-pauses the process of cell division [22].

The true picture is rather more complex than this, not least because of the fact that some signal molecules inhibit rather than simply activate others, and the resulting dynamics can have multiple steady states, possibly oscillatory. Nonetheless, this picture of information about stimuli being carried through the cell to trigger responses in regulation and expression by a kind of domino effect has gradually become widely accepted, and mutated proteins in this network are implicated in many known cancers [2, 21].

### 1.1.3 Adhesion

At the cell membrane, the presence of intermolecular forces between the molecules present on the membrane and those in the external environment determine the strength of the cell’s adhesion to that environment. As in other materials, the strength of adhesion between two surfaces  $i$  and  $j$  is measured by the surface free energy  $\gamma_{ij}$  associated with the interface: how much work is needed to create a given area  $A_{ij}$  of that interface. This is essentially how sticky  $i$  and  $j$  are. It is closely related to surface tension, and corresponds to the change in free energy  $\Delta F$  when peeling the surfaces apart over a given area [23],

$$\gamma_{ij} = \frac{\partial \Delta F}{\partial A_{ij}}. \quad (1.1)$$

Despite the variety of molecules usually present, the interfacial free energy between two cells of different types is currently believed to be determined by the gross quantity of cell adhesion molecules present rather than their specific types. Cells tend to sort into regions of different homogeneous types with similar surface energies under the action of adhesion, which provides a purely mechanical contributing mechanism to pattern formation during morphogenesis [24, 25].

#### 1.1.4 Cytoskeletal stiffness and migration

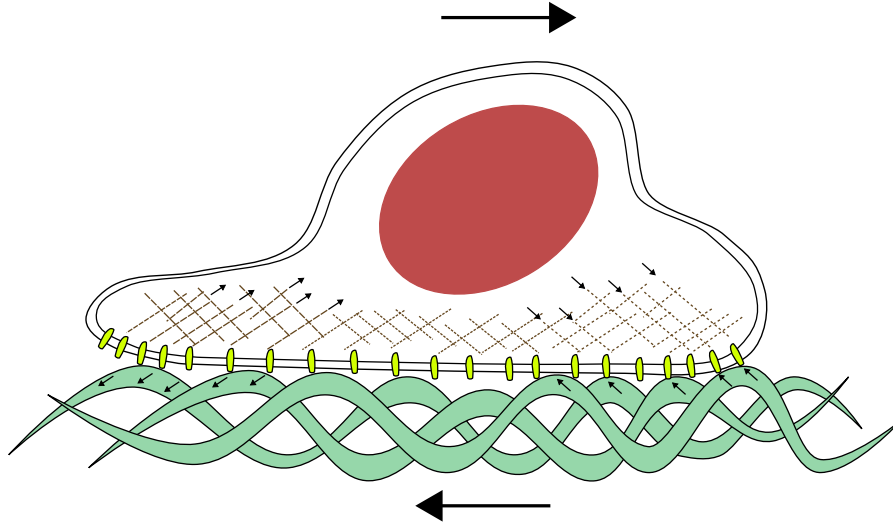


**Figure 1.4** *A cartoon to show the generation of forces on a motile cell by dynamical polymerization of actin and interactions with cell adhesion proteins, showing forces due to polymerization of actin filaments and the resultant tractive force on the cell and equal and opposite force acting on the surrounding matrix.*

Cells' resistance to mechanical deformation consists of both the resistance to applied pressure common to all materials, the bulk modulus, and from the tensile and compressive resistance of the cytoskeleton. The cytoskeleton is complex and active in structure, and is composed of a network of actin filaments. Actin is an active polymer, and in addition to contributing to the mechanical stiffness of the cell plays important roles in the dynamics of signal transduction and motility [4].

The properties of most immediate interest to us are the contribution to mechanical stiffness and the generation of forces during motility. Forces between the cell and the surrounding matrix are generated by chemical reactions in the actin network, and its connection to transmembrane cell adhesion proteins. The depolymerisation and shrinkage of actin filaments near the leading edge of the cell “pulls”, while the polymerisation and expansion at the trailing edge “pushes” [26]. See Figure 1.4 for a sketch of the process.

## 1.2 Why mathematical models?

Many mathematical and computational models in this field are scrupulous in their inclusion of all imaginable complications that can be found in real biological systems. Many different systems are coupled together in ways observed to occur experimentally, at many different scales: such multi-scale models, although they can be successfully fitted and in many cases can be used to predict the behaviour of individual systems, sometimes requiring more than a dozen adjustable or empirically set free parameters.

I deliberately want to avoid developing models that are “too realistic” in the course of my research here for a number of reasons, some practical and some philosophical.

Firstly, models with a large number of complex systems which are themselves complex, having dozens of free parameters, are opaque. Their investigation and empirical fitting can usually only be carried out computationally, often involving elaborate numerical estimation procedures in addition to the complex numerical integration of the underlying differential equations or master equations. The freedom that comes from having so many adjustable parameters, a situation that is almost inevitable in any field with a large number of experimental unknowns, means that often a model will have a good fit, and can even turn out to have a decent amount of predictive power, but the complexity makes the models essentially impossible to interpret in simple terms. This approach encourages a “black box” approach to science, in which verifiable results are arrived at, along with means for predicting them, with little or no increase in human understanding of the things being studied.

Secondly, computational models with an abundance of degrees of freedom are very difficult to falsify. Enormous differences in qualitative behaviour can be achieved with relatively small parameter changes in many such models: if we take the view that the scientific method has to do with ruling out one of a number of different alternative hypotheses through experiment, then models which display many different qualitative behaviours, and can be fitted to a variety of different empirical curves in each regime, are very difficult to rule out.

On the other hand, deliberately simplistic toy models have the opposite set of problems. Simple and tractable models which share only a qualitative resemblance to the system they are ostensibly a theory of can produce the feeling of understanding in the scientist who studies them, and can be coaxed into providing predictions about behaviour which are eminently falsifiable.

There seems to be a gap in the literature of theoretical frameworks that fall in between: imperfect but decent in predictive power, and decent but not exhaustive in explanatory power. It is this particular void that we want our research to fill: a simple theory which explains and predicts the effect of a few specific phenomena well. Here, we attempt to develop such a framework and set of models for the problem of determining the dynamics of cancer evolution in terms of the biophysical properties of their constituent cells, models which are simple enough to be understood fully, but which still attempt to maintain a testable correspondence to experiment: as simple as possible but no simpler.

With this goal in mind, we will set out to develop and elucidate a theoretical framework within which we can begin to understand and predict the interaction between evolutionary dynamics and invasion in late-stage cancers, and which can serve as a starting point for future work in the field. I will now take a moment to discuss the most commonly encountered mathematical models of tumour growth in oncology, before offering a critique of their specific relevance to full-blown invasive cancer and beginning my development of analytical and computational models which attempt to bridge the gap and provide a framework for the modelling of evolution during invasive cancers.

### **1.2.1 Basis of commonly used growth models**

There are a variety of mathematical models currently in use to describe the growth curves of individual tumours, or the total tumour burden in advanced cases of metastatic cancers. An exhaustive survey of current models, and their applicability to different cases and diseases, can be found elsewhere [27–29]. Here, I will provide a summary of the different classes of models, their empirical basis, and a brief discussion of their limitations.

The purpose of a mathematical model of growth is to provide some description of observable growth curves in terms of a few underlying parameters. Ideally, the parameters and terms of the model interpreted in terms of physiological mechanisms at play during the process of biological growth.

Models with more parameters will obviously tend to provide better fits to data, but this does not always correspond to stronger predictive power, in that future extrapolations of the curve do not agree with experimental data for very long after the parameters have been set. Many models with a large number of parameters are prone to numerical stiffness, having many local minima in fitting procedures, as well as tending not to have a clear interpretation in terms of physiological mechanisms [29, 30].

Models can be aggregated, very crudely, into groups whose growth curves display long-term slowdown to stable maximum sizes (plateaus) and those that instead display unbounded growth. The simple reason to expect long-term slowdown and plateaus in the growth rate is that a given individual solid tumour will be limited in terms of the supply of nutrients (namely, oxygen and glucose) that it has access to, and in terms of how much space is available for it to occupy. Growth can only continue as long as both nutrients and volume are available for the tumour to expand [29, 31].

It is not obvious that a model for the growth of non-solid, diffuse tumours or more highly invasive cancers should have a slow-down in terms of growth rate — in fact, it may not be true at all. I will return to this point after discussing the most commonly encountered growth models in the literature.

### 1.2.1.1 Two parameter models

The simplest two models which display unlimited growth are exponential and power-law growth. Writing the initial size as  $n(0)$ , and the size at time  $t$  as  $n(t)$ , exponential growth corresponds to the differential equation

$$\frac{dn}{dt} = Gn(t) \quad (1.2)$$

which may be interpreted as every cell in the population dividing at a frequency equal to  $\ln(2)G$ , with the resulting growth curve given by the solution

$$n(t) = n(0) \exp(Gt) \quad (1.3)$$

with  $G$  the exponential growth rate of the model. See figure 1.5 for representative solutions. The initial size and growth rate  $G$  are the defining two parameters of the model [29].

The power-law model corresponds to the differential equation

$$\frac{dn}{dt} = an^p \quad (1.4)$$

with  $p$  some dimensionless number between 0 and 1, and  $a$  some constant. Solutions of this equation,

$$n(t) = C(t - t_0)^{\frac{1}{1-p}} \quad (1.5)$$

with  $C = ((1 - p)a)^{\frac{1}{1-p}}$  and  $t_0$  determined by initial conditions, display unlimited growth, and are exhaustively characterised by two parameters (see figure 1.5 for representative solutions), but also have the property that the size of the tumour is always 0 at some point in time. The power-law model is therefore not suitable for very small tumours. The parameter  $p$  often has an interesting

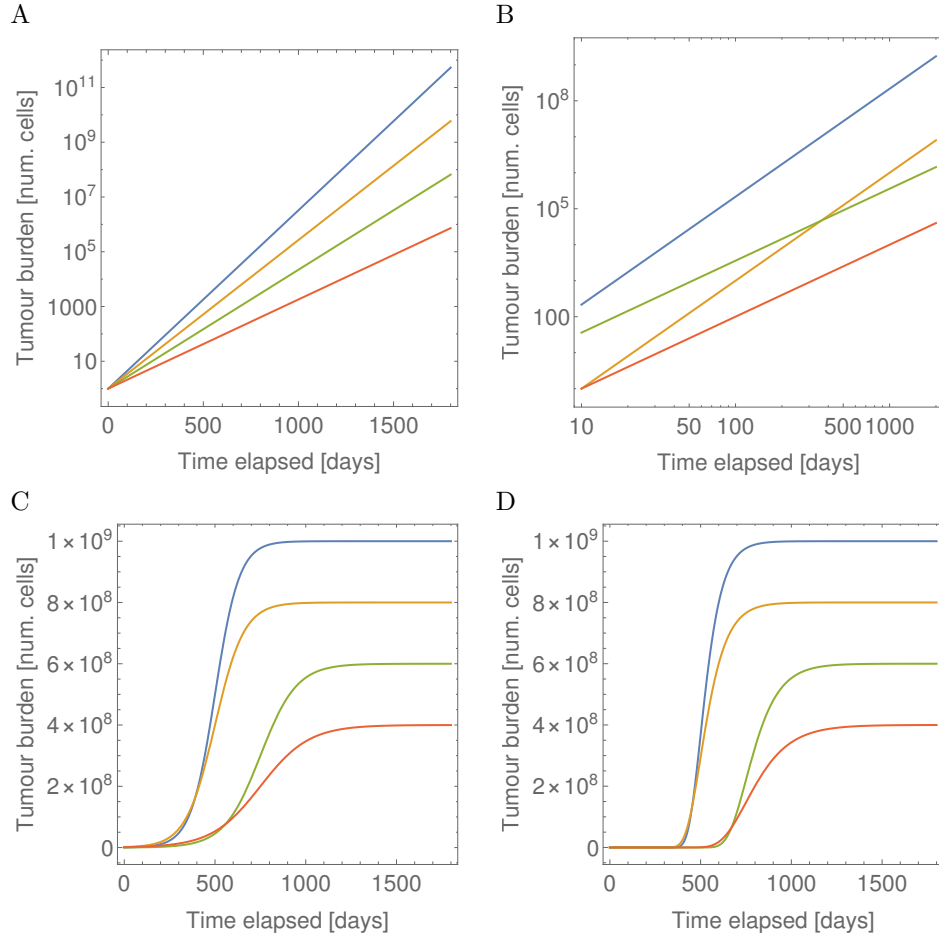


**Figure 1.5** A comparison of example growth curves for the two- and three-parameter models discussed in this section. A: four solutions of the exponential growth model with identical initial populations  $n(0) = 1$  and growth rates  $G = \{0.015, 0.0125, 0.01, 0.0075\}$ . Note the logarithmic scale. B: four representative solutions of the power-law growth model with parameter values of  $C = 0.216, p = 2/3$  (blue curve);  $C = 10^{-3}, p = 2/3$  (yellow curve);  $C = 0.216, p = 1/2$  (green curve); and  $C = 10^{-3}, p = 1/2$  (red curve). Note the log-log scale. C: four examples of logistic growth, with  $n(0) = 5.53 \times 10^5$ ,  $G = 0.015$ , and  $K = 10^9$  (blue curve);  $n(0) = 1.54 \times 10^6$ ,  $G = 0.0125$ , and  $K = 8 \times 10^8$  (yellow curve);  $n(0) = 3.31 \times 10^5$ ,  $G = 0.01$ , and  $K = 6 \times 10^8$  (green curve);  $n(0) = 1.43 \times 10^6$ ,  $G = 0.0075$ , and  $K = 4 \times 10^8$  (red curve). D: four representative solutions of the Gompertz differential equation, with  $b = 1808$ ,  $\alpha = 0.015$ , and  $K = 10^9$  (blue curve);  $b = 518$ ,  $\alpha = 0.0125$ , and  $K = 8 \times 10^8$  (yellow curve);  $b = 1808$ ,  $\alpha = 0.01$ , and  $K = 6 \times 10^8$  (green curve); and  $b = 277$ ,  $\alpha = 0.0075$ , and  $K = 4 \times 10^8$  (red curve).

interpretation in terms of the geometry or perfusion (how efficiently blood vessels can penetrate the tumour) of individual tumours. If all of the nutrients that flow into the tumour get used for additional growth, and perfusion is perfect (by which I mean that every cell in the tumour has good access to nearby blood supply, and the capillaries reach throughout the tumour perfectly efficiently) then the coefficient  $p = 1$ . If, on the other hand, the capillaries can only reach cells on the surface of the tumour, and the tumour is spheroidal, then  $p$  will be substantially lower, at  $p = 2/3$ . If perfusion falls somewhere in between these values, then  $p$  will fall somewhere in between  $2/3$  and  $1$  [29].

Despite the simplicity of the exponential growth model, it should be emphasised that it is, in practice, the most popular model for tumour growth by a substantial margin, both among clinicians in need of a quick and simple estimate for the purposes of extrapolating growth or characterising it in exploratory studies in which dynamical data may be sparse, in studies of drug effectiveness, and also among mathematical biologists in the context of a basis for more complex models [29, 30]. For example, one can readily generalise the underlying equations of the model to a more complex system of linear differential equations, representing different sub-populations of cancer cells, and analyse the resulting dynamics very easily, often even giving some meaningful interpretation to the underlying parameters. I will return to this paradoxical popularity shortly.

However, even though this is the most commonly encountered model in practice, individual tumours often show a gradual slow-down in their growth, tending towards some sort of plateau. Although it should be pointed out that plateaus are not always observed clinically [29]. The basic inability of simple exponential growth to capture this motivates the development of more complex models.

### 1.2.1.2 Three parameter models

The simplest models displaying such a plateau in growth are the logistic model

$$\frac{dn}{dt} = Gn(1 - n/K) \quad (1.6)$$

with a carrying capacity  $K$ , and the Gompertz model

$$\frac{dn}{dt} = \alpha \log(K/n)n \quad (1.7)$$

with some “growth rate”  $\alpha$ , respectively [29, 30]. Solutions to these models can be expressed analytically,

$$n(t) = \frac{K}{1 + e^{-G(t-t_0)}} \quad (1.8)$$

for the logistic model, with  $t_0$  a constant set by initial conditions; and

$$n(t) = Ke^{-be^{-\alpha t}} \quad (1.9)$$

for the Gompertz model, where  $b$  is a constant that is set by initial conditions, and can be related to the initial population size  $n(0)$  by

$$b = \log\left(\frac{K}{n(0)}\right) \quad (1.10)$$

where  $\log$  is the natural logarithm. Examples of solutions are displayed in figure 1.5.

Both of these models' growth curves show an initial period of growth, which then decelerates as the tumour grows larger, as is easily seen in all examples given in figure 1.5. Both models' growth curves are characterised by three parameters, displaying an initial period of rapid growth followed by a slow-down and plateau. The main visible difference between the two is that the logistic growth curves are symmetric, whereas the Gompertz model's growth curves are asymmetric, showing fast initial growth and a very gradual slow-down. Of the two, Gompertzian growth tends to perform somewhat better than logistic empirically, and was historically more popular than many competing models, but has a number of serious problems, among which are the behaviour of the model at small sizes. When  $n \ll K$ , the replication rate of cells blows up to infinity, indicating discontinuities in growth. Furthermore, the difficulty of interpreting  $\alpha$  or justifying the strange dependence on population size on physiological grounds. For these reasons, and more importantly for its empirical failures, Gompertzian growth is decreasingly popular [29].

### 1.2.1.3 Four and more

More complex models, such as Gomp-ex, can be constructed from these simple models in a piecewise manner, typically introducing new adjustable parameters with each "switch" between different models. One may use Gompertzian growth for tumours larger than  $n_c$ , and exponential for tumours smaller than this size, treating  $n_c$  as an adjustable parameter [29].

One type of model which is not constructed in this way, and which has the additional advantage that it has a straightforward physiological interpretation, is the von Bertalanffy growth model characterised by the differential equation

$$\frac{dn}{dt} = an^p - bn \quad (1.11)$$

with  $a$  and  $p$  constants characterising uptake and use of nutrients and oxygen, and  $b$  a rate related to turnover and the breakdown of cells and biomass (catabolism) which also controls plateau size, as this is the size at which all nutrients taken in are used simply to maintain the tumour at its current size.

These may be interpreted physiologically as follows, in terms of simple conservation of mass and the energy budget of an organism (or tumour, in our case). The rate at which mass of nutrients can be taken in and used in metabolic processes should be bounded from below by the surface area (if perfusion is very poor, and capillaries don't penetrate into the tumour very effectively at all) and from above by the total volume (if perfusion is very thorough). A simple model therefore has metabolic rate  $= an^p$ , with  $p$  between  $2/3$  and  $1$ .  $p$  can therefore be interpreted as how well vascularised a tumour is.

This biomass can be used either for additional growth or for the maintenance of the system at a given size. The mass used to compensate for catabolic processes should be proportional to the amount of living material present (i.e. tumour size), with the remainder resulting in growth. Conservation of mass then implies

$$\underbrace{an^p}_{\text{metabolic rate}} = \underbrace{bn}_{\text{catabolic rate}} + \underbrace{\frac{dn}{dt}}_{\text{new growth}} \quad (1.12)$$

and the von Bertalanffy equation comes from a simple rearrangement [29].

For  $p < 1$ , interpretable as less-than-perfect perfusion, this model displays an initial burst of power-law growth, tending towards a plateau determined by  $a$ ,  $b$  and  $p$ .

One remarkable feature of this model is that it contains both simple exponential growth and power-law as limits. The first, in the limit that  $p = 1$ , and the second in which  $b = 0$ .

It is also worth noting that in many cases the Bertalanffy growth model performs much better than other four-parameter models such as Gomp-ex, and has the additional advantage that the parameters have a straightforward interpretation. Despite these points in its favour, it is still somewhat obscure at the time of writing, and sees a rather limited use. It is rarely used in studies of drug effectiveness despite its many advantages [29].

### 1.2.2 How applicable are these to invasive cancers?

Comparisons of these models (and a preponderance of others) are typically carried out on observations of single tumours in mouse models. A serious limitation here is that it is not obvious that models which are well-suited to single tumours will carry over to collections of multiple, diffuse tumours. It isn't very hard to see that a collection of metastatic or locally invasive lesions could have a very different growth curve than an individual lesion. A single lesion might only grow for a limited time up to some plateau size, but continue to send out invasive cells to other regions in which growth can continue. The whole may grow differently from the individual parts.

Imagine a population of rabbits. An individual rabbit can only grow for an initial short period of time, for about six months, after which they have basically reached their adult size and will not grow any larger. A field of rabbits, on the other hand, can support a continuously growing number of rabbits for a much longer length of time, and it's possible to see exponential growth of the population. This is despite the fact that individual rabbits can only grow for a certain limited period of time. The important idea here is that a *population* can experience exponential growth despite quite different growth curves for its *individual* constituents.

Exponential growth can still describe the growth of the whole population, even when individuals in it only grow a limited amount. Similarly, in the case of metastatic cancers, the growth curve of the entire tumour burden may be very different from the growth curve of an isolated tumour. The feedback due to migration and metastasis may have a complex effect. We analyse and extend models of this feedback mechanism to account for evolutionary dynamics in chapter 3.

As previously noted, despite widespread knowledge of its inability to display plateaus commonly observed in single-tumour growth curves and many other complex behaviour, the exponential growth model is still the most commonly encountered in practice, both among clinicians and applied mathematicians. That such a simple and “stupid” model should see such widespread use, despite not being taken seriously by the majority of those who do use it is surprising, and bears some explanation.

Two basic reasons why this is the case are the fact that the model is easy to fit and apply, having only two parameters, and the fact that it is often impossible to get long-term dynamical data about tumour burden. It is also easy and tractable to use, and due to a scarcity of data for ethical reasons is usually difficult to rule out.

This results in the remarkable situation that two scientific communities widely use and apply a model which, despite its popularity and debatable success, is not taken “too seriously” by any member of these communities. Considering the fact that it is clearly useful in many cases owing to its tractability and simplicity, it is my belief that the paradoxical popularity of exponential growth warrants a serious investigation. How might exponential growth arise in the context of more detailed and realistic models? I address this in chapters 2 and 3.

### 1.2.3 Mathematical modelling of cancer evolution

The picture of cancer as an evolutionary process has become well established [14, 32]. Many genes have been found which code for proteins which, in their mutated form, are important in the start and progression of cancer. Identifying their ordinary functions is an active and rewarding program in current research, and fits well into the picture of an accumulation of mutations which give abnormal cells an “advantage” over normal cells. In addition to the initiation of tumours, the emergence of resistance to therapy is also suspected by many to involve a Darwinian process of selection [18, 19].

However, detailed measurements of the dynamical course of cancer are extremely difficult to obtain. For obvious ethical reasons, collecting an exhaustive life history of the untreated disease is usually impossible due to the suffering that this entails. As a result, although the idea that the underlying process can be described as evolutionary is quite widely accepted, the timing and detailed dynamics underlying these processes have not been definitively established.

There are several current proposals for the nature of the underlying dynamical process. These proposals can usually be described as variations on one of a few hypotheses, which differ first in the relative importance of selective pressure, and second in the timing of selective sweeps (if they occur). A selective sweep is an evolutionary event in which a new, fitter (“driver”) mutant rapidly overtakes other lines. This event pulls neutral (or passenger) mutations up in frequency of occurrence along with the driver mutation [18].

To summarise the current hypotheses:

- *Late evolution models* posit that additional driver mutations occur, and each carry some very small advantage. These successive drivers increase in frequency in a series of sweeps, which occur at an accelerating rate. As a result, most evolutionary change happens late in the life history of the cancer[33].
- *Early evolution models*, like late evolution models, posit that additional driver mutations occur, but carry diminishing returns. Only the first few drivers increase in frequency at an accelerating rate, after which the pace of evolutionary change slows dramatically. Most evolution occurs early in the course of the cancer in these models[15, 34].
- *Neutral models* attempt to explain high levels of intra-tumour heterogeneity by positing that only the very earliest, initiating mutations carry a significant advantage, and subsequent mutations are essentially neutral, with fixation due to the effects of rapid early expansion. The so-called “Big Bang” model falls into this class [35].

In a little more detail, these models can also be related to different assumptions about the underlying fitness landscape available to mutant clones in a tumour, and what other factors affect the probability of fixation. However, how exactly underlying fitness landscapes should affect growth and the dynamics of selection if spatial constraints and geometry are important is an open question: one which we hope to address at least in part in chapter 3.

In the case of neutral models, selection pressure is hypothesised to be swamped by rapid growth. Selection due to small differences in cell survival needs to be stronger than random fluctuations, which in practice means that populations have to be sufficiently large that these “founder effects” can be avoided [36, 37]. But if only cells near the growing surface are able to divide, the active population is much smaller than the true population size, and stochastic effects like genetic drift are much more important. Neutral and even somewhat deleterious mutations can reach fixation on the surface of expanding tumours in theory [38, 39].

Recent proposals such as the “Big Bang” model for intratumour heterogeneity postulate that the majority of genetic variation in tumours is due to early fluctuations. These enable fixation of

almost neutral alterations. While notable for its novel prediction of characteristic backgrounds of heterogeneity that are independent of selective pressure, phenomena such as the appearance of resistance to chemotherapy in late stage cancers are easier to explain in terms of acquired selective advantages. Spatial constraints are not necessarily as relevant for metastatic cancers which are able to evade local factors that would otherwise inhibit their growth [35].

Quantitative experiments on bacterial colonies and numerical simulations of single tumours support the picture that spatially constrained growth can drastically increase the probability of fixation for non-advantageous mutant lines, even for somewhat deleterious mutations. A plausible example of this occurring in cancer would be a solid tumour with poor vascularisation, in which growth can only occur in a narrow rim at the surface [39, 40].

We will therefore treat neutral models as essentially null models. They are an important class of alternatives to selective pressure for the purposes of empirical tests, which we will occasionally revisit during the development of our theories of selection during metastasis. We should emphasise that the fixation due to early expansion and “freezing in” of primordial neutral mutations is a prediction which is hard to avoid on the basis of simulations and other experiments on bacteria, and which is an important component of our later, developed theories in chapter 3.

The first important class of models for selection in cancer are models which assume fitness increases to be linear, which corresponds to an accelerating pace of selection. Crucially, these models tend to assume well-mixed growth, analogous to the simple exponential growth model described in the previous section. The relevance of this class of models to spatially constrained growth with invasion has not been well studied.

One important recent mathematical model which attempts to predict driver accumulation, and furthermore relate this to measurable proxies of dynamical information akin to the molecular clock, is the work of Božić *et al.*’s [18]. This is a well-mixed model, which assumes that individual lineages grew exponentially with characteristic cell division time  $T$ , differences in fitness  $s$  determined purely by differences in survival and turnover probability (so that  $s = 1 - b/d$ ,  $b$  division rate and  $d$  death rate), and driver mutation occurrence rate  $u$ . The core prediction of this framework is an exponential increase in the frequency of driver mutations over time. Although many models of tumour growth are dynamical, data on the course of growth over time is difficult to obtain for ethical reasons. To address this, this model also includes the accumulation of passenger mutations. Passenger mutations by definition do not alter the rate of growth of tumours, and as such the number  $n_p$  of passengers present grows at a constant rate over time. Namely

$$n_p = \nu t/T \tag{1.13}$$

where  $\nu$  is the product of the point mutation rate per base pair and the number of base pairs at which mutations are neutral, and  $T$  is the time in between divisions. This assumption of a molecular clock enabled the authors to attempt to test their model empirically, which is a significant achievement. But the assumption of a constant driver accumulation rate is not obviously consistent with the genetic hitch-hiking of passenger mutations, in which they increase in frequency due to their coincidental association with drivers. The assumption of a constant rate can be justified on the basis that in this model, the cell cycle time is constant. As a result, only changes in the probability  $d$  that a cell survives to divide more than once can affect fitness. The frequency of actual divisions, and hence the rate at which new passenger mutations occur, must therefore also be constant. There is evidence that passengers accumulate broadly linearly prior to cancer initiation, though, since tumours in 90-year old patients have roughly twice as many mutations as in 45-year old patients at the same stage of tumour progression [14].

This model is a good example of a steady, incremental increase in fitness that is reminiscent of classic Darwinian selection, and predicts an exponential accumulation of drivers [18]. This exponential increase in the average number of drivers corresponds to a so-called “late evolution” model, in line with what we might expect. However, this model’s tractability hinges on its

assumption of a well-mixed model, and the derivation of the time constant of the accumulation depends on the assumption that sweeps are “hard” and widely separated in time. This requires only one clone to be prominent in the population at any one time, which is a rather strong requirement. In chapter 3, we propose a theoretical framework in which similar predictions about the accumulation of drivers can be made with weaker assumptions about the dynamics.

Like many others, this model is “well-mixed” — it does not consider the effects of shape on growth. One attempt to include geometrical constraints on the emergence of new drivers is the model by Antal *et al.* of a single spheroidal tumour [41]. Two important results from this work are the time for a new driver mutation to reach fixation on the surface of a tumour, and the probability that a cell at a chosen radius belongs to the wild-type or the mutant line. Equivalently, the shape and size of the spatially contiguous mutant sector. This geometrical model treats the nucleation of new driver mutations as stochastic and the growth of existing lines as deterministic, which heavily influences the analytical model developed in chapter 3. Growth in this model only occurs on the surface of the (initially spherical) tumour: the rate at which new driver mutations occur is therefore also proportional to the area of this growing surface. This geometrical constraint strongly restricts the effective population size, and growth and mutation occur more slowly than in well-mixed models [41].

Despite being a significant step away from the widespread assumption of well-mixed models, this is strongly constrained in two regards. The first is the idealised picture of perfectly smooth spheroids. Real tumours are unlikely to be perfectly smooth. It has been found in the case of bacterial colonies that roughness can strongly affect the probability of survival of mutant clones on the surface [39]. This may substantially revise one of this model’s core predictions. The second limitation for our purposes is the model’s lack of attention to migration. We revisit and attempt to address these issues in chapter 3.

Finally, the possibility of more complex fitness landscapes and evolutionary processes cannot be conclusively ruled out [42]. In this case, the pace of selection could intermittently accelerate and decelerate. This results in a picture of selective sweeps occurring in a few evolutionary bursts between long periods of slow evolutionary change, similar to what are known in evolutionary biology as punctuated equilibria [43]. One plausible and simple scenario is one in which only a few initial drivers after initiation carry a substantial advantage, followed by diminishing returns. This would result in an early, rapid succession of selective sweeps, followed by a period of relative stasis. This picture is intermediate between neutral models and the gradualistic late-evolution models. However, we should emphasise that this connection between the fitness landscape and evolutionary dynamics is based largely on expectations from well-mixed models. Studying the combined effects of space and invasion will be a major theme of this thesis.

#### 1.2.4 Our research in context

The interpretation of any experiment can only be as clear as the theory that it sets out to test. There is a clear need for a theoretical scheme which enables the evolutionary dynamics of metastatic cancers to be connected to the statistical behaviour of individual cells. Statistical properties of the large population should be related to mechanisms at play in the smallest members of the population. This search for a connection between aggregate behaviour and individual dynamics is a long-standing theme in both statistical physics and cell biology.

The work presented in this thesis was carried out in the spirit of connecting the world of the microscopic with that of the macroscopic. This should contribute to making possible the eventual prediction of the dynamics of cancer evolution from known properties of the cells that comprise it. Another outcome is that observations of the course of cancers could be used to draw inferences about the mechanisms at play on a smaller scale. While the achievement of both of these will in all likelihood take many more years of intensive research, we hope that our work here represents an incremental advance towards making mathematical models which are simple enough to be

straightforwardly interpreted, whilst also being brought closer to realistic situations.

To summarise, two important open problems in the dynamics of cancers are the growth curve of the tumour burden over time, and the timing of evolutionary events such as those suspected to produce resistance (see section 1.1.1). Whilst there are too many unknowns in our current knowledge of cancer to model these phenomena in full, we will attempt to advance our understanding of how growth and the speed of evolution are affected by tumour geometry and local invasion.

In chapter 2, we use a set of numerical simulations to investigate how the growth curve of an ensemble of tumours may be affected by changes in the properties of individual motile cells. Namely, how changes in elastic stiffness affect the speed of cells' migration through tissue; and how changes in cell type and speed affect the form of growth curves of tumours. We also study whether it is possible, and if so under what conditions, for growth curves to be truly exponential even when individual lesions in the ensemble grow much slower than exponentially.

We elaborate substantially on the last question in chapter 3, in which we present a stochastic theory for the growth of cancers with several constituent genotypes. The goal is to relate the fitness landscape of the different mutant types to the relative frequencies and average number of mutations present after a given time. We find a sophisticated way of doing so, and show that the mean-field limit of our theory is analytically solvable with complex analysis. The analytical approach enables some fundamental results about the growth of populations to be generalised, and permits exact solutions in a number of cases.

Finally, in chapter 4 we outline our contributions to an experimental study of a novel form of combined chemotherapy. The new therapy is based on a hypothesis that resistance to chemotherapy is acquired through several independent mutations. We discover that a simple model of tumour growth based on two independent populations provides a decent description in several cases. The results seem to refute the original hypothesis, and we provide some possible explanations as to why this may be.

## Chapter 2

# Individual-based models of local invasion

### 2.1 Introduction

Cancer involves the escape and migration of cells from primary tumours to form new tumours elsewhere in the body. This process is termed *metastasis* and is one of the most important features of advanced cancer [2]. Most experiments studying the migration of cancer cells around the body involve the injection of mice with human cancer cells, and measuring the locations and sizes of the resulting tumours [27, 29]. Since the results show new tumours forming in similar ways to untreated metastatic cancers, the current theory of how metastasis occurs is that a small number of cells become invasive and enter the bloodstream, before escaping again to start a new tumour elsewhere [27, 44].

However, the presence of cells in the margin surrounding tumours is another important indicator of the success of surgical therapy and forms part of the standard process of tumour biopsy. In addition to distant migration, escaping cells can also be found wandering around the margins of existing tumours, not yet having escaped to remote locations [45, 46]. It is routine practice to check that the margins of a tumour are clear of invasive cells, as this is an indicator of how likely the tumour is to have produced metastases either locally (in the same organ or tissue) elsewhere in the body [47].

We will explicitly *not* attempt to model the process of escape and metastasis in full detail, and will deal primarily with abstracted models that attempt to answer specifically how local migration affects growth. It is nonetheless worth giving an overview of what is currently known about the process of *distant* metastasis. This is to put our work into context, and to show what questions we can and cannot answer with our emphasis on local migration.

For distant metastasis to occur, invasive cells have to escape the lesion and surrounding tissue that they come from. The most common types of cancers are carcinomas, which are cancers of specialised epithelial tissue: this is tissue which forms layers of cells, like in glands or skin or in the lining of the digestive tract. Supporting any epithelial tissue is a larger bulk of connective tissue (see figure 2.1, upper structures). The two are separated by a thin layer called the basement membrane, which is mostly made of collagen fibres [48]. After escaping into the connective tissue, the invasive cells have to squeeze back through another basement membrane, and through layers of cells lining blood vessel walls, to escape into the bloodstream. From here, the cells undergo the reverse process, escaping first the bloodstream, travelling through connective tissue, and escaping another basement membrane, to found a new tumour [2, 44].

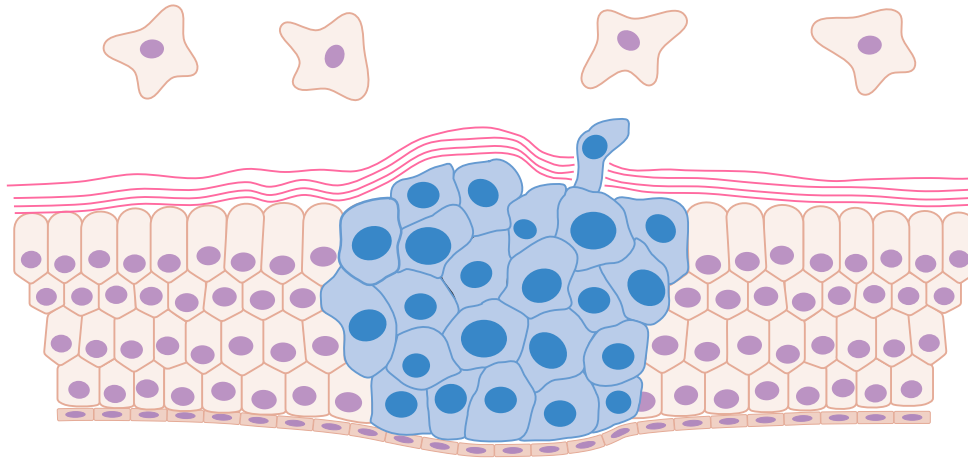


**Figure 2.1** *Diagram of the structure of a cancer of epithelial tissue (dense, orderly layer), showing the tumour itself (in blue), surrounding connective tissue (above, scattered cells) and the basement membrane separating them (red lines). A tumour cell is shown escaping through a hole in the basement membrane. Modified, from [6].*

By “lesion” or “micro-lesion”, we mean a single, small mass of cancer cells which is basically uniform in composition. By “tumour”, we mean instead larger and more complex structures, which possibly include new vasculature (capillaries), and some normal and necrotic tissue interspersed with the cancerous cells. Tumours can then be seen as aggregates of smaller microscopic lesions. Neither of these terms has a strict, hard-and-fast definition in the literature, and this choice of meanings is purely for technical convenience.

We are not interested in modelling every step of this process explicitly, as the number of unknowns alone would force us to include a large number of adjustable parameters. We shall instead focus on local migration, consisting of lateral movement through the same layer of tissue before invasive cells escape the basement membrane. This is intended to capture the process by which cells arrive in the surgical margin, the region surrounding malignant tumours. In particular, we will investigate how changes in individual cell properties affect the speed of the cell’s movement through layers of tissue, and how this affects the growth of tumours over time.

Changes in these properties could imaginably be achieved with novel drugs that make migratory cells stiffer [40, 49]. However, what effect this has on the rate of migration and escape is not obvious, let alone the knock-on effects on growth rates, and extremely difficult to measure in living test organisms such as mice. This is the main motivation for our set of virtual experiments, which attempt to measure the effect on tumour growth of changes in various factors that affect cell invasion.

## 2.2 Mechanistic simulation

Whether or not cells are invasive or stay in place is connected to their *type*, how specialised the cell is. Cell specialisation consists of which functional proteins it produces, and what these do. For example, a cell that formed the lining of a gland may produce protein complexes that speed up the synthesis of some hormone, which the gland secretes into the body; muscle cells produce larger amounts of actin and myosin, which form fibers which enable the cell to contract. Other types of cells produce other functional proteins [4]. This specialisation also manifests as differences in physical and mechanical properties of cells. How stiff cells are mechanically, and how many

adhesion molecules are present on their membranes, are two examples particularly relevant to us.

The question that we are trying to answer here is how quickly invasive cells are able to move through layers of epithelial tissue (or monolayers of cancer cells), and how this is affected by mechanical stiffness. Put more mathematically, these simulations are to measure how the speed of cell migration depends on the elastic modulus of invasive cells. While it is possible to study individual cancer cells' migration in isolation on a growth medium, it is much harder to experimentally investigate how their migration is affected by mechanical interactions with other cells around them in dense tissues.

To this end, we write and perform several set of centre-dynamical simulations which resolve the forces acting on each cell in a virtual monolayer of cells, treating each cell as a deformable sphere with a radius  $R_i$ . We adopt a fairly standard approach to other centre-dynamical models in the field, but make a few choices regarding different types of cell and how neighbouring cells interact that distinguish our simulation from others. For the unfamiliar with centre-dynamical models, we will briefly summarise the approach and the most unusual of our choices about what to model before going into details about the equations of motion and other technical choices.

The drag force acting on each cell is simply proportional to their velocity and in the opposite direction, and we use the classical expression for Stokes' drag on a sphere. This is a standard assumption in centre-dynamical models [50]. The surrounding interstitial fluid is assumed to have a viscosity similar to water. This means that at these small length-scales viscous drag is considerably larger than inertia, allowing for substantial simplifications to the equations of motion.

Cells experience forces due to interactions with their neighbours in addition to the viscous drag force, and an additional traction force if they are of the motile type. Cells can switch between a static type, which do not migrate and which divide; and a motile type, which migrate and which do not divide. These two types of cell correspond roughly to what are called epithelial and mesenchymal types in the literature, and the transition between them is a simple model of epithelial-mesenchymal transition (EMT) [51–53].

As we re-use our model of EMT in later models essentially unchanged, we will summarise it before moving on to the mechanical model.

## 2.2.1 Equations of motion and algorithm

### 2.2.1.1 Epithelial-mesenchymal transition

We model epithelial-mesenchymal transition as a Markov process: there is a rate  $k_{EMT}$  at which an epithelial cell transitions to a mesenchymal one, and a reverse rate  $k_{MET}$  at which mesenchymal cells switch back to being epithelial again. After an interval of time  $\Delta t$ , there is thus a conditional probability  $P_{E \rightarrow E}$  for  $E$  cells to remain  $E$  cells of

$$P_{E \rightarrow E}(\Delta t) = e^{-k_{EMT} \Delta t} \quad (2.1)$$

and a conditional probability to have switched to  $M$ -type  $P_{E \rightarrow M}$  of

$$P_{E \rightarrow M}(\Delta t) = 1 - e^{-k_{EMT} \Delta t} . \quad (2.2)$$

Similar formulae hold for  $M$  types to switch back to  $E$  types, substituting  $k_{MET}$  for  $k_{EMT}$  in the formulae above. These transition probabilities imply that the overall probabilities  $P_E$  and  $P_M$  that a given cell will be found to be type  $E$  or  $M$  after a period of time  $t$  obey a set of simple ordinary differential equations,

$$\frac{dP_E}{dt} = -k_{EMT}P_E + k_{MET}P_M \quad (2.3)$$

$$\frac{dP_M}{dt} = -k_{MET}P_M + k_{EMT}P_E \quad (2.4)$$

and since there are only two possible types of cell,  $P_E + P_M = 1$ .

In the limit that we have very large numbers of cells, these probabilities  $P_E$  and  $P_M$  correspond to the proportions of the population of each type. These proportions can be seen to relax exponentially towards an equilibrium point, regardless of the choice of initial conditions. This steady state corresponds to the solution of the two linear equations

$$-k_{EMT}P_E + k_{MET}P_M = 0 \quad (2.5)$$

and

$$P_E + P_M = 1 . \quad (2.6)$$

These have the unique solution

$$P_E = \frac{k_{MET}}{k_{EMT} + k_{MET}} , \quad (2.7)$$

$$P_M = \frac{k_{EMT}}{k_{EMT} + k_{MET}} , \quad (2.8)$$

and as a result, the relative numbers of  $M$  and  $E$  cells can (in principle) be tuned by choosing different values of the forward and reverse rates of EMT.

This choice of model was primarily for simplicity, as differentiation hierarchies can be very complex and involve several different populations, but very similar Markov chain models have been found to provide a remarkably good description of type switching behaviour in breast cancer cells *in vitro* [53].

### 2.2.1.2 Simulation units and parameter values

Motility is assumed to be due to adhesion of motile cells to a substrate such as the basement membrane or a culture medium, along which motile cells drag themselves (see figure 1.4). We make the deliberate choice not to model the mechanics of the underlying substrate or actin treadmilling [26], and instead simply apply a constant traction force to each motile cell, and treat the population of cells as a simple two-dimensional layer of interacting spheres. We then vary the motile cell's elasticity to see how this affects the motile cell's speed. The simple expectation is that the more strongly motile cells interact with the non-motile epithelial cells surrounding them, the slower they will be able to move.

The choice of a plausible traction force can be done by reviewing experimental results on how quickly motile cells of the same size move, and calibrating the traction force on motile cells in the simulation in the absence of other cells until the simulated speed and experimental speeds agree. Ideally these experiments would use cancer cells, but in many experiments amoebas or immune

cells called neutrophils are also used. This results in speeds in the range of  $0.03\text{--}1.0\mu\text{m} \cdot \text{s}^{-1}$  [26, 54–56].

We should point out that many of these experiments involve migration of cells on clean surfaces rather than dense tissue cultures, and so the speeds involved will likely be much higher than in our simulations.

To judge how relevant inertial effects are, we can use the above typical scales and combine them to determine an upper bound on the Reynolds’ number for our system, a dimensionless quantity representing the relative importance of viscous damping (in this case due to the interstitial fluid) and inertia (due to density).

Given that the interstitial fluid surrounding these cells is composed of a complex fluid containing water and other much more viscous substances and proteins, it will be at least as viscous as water: so,  $\mu \sim 10^{-3} \text{ Pa} \cdot \text{s}$  [50].

Both the interstitial fluid and the cellular substructure will, as they are composed of both water and proteins which in bulk are less dense than water, be somewhat less dense than water overall. The density of either the cells or the interstitial fluid will therefore be  $\rho \approx 10^3 \text{ kg} \cdot \text{m}^{-3}$  [50].

Finally, the cells of interest will be between  $L = 10 - 20\mu\text{m}$  in diameter, and neutrophils move at around  $U = 1\mu\text{m} \cdot \text{s}^{-1}$  [26, 54–56], which puts the Reynolds number of the flow around the cell at

$$\text{Re} = \frac{\rho UL}{\mu} = 10^{-5} \quad (2.9)$$

which is indeed much smaller than 1, meaning that inertial effects are  $10^{-5}$  times the strength of viscous and other effects. This justifies the use of the over-damped limit in which cell motility is usually analysed [25, 50].

The most “natural” choice of units for these simulations is one in which the most commonly encountered quantities are all close to 1. We are also not interested in electromagnetic effects, or other “exotic” physics: these simulations and models concern mechanics and motion of cells. Base units for our simulations should therefore consist of a mass M, a length L, and a time T.

An obvious choice for L is based on the typical size of eukaryotic cells, at around  $10\mu\text{m} = 10^{-5}\text{m}$  [55], so that average cell sizes are all around 1.0 L. Cell speeds should also, conveniently, be on the order of  $1.0 \text{ LT}^{-1}$ , which given a typical speed of  $0.1\mu\text{m} \cdot \text{s}^{-1}$  from above suggests a time unit of  $1\text{T} = 100\text{s}$ .

The mass of a typical cell is probably not a good choice for M, as inertia is much less important than drag here: we shall therefore choose units so that the viscosity of the interstitial fluid (assumed to be similar to that of water)  $\mu = 1.0 \text{ ML}^{-1}\text{T}^{-1}$ , which determines drag on these microscopic scales, is close to 1. It follows from straightforward dimensional analysis that the corresponding mass scale is  $M = \mu\text{LT}$ .

Given a viscosity of  $\mu \approx 10^{-3}\text{Pa} \cdot \text{s}$  and cell size of  $R \approx 5\mu\text{m}$ , a velocity of  $1\mu\text{m} \cdot \text{s}^{-1} = 10\text{L} \cdot \text{T}^{-1}$  on the upper end of the range of possible speeds requires a traction force of about  $9.4 \times 10^{-14}\text{N}$ , or  $94\text{ML} \cdot \text{T}^{-2}$ .

The various different units and adjustable parameters in these simulations can then be expressed as:

Quantity	Magnitude	Typical values & reference
Mass unit M	$= \mu L T = 10^{-6} \text{kg}$	Calculated, see above. [50]
Length unit L	$1L = 10^{-5} \text{m}$	Cell diameter, [55]
Time unit T	100s	Calculated, see text.
Traction force $\ \vec{F}_T\ $	$94 \text{ML} \cdot \text{T}^{-2}$	Calculated. [26, 54–56]
Interstitial fluid viscosity $\mu$	$1.0 \text{ML}^{-1} \text{T}^{-1} = 10^{-3} \text{Pa} \cdot \text{s}$	$10^{-3} \text{Pa} \cdot \text{s}$ [50]
Cell elastic modulus $E^*$	0–10 kPa for $M$ cells, 1 kPa for $E$ cells	1–13 kPa [57]
Work of adhesion $\gamma$	$10^{-2} \text{N} \cdot \text{m}^{-2}$	$1–9 \times 10^{-3} \text{N} \cdot \text{m}^{-2}$ [23, 25]
Cell bulk modulus $B$	10 kPa	Same as $E$ -type elastic modulus
Critical pressure $p_C$	$1 \text{M} \cdot \text{L}^{-1} \cdot \text{T}^{-2} = 10 \text{pPa}$	Estimated, see text.
Simulation area	$40 \text{L} \times 40 \text{L}$	NA

### 2.2.1.3 Equations of motion

As in other centre-dynamics models of tissue layers, inertia is neglected [25, 58, 59]. Otherwise, our equation of motion for each cell  $i$  would be

$$\sum_j \vec{F}_{ij} - b_i \vec{v}_i = m_i \vec{a}_i, \quad (2.10)$$

where  $\vec{v}_i$  is the velocity of cell  $i$ ,  $\vec{a}_i$  the acceleration of cell  $i$ ,  $b_i = 6\pi\mu R_i$ , and  $\sum_j \vec{F}_{ij}$  the resultant of all forces *other than drag* acting on cell  $i$ . This is considerably simplified by taking  $\text{Re} \approx 0$ , resulting in the quasi-static approximation [50]

$$\sum_j \vec{F}_{ij} - b_i \vec{v}_i = 0, \quad (2.11)$$

which can be more conveniently written in terms of cell mobility  $\zeta_i = b_i^{-1}$ ,

$$\vec{v}_i = \zeta_i \sum_j \vec{F}_{ij}. \quad (2.12)$$

The idea is that at such low Reynolds' numbers, the balance of forces is in instantaneous equilibrium with viscous drag, to an approximation as good as  $\text{Re}$  is small.

To integrate these equations, we use Euler integration, the simplest possible scheme. With a time step size of  $\Delta t$ , the position of each cell  $\vec{r}_i$  evolves according to

$$\vec{r}_i(t + \Delta t) = \vec{r}_i(t) + \Delta t \zeta_i \sum_j \vec{F}_{ij} \quad (2.13)$$

The forces  $\vec{F}_{ij}$  represent the interactions between cells and their neighbours, and the traction force experienced by motile cells. The interactions between cells and their neighbours consist of attractive and repulsive forces which act on lines between their centres: since we have abstracted away all of the details of a cell's shape except for its “size”, given by its radius  $R_i$ , the physics of our layer of virtual tissue seems vaguely reminiscent of the physics of a system of particles suspended in a viscous solution. The crucial differences consist of the growth of cells, to which we will return shortly, and the active “driving” of motile cells, represented with this constant traction force  $\vec{F}_T$ .

With the exception of this traction force, the interaction forces can be calculated from a potential  $U_{ij}$  which encodes all information about the physical interaction between cell  $i$  and its neighbour  $j$ ,

$$\vec{F}_{ij} = -\nabla U_{ij} , \quad (2.14)$$

which we represent as a sum of attractive and repulsive components,

$$U_{ij} = U_{ij}^{(\text{adh.})} + U_{ij}^{(\text{rep.})} + U_{ij}^{(\text{press.})} , \quad (2.15)$$

arising from adhesive and elastic interactions respectively. As in other centre-dynamical models, each of these is interpreted as due to a distinct physical interaction between the cells, and the aggregate potential  $U_{ij}$  should have a minimum at some distance between the two cells close to the average radius  $\bar{R}$ . This is so that the tissue has a stable mechanical equilibrium.

#### 2.2.1.4 Adhesion

We assume that the only attractive forces which act between cells are those due to cell adhesion. Most adhesion between cells is caused by the formation of chemical bonds between molecules on the cell membranes, and is primarily determined by the concentration of cell adhesion molecules called cadherins on the cell membrane [23–25, 60].

This contribution  $U_{ij}^{(\text{adh.})}$  to the interaction potential  $U_{ij}$  is simply the work done by adhesion, or the interfacial free energy due to bonds between these cell adhesion molecules. This interfacial free energy between two cells  $i$  and  $j$  depends on their respective types, but if the surface free energy (work of adhesion per unit area, analogous to surface tension) of their interaction is  $\gamma_{ij}$ , and the contact area between them  $A_{ij}$ , then the work done by adhesion is

$$U_{ij}^{(\text{adh.})} = -\gamma_{ij} A_{ij} , \quad (2.16)$$

and what remains is to specify  $\gamma_{ij}$  for the different possible cell types and calculate  $A_{ij}$ .

Different types of cadherins do not bind to each other very specifically. One type of cell with a high concentration of one type of cadherin and another type of cell with a similar concentration of a different type of cadherin will stick together with similar  $\gamma_{ij}$  than they would to each other. The interfacial free energy  $\gamma_{ij}$  is therefore believed to depend only on the concentration of adhesion molecules present on each type of cell, and not on the type of cadherin present [23–25, 60, 61].

However, direct measurements of the different possible  $\gamma_{ij}$  are extremely difficult, and despite many studies of adhesion between cells of the same type, we are not aware of any simple model of adhesion that is both founded on quantitative measurements of the work of adhesion between cells of different types and generally agreed upon [61, 62].

In our simulations, we choose simply set all  $\gamma_{ij}$  to be the same value, so that  $\gamma_{ME} = \gamma_{MM} = \gamma_{EE} = 10 \times 10^{-3} \text{N} \cdot \text{m}^{-2}$ . This is on the same order of magnitude as many measurements of the strength of cell adhesion [23–25, 60, 61].

Now, to calculate  $A_{ij}$ . Suppose two spherical cells  $i$  and  $j$  with radii  $R_i$  and  $R_j$  come into contact each other: we take the contact area to be circular and flat, with radius  $r_{ij}$ . (See figure 2.2.) We also assume for convenience that the shape and area  $A_{ij}$  of contact are unaffected by the cell's contacts with other neighbours, and that there are no complex effects like hysteresis. This is purely for convenience and simplicity: other authors do take into account hysteresis, or use Voronoi

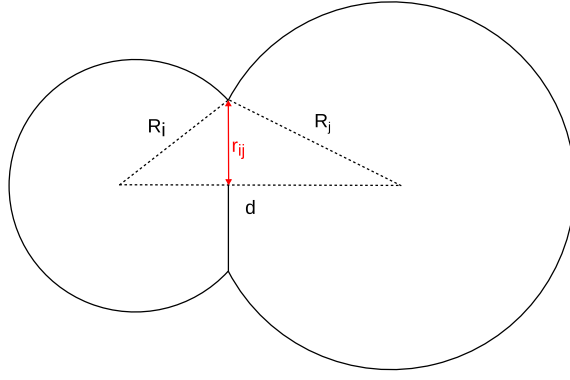


**Figure 2.2** Cross-sectional view of the assumed geometry for the contact area (radius marked by red arrow) of two neighbouring cells  $i$  and  $j$  of radii  $R_i$  and  $R_j$ .

contact areas [63, 64]. However, we are not interested in the effect of hysteresis *et cetera* on cell motility, so this will suffice.

Call the distance between the two cell centres is  $d$ , and define

$$\epsilon = R_i + R_j - d \quad (2.17)$$

and

$$R = (R_i^{-1} + R_j^{-1})^{-1} \quad (2.18)$$

to be the overlap  $\epsilon$  and harmonic mean radius  $R$ . The contact area  $A_{ij}$  is then given by

$$A_{ij}(\epsilon) = \pi r_{ij}^2(\epsilon) = 2\pi R\epsilon - \frac{\pi}{4}\epsilon^2 \quad (2.19)$$

and so the adhesion interaction potential is

$$U_{ij}^{(\text{adh.})}(\epsilon) = -\gamma_{ij}A_{ij} = -\gamma_{ij}\left(2\pi R\epsilon - \frac{1}{4}\epsilon^2\right) \quad (2.20)$$

for an interaction force of

$$\vec{F}_{ij}^{(\text{adh.})} = -\nabla_{\epsilon} U_{ij}^{(\text{adh.})} = \gamma_{ij}\left(2\pi R - \frac{1}{2}\pi\epsilon\right)\vec{n} \quad (2.21)$$

where  $\vec{n}$  is the unit vector pointing from the centre of  $i$  to that of  $j$ .

### 2.2.1.5 Hertzian repulsion

In addition to adhesive forces, there must also be repulsive forces due to the cells' elastic resistance to applied stresses [65]. When any two elastic bodies are brought into contact, they must be deformed at least slightly, and this requires mechanical work. The simplest such model of the work required to bring two spheres closer than possible in their undeformed state is Hertzian repulsion:

$$U_{ij}^{(\text{rep.})} = \frac{2E_{ij}^* R^{1/2}}{5} \epsilon^{5/2} \quad (2.22)$$

where  $E_{ij}^* = (E_i^{-1} + E_j^{-1})^{-1}$  is an “effective” elastic modulus accounting for the fact that the more elastic of the two bodies will do more of the deformation. For example, a rubber ball squashed into a much more rigid concrete surface will be strained much more dramatically than the concrete. Because most of the work will go into straining the rubber ball, the force required to squash the two together will be determined by the elastic modulus of the ball, rather than the concrete.

$R$  is once again the harmonic mean of the radii of the two cells, given by equation (2.18).

With  $\epsilon$  defined as above in equation (2.17), the repulsive force between  $i$  and  $j$  due to Hertzian repulsion is

$$\vec{F}_{ij}^{(\text{rep.})} = -E_{ij}^* R^{1/2} \epsilon^{3/2} \vec{n} \quad (2.23)$$

where  $\vec{n}$  is again the unit vector pointing from the centre of  $i$  to the centre of  $j$ . One can easily verify that the corresponding reaction force on  $j$  due to  $i$  is equal and opposite [65].

### 2.2.1.6 Internal pressure

In addition to Hertzian repulsion due to elastic deformation, we also include repulsion due to bulk compression. Even balloons full of any given liquid will avoid being forced into one another, despite the lack of resistance to shear stress. All media, whether elastic or fluid, have a bulk modulus  $B$  that describes their resistance to compression.

The internal pressure  $p$  of the cell is

$$p = B \frac{\Delta V(\epsilon)}{V} \quad (2.24)$$

in terms of the change in volume  $\Delta V$  as a function of the overlap  $\epsilon$  from equation (2.17),

$$\Delta V(\epsilon) = \frac{\pi}{4} R \epsilon^2 - \frac{\pi}{24} \epsilon^3, \quad (2.25)$$

with  $R$  as before from equation (2.18), and

$$V = \frac{4\pi}{3} R_i^3. \quad (2.26)$$

The true value of the bulk modulus, along with Poisson’s ratio, is typically unknown for most cell types [57]. We take the bulk modulus  $B$  to be the same as the elastic modulus of  $E$ -type cells,

$$B = E_E^* = 10 \text{ kPa} \quad (2.27)$$

corresponding to a Poisson’s ratio of  $\nu \approx 1/3$  [65].

The force corresponding to this internal pressure is, to leading order,

$$\vec{F}_{ij}^{(\text{press.})} = -pA_{ij}\vec{n} = -\frac{3\pi}{8}B\frac{R^2\epsilon^3}{R_i^3}\vec{n}, \quad (2.28)$$

which is cubic in overlap  $\epsilon$ . This means that this term will be dominated by Hertzian repulsion at  $\epsilon \ll R$ , only becoming relevant at extremely dense packings of cells. However, although the internal pressure  $p$  is not relevant to mechanical interactions, it does provide a useful way to track which cells are overcrowded and should not divide.

We will only allow cells with internal pressure  $p < p_C = 10^{-5}$   $\mu\text{Pa}$  to undergo cell division. This is to ensure that the population of cells in the tissue stay at a constant, predictable density: cell division will be naturally suppressed in regions where the internal pressure  $p$  is too high, but will continue if a cell dies, filling the void it leaves behind. We will elaborate on this shortly.

### 2.2.1.7 Traction

In addition to their distinct mechanical and adhesive properties,  $M$ -type cells do not divide, and also experience a tractive force  $\vec{F}_T$ . This force is constant in time and oriented in the  $x$ -direction. This is partially for convenience of calculation, but can be readily interpreted as the motile cells' being attracted up a concentration gradient, perhaps of oxygen, glucose or another chemical signal. Such sensing of chemical gradients and migration in more favourable directions is very well-established [26, 56, 66].

We assume that the traction force that  $M$  cells experience is constant in magnitude and direction, and equal to

$$\vec{F}_T = +94 \text{ ML} \cdot \text{T}^{-2} \vec{e}_x, \quad (2.29)$$

where  $\vec{e}_x$  is a unit vector pointing along the  $x$  axis.

As a cartoonish simplification of this process, one can picture the mechanical effect of the active stresses in the cytoskeleton, both contractile and extensile forces, as a taut rope connecting the cell to its external environment under tension  $F_T$ . The actively generated tension in the ‘‘rope’’ manifests as a traction force on the motile cell,  $\vec{F}_T$ , and a reaction force  $-\vec{F}_T$  acting on the cells microenvironment (see figure 1.4).

In our simulations, the reaction force is assumed to act on the non-cellular, rigid substrate on which the cellular monolayer grows and subsists: it does not explicitly enter our simulations. Some of the limitations of this treatment of tractive forces are discussed later, in section 2.2.2.

### 2.2.1.8 Cell division and algorithm overview

```

tt = 0
ttmax = 150 days
 $\Delta t = 1$  second
while (tt < ttmax):
    for each cell:
        if ( $p < p_C$ ) then
            grow cell:
                cell→  $R_i = R_i + \Delta t \times \text{growth\_speed}$ 
            if (cell→  $R_i > R_i^{\text{final}}$ ) then
                divide:
                     $R_{\text{new}} = R_i/2$ 
                    cell→  $R_i = R_{\text{new}}$ 
                    newcell→position = cell→position +  $R_{\text{new}} \times \text{random\_direction}$ 
                    newcell→type = cell→type
            if (rand < switching_probability) then
                switch type
            calculate forces:
                force = sum(forces from neighbours)
            move cell:
                mobility =  $1/(6\pi R_i)$ 
                cell→position = cell→position + mobility  $\times$  force  $\times \Delta t$ 
        tt +=  $\Delta t$ 
    save velocities and populations to file

```

Each time step, we loop over all cells present, and for each cell implement growth, type switching, cell division, resolve the forces on each cell, and move each cell. Although the choice of the precise order for these is arbitrary, cell type information and cell radii are needed to specify the forces acting on each cell, and are most conveniently calculated together.

Cells gradually expand over time until they reach a critical size, at which point they divide into two cells with half the volume of the parent cell each if the internal pressure  $p$  is not too high. If  $p$  is larger than a critical pressure  $p_C$ , which we set to  $1.0 \text{ M} \cdot \text{L}^{-1} \cdot \text{T}^{-2} = 1 \mu\text{Pa}$ . This ensures that cells only divide when there is plenty of room for additional cells, avoiding unrealistic “clumping” of the kind detailed in [62]. Again, we should emphasise that we are not interested in modelling cell adhesion or division very realistically: we just want to know how fast  $M$ -cells can move as their stiffness changes.

We include a small random variability in the threshold for division when the cell is initialised, although the expansion of the cell during this interphase period [4] and the sizes and types of the new cells are deterministic. In this way, the average size of cells falls in a set range, and the small random variability in sizes at division causes a gradual desynchronization of cell cycles between cells over time.

This is implemented by gradually increasing each cell’s radius  $R_i$  by a constant amount  $\Delta R_i$  each time step. When  $R_i$  reaches a threshold value  $R_i^{\text{final}}$  set when the cell was initialised, the cell divides. Both new cells have radii equal to  $2^{-1/3} R_i^{\text{(old)}}$  to conserve volume, and the new cell has a threshold

$$R_i^{\text{final}} = \bar{R}(0.9 + 0.2 \times \text{rand}) , \quad (2.30)$$

where  $\text{rand}$  is a random number in between 0 and 1 and  $\bar{R}$  is the specified mean radius. This insures that all cells have a threshold division size within ten percent of the specified average, and that their sizes all fall within the same reasonable range. In practice,  $\bar{R}$  is set to  $5\mu\text{m}$  to match typical cell sizes.

After changing the cell's size and performing division if it is large enough and not overcrowded, we calculate the net force acting on the cell,

$$\vec{v}_i = \zeta_i \left( \sum_j \left( \vec{F}_{ij}^{(\text{adh.})} + \vec{F}_{ij}^{(\text{rep.})} + \vec{F}_{ij}^{(\text{press.})} \right) + \delta_{T_i, M} \vec{F}_T \right) \quad (2.31)$$

where the sum is taken over all neighbours in contact with the cell  $i$  and  $\delta_{T_i, M} = 1$  if the type  $T_i$  of cell  $i$  is  $M$ -type and 0 otherwise. The position  $\vec{r}_i$  is then updated to

$$\vec{r}_i(t + \Delta t) = \vec{r}_i(t) + \Delta t \vec{v}_i \quad (2.32)$$

in accordance with equation (2.13), with  $\vec{v}_i$  from equation (2.31).

The determination of which cells should be considered neighbouring cells is not obvious, given that cells can move continuously around. One non-trivial optimization to accelerate the time taken to calculate all possible contact forces acting on a cell is the inclusion of a data structure that records which cells currently lie in which of a grid of larger boxes overlaid on top of the simulated area: when calculating the contact forces in equation (2.31), only cells in the same box as  $i$  and neighbouring boxes are checked. If a pair of cells are found not to be in contact ( $\epsilon < 0$ , from equation (2.17)), then the contact force between the two is zero.

This is a simple example of a bounding volume method: the bounding volume in all cases consists of the grid square containing the cell and its neighbouring squares [67].

## 2.2.2 Results

The total population of cells tends towards a stable equilibrium after an initial overshoot at about 20 days. As is visible in figure 2.3, the profile of the population's growth is not affected by the elasticity of the motile  $M$  cells.

As can be seen from figure 2.4(A), stiffer migrating cells with higher  $E_{MM}^*$  experience stronger resistance to their motion than cells with weaker interactions, and move slower under a constant traction force  $\vec{F}_T$ . As the stiffness  $E_{MM}^*$  of the motile cells increases, however, the speed at which the  $M$ -cells migrate levels off asymptotically. The underlying reason for this is the fact that the strength of Hertzian repulsion is determined by the more deformable of the interacting materials, as the more elastic material will deform more and consequently absorb more of the elastic strain energy. This is basically in line with the ‘‘rubber ball’’ argument described in subsection 2.2.1.5, and the dependence of speed on  $E_{ME}^*$  can be seen in see figure 2.4(B).

In theory, even a perfectly rigid  $M$  cell would only see a limited finite resistance to its motion, as its elastic interactions with the surrounding tissue would still be finite, and controlled by the magnitude of  $E_{EE}^*$ .

All this strongly suggests that the transition from stiff, slow cells to flexible and fast cells is controlled by the relative strengths of elastic interactions between  $M$  and  $E$  cells via the effective elastic modulus  $E_{ME}^*$ . Although this was not intended to model long-range migration through the extracellular medium, we can speculate that similar elastic interactions between the elasticity of cells and the elasticity of the fibrous extracellular matrix affect the speed of cell motility over much

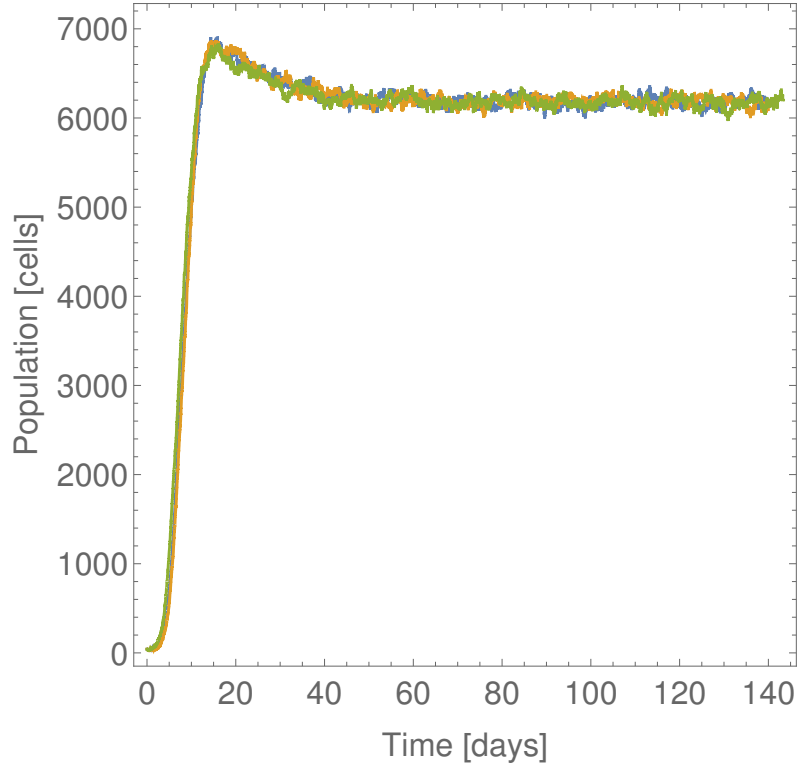


**Figure 2.3** *A plot of the change in population of the virtual monolayer, showing the approach to confluence and fluctuations around equilibrium population for three realisations with different values of effective elasticity of motile cells (blue:  $E_{MM}^* = 0.0$ , yellow:  $E_{MM}^* = 1.0$ , green:  $E_{MM}^* = 10.0$ ). Note the initial overshoot before relaxation to the equilibrium population density, and the fact that all three profiles look qualitatively similar. The overshoot and approach to confluence is not influenced by the properties of the motile cells.*

longer distances. Whether or not this is the case of course depends on experimental falsification or verification.

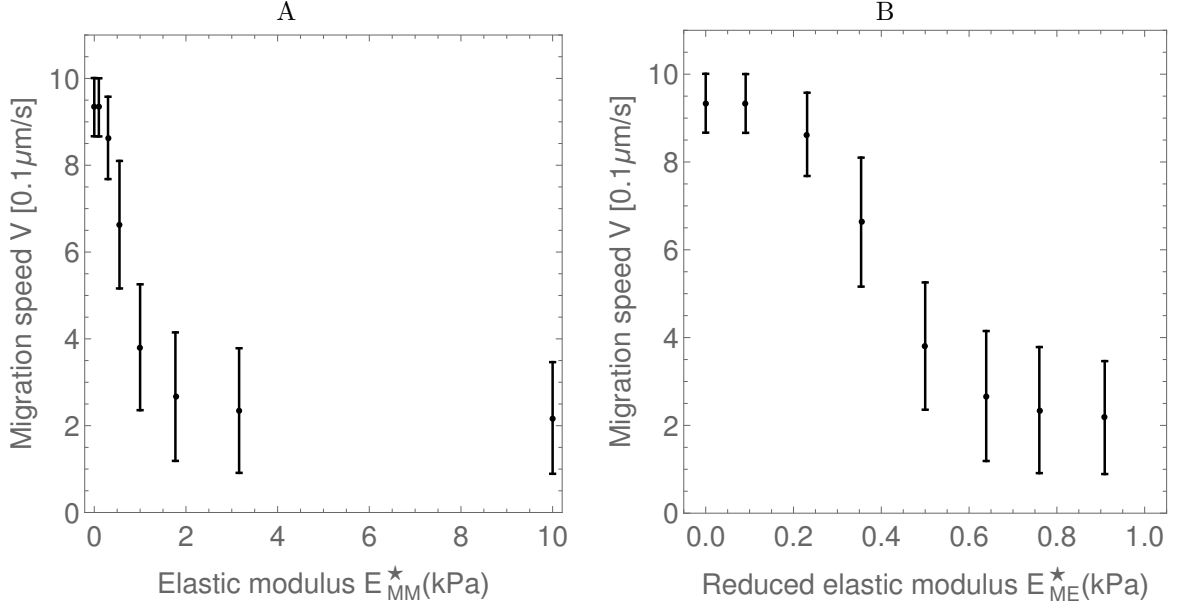


**Figure 2.4** *Plots showing the average speed of motile cells as (A) a function of the effective elastic stiffness of motile cells  $E_{MM}^*$ , and (B) a function of the reduced elastic stiffness of motile cells  $E_{ME}^*$ , corresponding to the interaction strength between epithelial and motile cells. Note the initial decline in  $|\bar{v}|$  followed by a levelling off at high values of  $E_{MM}^*$ , and that the interaction strength saturates at the stiffness of surrounding tissue, 1.0 in these units.*

One important shortcoming of this model is that cells are assumed to be internally homogeneous and isotropic continua, and so their mechanical interactions can be described entirely in terms of the strength of adhesion and their elastic moduli. However, cells are known to not be internally homogeneous, and the cell nucleus can have a very different elastic response from the cytoplasm and cytoskeleton that surround it [68]. If it is the case that the degrees of freedom of the nucleus are important, centre-dynamical approaches that take cells to be homogeneous spheres may be inadequate, and could be extended to include the position and shape of the nucleus as well. Many of the “standard” approaches in the field, even more sophisticated vertex-dynamical models or those which treat individual cells as continuously deformable bodies also ignore nuclear degrees of freedom [62, 69]: although there has been some progress in including the mechanics of the nucleus in lattice models [70], we are not aware of any successful attempts to do so in off-lattice, continuous models..

Another shortcoming is that this approach was also very computationally intensive, requiring six months of runs to produce useful quantities of data (seen in figures 2.3 and 2.4), and being limited to populations of a few thousand cells in two dimensions rather than the many millions in complex three-dimensional configurations that real tumours are often composed of. Some rather aggressive coarse-graining is necessary to generalise our results to large and realistic tumour sizes.

Despite these shortcomings, this simple model shows that increases in elastic stiffness of motile cells can enhance the resistance to motile cell’s motion through epithelial tissue. It also shows that the degree by which motile cells can be slowed down by elastic interactions is limited by the elasticity of the surrounding tissue rather than the stiffness of the migrating cell. To answer what — if any — effect these changes in motile speed actually have on the growth rate of tumours composed of larger ensembles of lesions requires a look at a much larger length-scale.

## 2.3 Spatial lattice model of local migration

The off-lattice mechanistic model studied in section 2.2 is too computationally demanding to scale easily to tumours that contain millions of cells, and in which cells are free to migrate in three spatial dimensions. But it is on these scales that most clinically relevant tumours exist and grow, so to understand how changes in the speed of cell motility affect growth, we need to develop a simpler model that can nonetheless preserve basic insights and phenomena from the more complex model.

To analyse how migration affects the growth curve of large tumours, we developed a simpler, lattice model that incorporated cell motility with an adjustable migration speed  $|\vec{v}|$ , kept the same model of changes in cell type as in 2.2.1.1, and which included some degree of randomness in the control of cell motility. We explicitly abstract away details such as the mechanical properties of cells and cell adhesion, and treat cell division and motility as stochastic processes.

In this lattice model, cells are particles which occupy single sites on a three-dimensional cubic lattice. Cells can be of type  $E$  or type  $M$ , as in section 2.2.1.1, and transition between the two types stochastically with forward and reverse rates  $k_{EMT}$  and  $k_{MET}$  respectively. The dynamics of growth and migration are treated with a combination of Eden-model growth for  $E$ -type cells and a persistent random walk to migration for  $M$ -type cells [71, 72]. In the Eden model of growth, a given cell will attempt to divide at a stochastic rate  $b$ , by attempting to place a new cell at a neighbouring lattice site chosen uniformly at random. The division is only successful if the chosen lattice site is free: otherwise, the cell does not divide this turn (see figure 2.5 for an illustration). Only type  $E$  cells are able to divide.

An  $E$ -type cell that is completely surrounded will effectively not divide at all, whereas one which is not entirely surrounded will divide at a progressively slower effective rate as its neighbours become full [71]. In this model of growth, constraints from overcrowding of cells naturally emerge from a very simple set of rules. The growth of large tumours is naturally slower than exponential, and tumours are roughly spheroidal (see figure 2.11 in the results section).

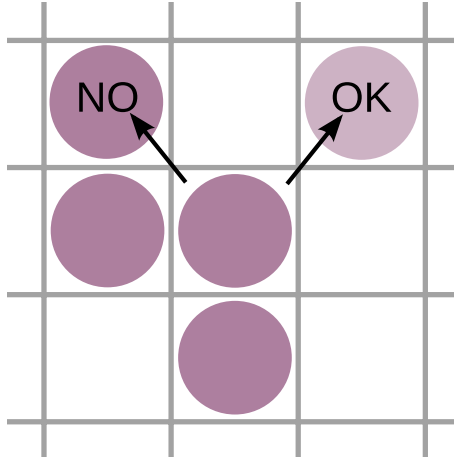


**Figure 2.5** A figure showing the basic growth rule in the Eden model of growth. With a probability  $b\Delta t$ , the cell in the centre of the diagram attempts to divide, choosing a neighbouring lattice site at random. The upper-left lattice site (marked NO) is occupied, so an attempt to divide here will fail. The upper-right lattice site (marked OK) is unoccupied, so an attempt to divide here will succeed, and a new cell (light colour) will be placed here.

Cells of type  $M$  do not divide, but are motile. Each motile cell has the same characteristic speed  $|\vec{v}|$  and an individual *polarity*  $\vec{P}$ , corresponding to its instantaneous direction of motion. The polarity of a cell corresponds to the direction of one of its neighbouring sites on the lattice. Each time step

$\Delta t$ , the  $M$ -cell attempts to move  $V\Delta t$  times by hopping to the next lattice site in its direction of motion: if the lattice site it is attempting to move to is occupied, it stays still. These cells also “tumble” with a rate  $\alpha$ , meaning that there is an expected probability to tumble of  $\alpha\Delta t$  per time step  $\Delta t$ . With a probability of  $\alpha/V$  per hop, cells tumble, meaning that they choose a new polarity from the set of possible neighbouring lattice sites.

This probability to tumble per hop  $\alpha/V$  can also be expressed as an average length  $L = V/\alpha$  between tumbling events.

This model of the motion of an active particle belongs to the “run-and-tumble” class of models [72]. Although more commonly used as models of bacterial locomotion [72, 73], here we are using it to describe invasive mesenchymal cancer cells. Many of the details of the precise dynamics of how cancer cells move through tissues in reality is unknown: our use of this type of model is intended to capture the idea that cells move with some characteristic speed  $|\vec{v}|$ , and the environment surrounding them is heterogeneous, which causes their motion to gradually decorrelate. One plausible justification for why cells might “tumble” in this way would be that they are following shallow chemical gradients (*chemotaxis* [69]) which fluctuate over time, causing the cell’s direction of motion to wander.

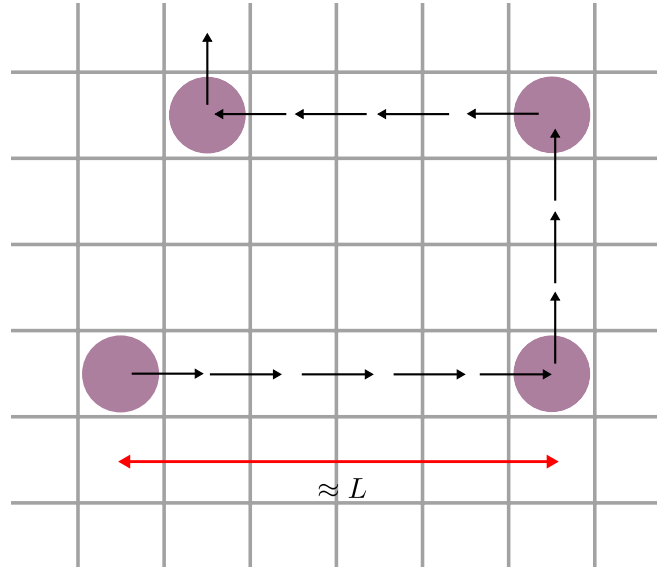


**Figure 2.6** *Cartoon of cell motility in the “run-and-tumble” lattice model. A motile  $M$ -type cell has a “polarity” or instantaneous direction of motion, marked with an arrow, and proceeds in this direction at a speed  $|\vec{v}|$ . This is modelled by having the cell move  $V\Delta t$  hops per time step  $\Delta t$ . Each hop, there is a probability  $\alpha/V = 1/L$  (see main text) that the cell will tumble, re-orienting so that its polarity points in a different, randomly chosen direction.*

We measured the total population of cells of both types over time, running multiple replicates for different values of the type transition rates  $k_{EMT}$  and  $k_{MET}$ , tumbling rate  $\alpha$ , and speed  $|\vec{v}|$ . Our expectation at the outset was that the rate of tumbling  $\alpha$  and the speed of migration  $|\vec{v}|$  would both have a relatively weak effect on the observed growth curves of the tumour, on the basis that neither of these should affect the cell division rate  $b$  or the population of motile cells, which from 2.2.1.1 we expected to be controlled by  $k_{EMT}$  and  $k_{MET}$ .

### 2.3.1 Algorithm

```

tt = 0
ttmax = 150 days
 $\Delta t$  = 1 second
while (tt < ttmax):
    for each cell:
        if (type  $M$ ) then
            for (i=0, i<speed $\times\Delta t$ , i++)
                newposition = position + polarity
                if newposition is empty then
                    position = newposition
            if (rand < tumbling_probability) then
                polarity = random_neighbour
            if (rand <  $k_{MET}\Delta t$ ) then
                change type to  $E$ 
                polarity = (0,0,0)
        else if (type  $E$ ) then
            if (rand <  $b\Delta t$ ) then
                try to divide to random neighbour:
                x = position + random_neighbour
                if (x is empty) then
                    add new cell at x
                if (rand <  $k_{EMT}\Delta t$ ) then
                    polarity = random_neighbour

    tt +=  $\Delta t$ 
    if (tt mod 10 == 0) then
        save populations to file

```

A lattice sites' neighbours consist of the sites in an octahedral neighbourhood surrounding the site, a choice known in the cellular automata research community as a three dimensional von Neumann neighbourhood [74]. Polarities of  $M$ -type cells are represented a position vector  $\vec{P}$  which points to one of these neighbours, and corresponds to which neighbour the cell will attempt to hop to next. For example, a cell with  $\vec{P} = (0, 0, 1)$  will attempt to move in the  $z$ -direction.

Each time step, the set of all cells, which consisted of their positions, types, and polarities, is iterated over. For simplicity, cell type is not stored separately from polarity. Instead, non-motile  $E$ -type cells are considered to have a polarity of  $\vec{P} = (0, 0, 0)$ , with any other polarity indicating that the cell is of type  $M$ .

If the cell is type  $M$ , it attempts to hop to a new position  $V\Delta t$  times per time step, succeeding only if the new lattice site is unoccupied. With probability  $\alpha/V$  per hop, the cell tumbles, adopting a new polarity from the set of von Neumann neighbours with uniform probability each. Finally, with a probability  $k_{MET}\Delta t$  it switches to an  $E$ -type cell, with  $\vec{P} = (0, 0, 0)$ .

If the cell is instead type  $E$ , then with probability  $b\Delta t$ , the cell attempts to divide. A lattice site at one of this cell's neighbours is chosen, and if free, becomes occupied by a new  $E$ -type cell. The cell division otherwise fails.

Every 10 time steps, the elapsed time, total size  $n$ , numbers of non-motile and motile cells, and instantaneous growth rate (additional cells per time step,  $\Delta n/\Delta t$ ) are calculated.

The mode of growth can be determined by plotting the instantaneous growth rate against the total

population: that is, what does  $\Delta n/\Delta t$  look like as a function of total size  $n$ ? We did not assume that growth would take a particular form, and are interested in how the resulting growth curve emerges from the underlying rule set. If the growth is exponential, we would expect  $\Delta n/\Delta t$  to be proportional to  $n$ . Otherwise, in the case that growth can only occur on the surface and the tumour is spheroidal, we might expect

$$\Delta n/\Delta t \propto n^{2/3}, \quad (2.33)$$

instead.

### 2.3.1.1 Choice of data structures

During initial tests of the simulations, it was found that one of the slowest steps of the algorithm was the procedure in which a cell's neighbouring sites were checked for the presence of additional cells, which was performed during both division and cell movement. This test is possibly related to the collision detection problems encountered in the off-lattice model, but a different way around the problem was found.

Although it would be the fastest in terms of algorithmic complexity, it would have been far too memory intensive to store every possible lattice site, including empty ones. This meant that in early versions of the simulations, a cell's neighbouring lattice sites were not explicitly stored. Instead, all information on cells was stored in a vector containing the position, type and polarity of a cell. New cells would always be added to the end of this vector, which necessitated that tests to find a cell at any given lattice point had to iterate over the whole vector of cells, which took  $\mathcal{O}(n)$  to achieve for a population of  $n$  cells. This significantly slowed down the simulations, as similar checks would have to be repeated for a constant fraction of all  $E$ -type cells present.

Attempted solutions included various ways to store and access every cell's set of neighbouring lattice sites directly, but these ran into the problem that memory requirements were greatly increased: those solutions which managed to reduce the time complexity to  $\mathcal{O}(1)$  tended to have a much larger memory requirement of at least  $\mathcal{O}(n)$ , strongly limiting the maximum size of tumours that could be simulated effectively. While related approaches may be able to solve the problem, this was eventually abandoned in favour of a compromise solution which reached a somewhat better time complexity without severely increasing memory requirements.

The solution which I eventually settled upon was to store information about all present cells in an associative array that took a cell's position as a key and returned the cell's type/polarity — but *only* if a cell was present at that location, as the position would otherwise be absent from the array. As the structure underlying maps is a binary tree, operations involving search, lookup, addition and removal are all of order  $\mathcal{O}(\log(n))$  in time. This method did not necessitate the storage of every cell's neighbour's, which would have exacerbated memory requirements, but nonetheless allowed an appreciable speed-up [75].

Whether or not a cell was present at any given position could be determined by a *count* operation, which counted the number of entries in the map with a given key (in this case, a given position). If no cell was present at a given position, the *count* operation would return 0, and movement or division could proceed to move or add a cell at the tested site.

Since all of the *count*, lookup, addition and removal operations have time complexity  $\mathcal{O}(\log(n))$ , the division and motility sub-procedures in the algorithm have the same time complexity, and iterating through all cells in one time step in the algorithm results in a total time complexity of  $\mathcal{O}(n\log(n))$ .

### 2.3.2 Results

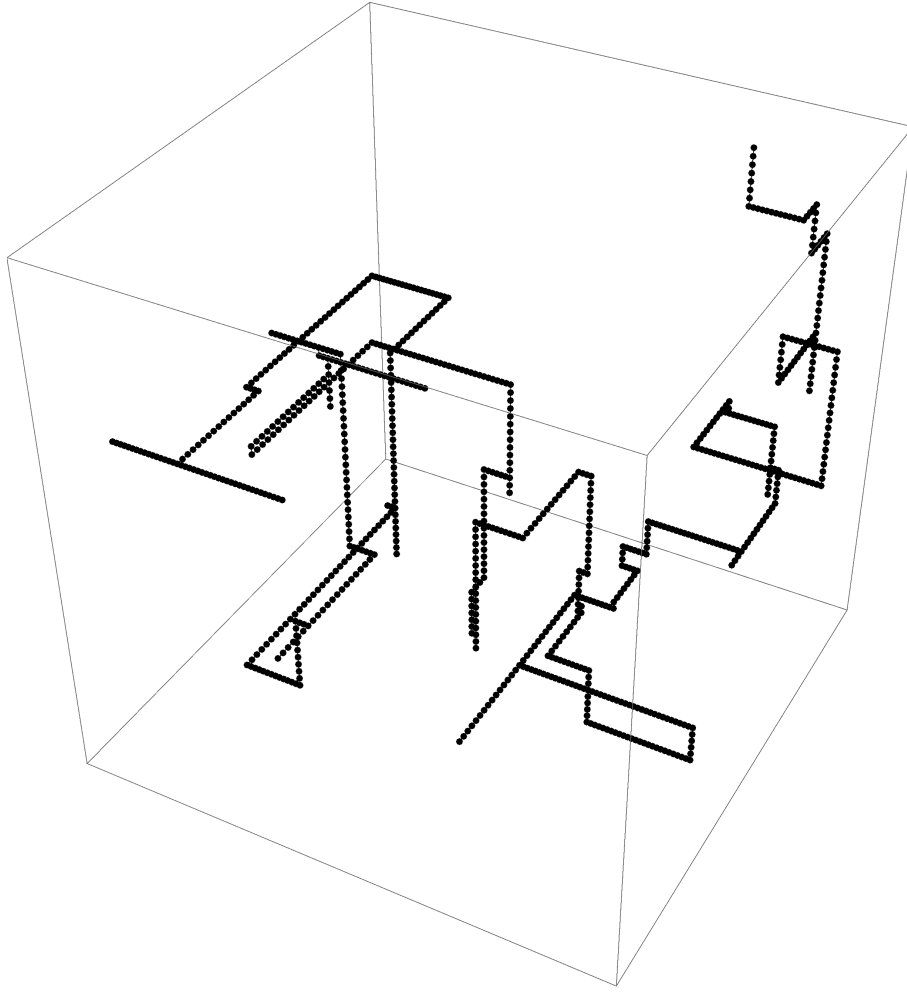


**Figure 2.7** *A trajectory of a single motile cell with tumbling rate  $\alpha = 0.1 \text{ day}^{-1}$  and speed  $V = 1 \text{ sites} \cdot \text{day}^{-1}$ , corresponding to mean run length  $L$  of 10 sites. There was no switching to the non-motile cell type or growth dynamics.*

#### 2.3.2.1 Single motile cell

Run-and-tumble models are closely related to the Telegrapher's equation [72, 73, 76]. The probability distribution  $\rho(x)$  for the position  $x$  of a particle undergoing a persistent random walk in one spatial dimension with speed  $|\vec{v}|$  and tumbling rate  $\alpha$  obeys the partial differential equation

$$\frac{\partial^2 \rho}{\partial x^2} + \alpha \frac{\partial \rho}{\partial t} = V^2 \frac{\partial^2 \rho}{\partial x^2}, \quad (2.34)$$

as detailed in [76]. While it would seem that a one-dimensional random walk won't provide a good description of a particle moving through a three-dimensional space, our motile cells are not allowed to take on arbitrary orientations. The choice of von Neumann neighbourhood means that they are forced to move along the axes of the lattice (see figure 2.7) and the random walk is not isotropic.

Without solving it explicitly, as long as the boundary conditions

$$\lim_{\|x\| \rightarrow \infty} \rho = 0 \quad (2.35)$$

and

$$\lim_{\|x\| \rightarrow \infty} \frac{\partial \rho}{\partial x} = 0 \quad (2.36)$$

hold, and  $\rho$  is normalized so that

$$\int \rho dx = 1, \quad (2.37)$$

then we can define the mean-squared displacement to be

$$\langle x^2 \rangle = \int x^2 \rho dx \quad (2.38)$$

and it follows from the application of integration by parts to equation (2.34) that  $\langle x^2 \rangle$  obeys

$$\frac{\partial^2 \langle x^2 \rangle}{\partial t^2} + \alpha \frac{\partial \langle x^2 \rangle}{\partial t} = 2V^2. \quad (2.39)$$

With the initial condition that, if the cell's initial position is already known,  $\langle x^2 \rangle = 0$  when  $t = 0$ , it follows that

$$\langle x^2 \rangle(t) = \frac{2V^2}{\alpha^2} (1 - e^{-\alpha t}) + \frac{2V^2}{\alpha} t \quad (2.40)$$

solves equation (2.39). This provides a theoretical mean-squared displacement to which we can compare the observed mean-squared displacement of an individual motile cell [76].

Two phenomena are clear from equation (2.40): on time-scales  $t$  much shorter than  $\alpha^{-1}$ , the mean-squared displacement is quadratic, indicating that the motile cell is initially moving ballistically in a straight line at constant speed. Due to tumbling, on time-scales much longer than  $\alpha^{-1}$ ,  $\langle x^2 \rangle$  slows down to growing linearly in time  $t$ . This indicates that after tumbling has set in, the cell begins to move diffusively through the available space, approximating a random walk.

As can be seen from figure 2.8 showing the mean square displacement averaged over a thousand replicate simulations of a single  $M$  cell, this classical theory shows a very good agreement with numerical results.

### 2.3.2.2 Aggregate tumour

Plots of  $\Delta n / \Delta t$  against  $n$  for different values of tumbling rate  $\alpha$ ,  $|\vec{v}|$ ,  $k_{EMT}$  and  $k_{MET}$  all show that initially, tumours grow slower than exponentially, with  $\Delta n / \Delta t \propto n^{2/3}$ . This can be easily interpreted as growth being dominated by a single lesion which grows only on its surface, in accordance with other results for the Eden model [71]. After some length of time controlled by the tumbling rate  $\alpha$ , growth accelerates for a while before settling down again to a similar dependency  $\Delta n / \Delta t \propto n^{2/3}$ , albeit with a larger prefactor (see figure 2.9).

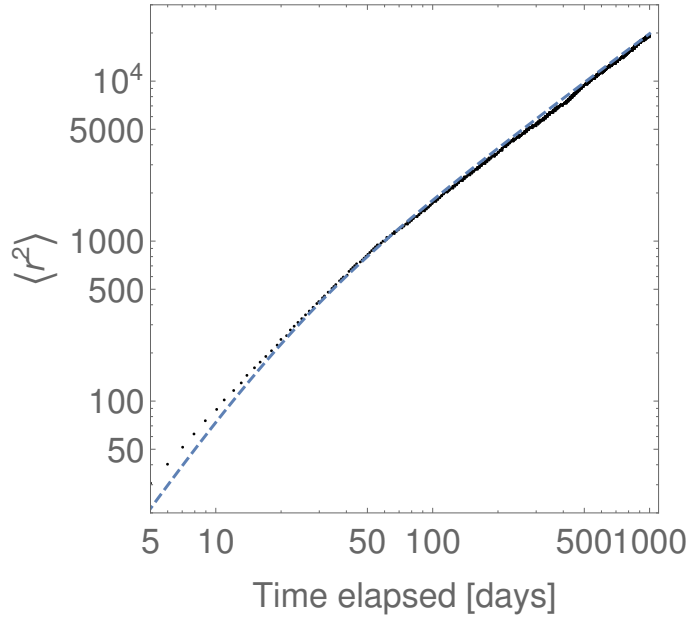


**Figure 2.8** *Plot of the mean square displacement averaged over 1000 replicate simulations of the motion of a single motile cell with the same parameters as above (black dots) compared to the theoretical mean square displacement from equation (2.40) (blue dashed line). Parameter values for both the simulations as theoretical curve were  $V = 10$  sites/day and  $\alpha = 0.1 \text{ day}^{-1}$ . Note the initial quadratic increase followed by a later diffusive tendency.*

It is very tempting to try to interpret this brief acceleration in growth as a period of exponential growth caused by the appearance of secondary lesions as motile cells switch back to  $E$  types and begin dividing again: it certainly seems from figure 2.11 that something like this is occurring. But it is difficult to pick out a clear and definite “exponential growth” regime either on any of the plots exemplified by 2.9 in which a simple proportionality between  $\Delta n/\Delta t$  and  $n$ , or a clear line on a logarithmic plot of  $n$  against elapsed time  $t$  as in 2.10. Although growth definitely seems to be accelerated by migration, as can be seen by increasing  $k_{MET}$  (see figure 2.10), it’s fairly clear from elementary calculus that one can draw a line tangent to any smooth enough curve and measure the gradient, so we should be very cautious before interpreting the rapid growth as “genuinely” exponential.

Nevertheless, for the purposes of comparing how much growth is accelerated by changes in the different microscopic processes, it’s useful to talk about an average growth rate. We find this by fitting a linear function

$$\frac{\Delta n}{\Delta t} = Gn + c \quad (2.41)$$

to data of the instantaneous growth rate  $\Delta n/\Delta t$  against size  $n$  by simple linear regression. The coefficient  $G$  would correspond to the exponential growth rate *if* growth was truly exponential. The use of simple linear regression means that  $G$  will be equal to the mean slope of  $\Delta n/\Delta t$  against  $n$ , so will in some sense be an “average” growth rate regardless of the true form of the growth curve.

Measuring the average growth rate  $G$  for various different values of  $k_{MET}$ ,  $k_{EMT}$ , and  $|\vec{v}|$  for many different replicates revealed several interesting dependencies of  $G$  on each of these variables.

As can be seen from figure 2.12(A), increases in  $k_{EMT}$  correspond to increases in the average

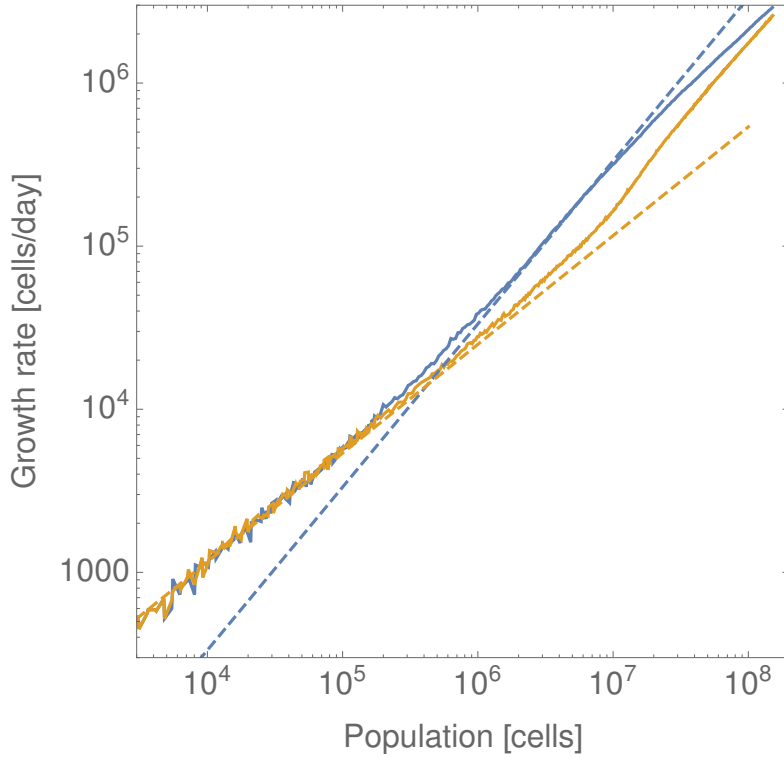


**Figure 2.9** A plot of the instantaneous growth rate (rate of cell division in cells per day) against the tumour size (in cells) for two different values of tumbling rate in the run-and-tumble model,  $\alpha = 0 \text{ day}^{-1}$  in blue and  $\alpha = 0.5 \text{ day}^{-1}$  in yellow. Theoretical relationships for exponential growth (growth rate  $\propto$  size, steep dashed curve) and surface growth (growth rate  $\propto$  size $^{2/3}$ , shallow dashed curve) are plotted for comparison, showing that in both cases surface growth initially dominates, before the tumour grows faster than for a single spheroidal lesion for a short period of time, before slowing down again. It is not clear that the tumour ever grows “truly” exponentially in this model, although growth is faster than for a single spheroid without migration. Other parameter values used were  $k_{EMT} = 10^{-2} \text{ day}^{-1}$ ,  $k_{MET} = 10^{-4} \text{ day}^{-1}$  and  $b = 1.0 \text{ day}^{-1}$ .

growth rate  $G$ . This is not very difficult to understand: from equation (2.8), the proportion of  $M$ -type cells increases with  $k_{EMT}$ . So, as we increase  $k_{EMT}$ , the number of motile  $M$ -cells present also increases, and the rate at which secondary lesions form (see figure 2.11) increases as well.

Somewhat more curious is the particular power-law dependence of  $G$  on  $k_{EMT}$ : approximately of the form  $G \propto k_{EMT}^p$ , with  $p = 0.22$ . Dimensionally,  $G$  and  $k_{EMT}$  are both rates with dimensions of  $[T^{-1}]$ . The parameter  $k_{EMT}$  is theoretically related to the fraction  $P_M$  of motile cells  $M$  (see equation (2.8), also chapter 3),

$$P_M = \frac{k_{EMT}}{k_{EMT} + k_{MET}} . \quad (2.42)$$

which is almost simply proportional to  $k_{EMT}$  when  $k_{EMT} \ll k_{MET}$ . We can hypothesise that the growth rate  $G$  in these cases is therefore empirically related to  $M$  as

$$G \sim b M^p . \quad (2.43)$$

To explain why this should be the case requires a more sophisticated analytical approach, which is

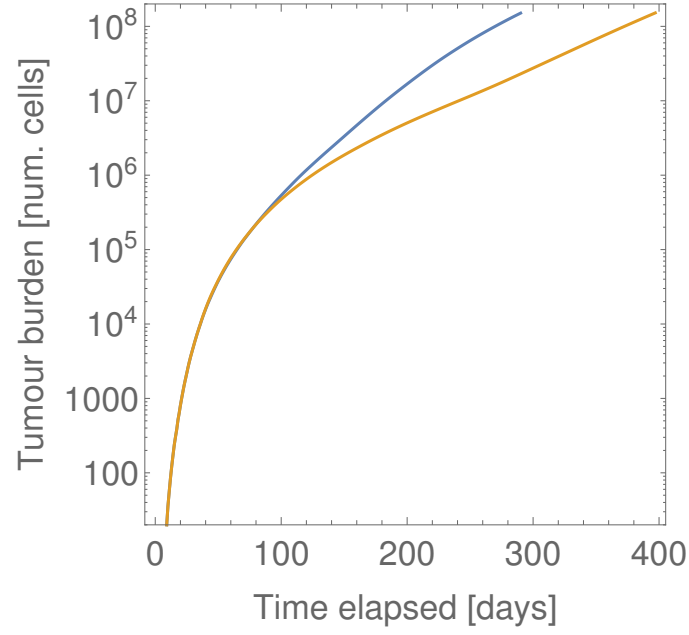


**Figure 2.10** *A figure showing the effect of changes in the mesenchymal-epithelial transition rate  $k_{MET}$  on the growth of the volume of the ensemble over time, in both cases with  $k_{MET} = 0.1 \text{ day}^{-1}$  (blue curve) and  $k_{MET} = 10^{-3} \text{ day}^{-1}$  (lower, yellow curve): initial sub-exponential growth characterised by one primary, followed by a cascade of micro-metastases driving exponential growth, and in the case with  $k_{MET} = 0.1 \text{ day}^{-1}$ , later slow-down and return to sub-exponential growth caused by coalescence of distinct lesions. Other parameters were set to tumbling rate  $\alpha = 0.01 \text{ day}^{-1}$ , rate of EMT  $k_{EMT} = 10^{-4} \text{ day}^{-1}$ , speed  $V = 30 \text{ sites} \cdot \text{day}^{-1}$  and birth rate  $b = 1.0 \text{ day}^{-1}$ .*



**Figure 2.11** *A visualisation of the positions of cells in the ensemble of lesions, showing the emergent cascade of migration and new growths that the model entails. Escaping motile cells can be seen circulating around the larger primary tumour and some of its secondaries. Parameter values used were  $b = 1 \text{ day}^{-1}$ ,  $k_{EMT} = 10^{-4} \text{ day}^{-1}$ ,  $k_{MET} = 10^{-2} \text{ day}^{-1}$ ,  $V = 10 \text{ sites/day}$  and  $\alpha = 0.1 \text{ day}^{-1}$ .*

developed in chapter 3. In a few special cases of related models of migration and growth, explicit analytical formulae for the exponent  $p$  can be derived.

Figure 2.12(B) shows that despite an initial increase when  $k_{MET}$  is small,  $G$  decreases with increasing  $k_{MET}$  once  $k_{MET}$  is higher than about  $1 \text{ day}^{-1}$ , which seems to correspond to the cell division rate  $b$  in the model. The reverse switching rate therefore has two competing effects on  $G$ : increasing the growth rate when small, and decreasing it again when it takes on sufficiently large values. This may be related to the effects that  $k_{MET}$  has on the length of time motile cells remain in the motile phase, and the proportion of all cells that are motile.

Let's remind ourselves that  $k_{MET}$  represents the rate at which motile cells switch back to being non-motile tumour cells. Slower rates  $k_{MET}$  will mean that cells spend longer as type  $M$  before transitioning back to type  $E$ : slower rates therefore induce a delay between becoming motile and switching back. This means that when  $k_{MET}$  is very low, there will be a long delay before cells which escape form new lesions elsewhere: this delay is shorter when  $k_{MET}$  is faster. By decreasing the delay between cells escaping and their founding new lesions, increases in  $k_{MET}$  can accelerate growth.

A countervailing effect is that the proportion  $M$  of cells which will be motile will correspond to  $k_{EMT}/(k_{EMT} + k_{MET})$ , so when  $k_{MET}$  is high,  $M$  will be small (all else being the same). When the reverse switching rate  $k_{MET}$  is much faster than the forward switching rate  $k_{EMT}$ , relatively few cells will be motile, and capable of founding new lesions. By decreasing the relative number of

invasive cells, increases in  $k_{MET}$  can therefore also decelerate growth: there are two countervailing effects from  $k_{MET}$ , as visible in 2.12(B).

The average growth rate seems to be more sensitive to  $k_{EMT}$  than to  $k_{MET}$ : that is, the rate at which cells become motile and escape is more important than the rate at which motile cells revert to tumour cells and form new lesions. In order for cells to be predominantly non-motile, and thus for a very small proportion of cells to be motile, the reverse rate  $k_{MET}$  must be much larger than the forward rate  $k_{EMT}$ . This means cells are removed from the “pool” of circulating motile cells very quickly, after a mean time of around  $k_{MET}^{-1}$ , almost as fast as they can be added to the pool. As a result, the rate at which cells are added to the pool, determined by  $k_{EMT}$ , will be almost the same as the rate at which they are removed from the pool.

The rate at which cells are released from lesions will be proportional to the number of cells on the free surface  $n_{surf}(t)$ , which is in turn determined by the growth of the underlying lesion,

$$J_{\text{release}} = \alpha k_{EMT} n_{surf}(t) \quad (2.44)$$

with  $\alpha$  some factor representing geometrical constraints, as only some fraction of cells will be able to face the right direction to escape. The rate at which motile cells revert back into epithelial-type cells, and in so doing form new tumours, will be proportional to the number of circulating motile cells,  $x$ , and  $k_{MET}$

$$J_{\text{revert}} = k_{MET} x . \quad (2.45)$$

The rate at which new micro-lesions are formed,  $\phi$ , is simply equal to the rate at which motile cells revert,

$$\phi(t) = J_{\text{revert}} = k_{MET} x \quad (2.46)$$

and the dynamics of the population of motile cells will be determined by

$$\dot{x} = J_{\text{release}} - J_{\text{revert}} = \alpha k_{EMT} n_{surf}(t) - k_{MET} x . \quad (2.47)$$

In terms of chemical kinetics, equation (2.47) can be taken to be instantaneously “in equilibrium” if  $k_{MET} x \gg \alpha k_{EMT} n_{surf}$ , and consequently  $\phi \approx \alpha k_{EMT} n_{surf}$ . More rigorously, however, one can show that

$$x(t) = \int_0^t n_{surf}(t - \epsilon) \alpha k_{EMT} e^{-k_{MET} \epsilon} d\epsilon \quad (2.48)$$

solves equation (2.47). Writing  $n_{surf}$  as a Taylor series, one can then find

$$\phi(t) = k_{MET} x(t) = \alpha k_{EMT} \sum_{j=0}^{\infty} \frac{(-1)^j}{k_{MET}^j} n_{surf}^{(j)}(t) = \alpha k_{EMT} n_{surf}(t) - \alpha k_{EMT} \frac{n'_{surf}(t)}{k_{MET}} + \mathcal{O}(k_{MET}^{-1}) \quad (2.49)$$

which shows that the rate at which new lesions can form is proportional to  $k_{EMT}$ , but asymptotically insensitive to  $k_{MET}$ . The effect of changing  $k_{MET}$  is to effectively introduce a delay in  $\phi$  of  $k_{MET}^{-1}$ , which will be as small as  $k_{MET}$  is large: this is consistent with the behaviour

observed in the second run of simulations, in which  $k_{MET}$  only had a strong affect on  $G$  when  $k_{MET}$  was relatively small.

Intuitively, this can be understood as the fact that as  $k_{MET}$  controls the delay between invasive cells' release and their founding of new micro-lesions, slower  $k_{MET}$  rates correspond to longer delays, and exponential growth will take longer to start. This explains how  $\phi$ , the rate at which new secondary tumours are founded, is generally more sensitive to  $k_{EMT}$  than  $k_{MET}$ . As the period of rapid growth is driven by a cascade of secondary micro-metastases,  $\phi$  in turn indirectly determines the growth rate: the exponential growth rate is thus more sensitive to changes in  $k_{EMT}$  in a related way.

A more detailed treatment of how precisely the rate at which new lesions are seeded by older primary tumours  $\phi$  determines the exponential growth rate is developed in chapter 3, but in essence the relationship is determined by the Euler-Lotka equation

$$\int_0^\infty \phi(t)e^{-Gt}dt = 1 \quad (2.50)$$

at the growth rate  $G$ :  $G$  can thus be written as a functional of  $\phi$ , although not usually in terms of elementary functions. One effect that this argument misses out is that at very high rates  $k_{MET}$ , motile cells will only be present for a vanishingly short time, not long enough to actually escape, and therefore above a certain value increases in  $k_{MET}$  can serve to slow growth down rather than accelerate it.

Finally, one can see from figure 2.12 that the average growth rate  $G$  also depends on the speed of migrating cells  $|\vec{v}|$ . We did not expect to find any interesting dependence between the two, and I did not find either an approximate functional form that could convincingly describe the dependency or a convincing simple argument as to why this should be the case. It might be important that since  $\alpha$  was held constant at  $0.01 \text{ day}^{-1}$  in these runs, increasing  $|\vec{v}|$  had the effect of increasing  $L$ : as to *why* this should be important, I am unfortunately at a loss.

An outstanding issue raised by these simulations is if the period of rapid growth enabled by migration that is observed here does indeed correspond to a period of *exponential* growth as such. While the tumours observed here seem to decelerate again after a brief period of faster growth, the strict answer seems to be no: but whether or not some phenomenon of exponential growth of an ensemble of small tumours could somehow *underlie* the acceleration observed here is quite a different question.

For growth to be truly exponential, the additional secondary lesions would have to grow totally independently of one another: in this model, they all grow on the same lattice, finite distances from each other, and may inhibit each others' growth when they coalesce. To answer what would happen if they were truly independent requires another, even more coarse-grained model.

## 2.4 Lattice model with instantaneous migration

Although the lattice model developed in section 2.3 allowed the effect of migration on the growth of tumours consisting of up to  $10^8$  cells to be studied, the results raised a number of questions that simulations of the model were not able to answer. Namely, whether truly exponential growth can be enabled by cell migration. Growth that is confined to a limited region of space, such as the region that can be explored by motile cells in the previous lattice model, or the volume of an isolated tumour or cluster in the Eden model [71], can never be exponential for an arbitrarily long period of time if that region expands slower than exponentially.

For example,  $M$  cells in the previous model can travel at a speed  $|\vec{v}|$ . The largest possible volume

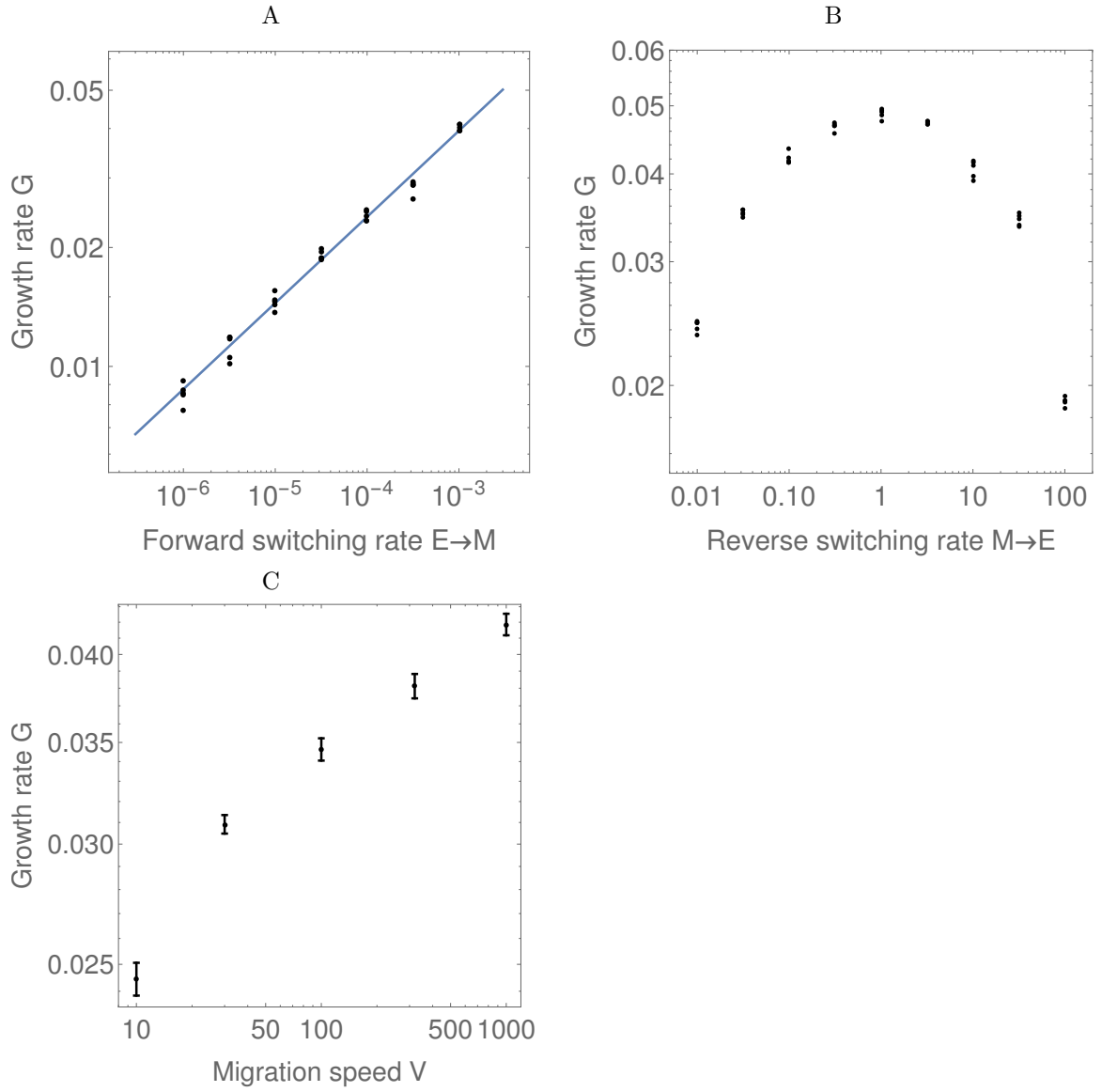


**Figure 2.12** Plots showing the dependence of the average growth rate on (A) the rate of the EMT transition  $k_{EMT}$ , with an approximate power law dependence on  $k_{EMT}$  showing the measured average growth rate with black points and the power-law of best fit in blue,  $G = ck_{EMT}^{0.22}$  (other parameter values were  $k_{MET} = 0.01 \text{ day}^{-1}$ ,  $V = 10 \text{ sites/day}$ , and  $\alpha = 0.01 \text{ day}^{-1}$ ); (B) the rate of the reverse MET transition  $k_{MET}$ , holding  $k_{EMT} = 10^{-4} \text{ day}^{-1}$  (other parameter values were  $V = 10 \text{ sites/day}$  and  $\alpha = 0.01 \text{ day}^{-1}$ ); and (C) the speed of migrating cells  $|\vec{v}|$ , holding  $k_{EMT} = 10^{-4} \text{ day}^{-1}$  and  $k_{MET} = 0.01 \text{ day}^{-1}$ .

that could be explored by a time  $t$  is therefore a sphere (really an octahedron due to lattice anisotropy) of radius  $Vt$ . If this volume is fully occupied by cells, the number of cells  $n$  after a time  $t$  can be at most on the order of  $(Vt)^3$ : really, as the volume will in practice be much emptier than this, this is a large upper bound. No exponential curve can stay under  $\mathcal{O}(t^3)$  for an indefinite period of time, so growth which is confined to a finite region which grows slower than exponentially must also be sub-exponential in the long run.

But what if we don't impose the constraint that the cells have to migrate to some finite distance away? Biologically, of course, bodies and tissues are only so big, but distinct lesions could plausibly be essentially non-interacting. Perhaps they are separated by some glandular structure, separated from each other by tissue in a duct [77].

This motivates a further abstraction to the previous model: to address how the growth of tumours was affected by migration to more distant regions (but still under similar environmental conditions), we developed a lattice model that treated local invasion as an instantaneous event, that founded a new lesion that did not interact with its founder.

### 2.4.1 Algorithm

The cell division dynamics were identical to the previous model. Cells attempt to divide at some rate  $b$ : each time step  $\Delta t$ , with probability  $b\Delta t$ , cells attempt to place a new daughter cell at a randomly chosen neighbouring lattice site. If the neighbouring lattice site is unoccupied then the attempt succeeds, otherwise it fails. Once again, cells were considered neighbours if they were von Neumann neighbours [74].

In contrast to the previous model, cells do not have an explicit phenotype, and migration does not involve the detailed, explicit movement of individual cells through space. New cells on the surface instead have some aggregated overall probability  $M$  to escape immediately after being produced in a replication event, to found a new lesion far removed from the original. These new lesions are indefinitely far away from the lesions that originated them: they do not interact with each other at all, indefinitely prolonging the intermediate phase of exponential growth in the model above.

Only new cells on the surface were capable of escaping and founding new lesions in this way. This is to reflect the fact that in the model developed in section 2.3,  $M$ -cells can only migrate to free lattice sites, so  $M$ -cells which happen to find themselves embedded deep inside a tumour are stuck. Only  $M$ -type cells on the free surface were able to escape.

This model abstracts away the process of phenotypic switching and migration into a one-step process: cells do not have an explicit type, but new cells may escape and form a new, distant lesion instantaneously with probability  $M$  per division. All cells in this model are able to divide and produce new cells, providing there is enough room in their immediate environments: there are no distinct types as such, as the migration process is instantaneous, and as such cells are assumed to spend a vanishingly small time as motile  $M$ -type cells. Each given site in the model may therefore be occupied or unoccupied, but if occupied by a cell does not, as previously, have an explicit type as such.

### 2.4.2 Results

This model shows some clear qualitative resemblances to the previous lattice model: an initial stage of sub-exponential growth in which the original primary tumour dominates the mass of the whole ensemble, and a second later stage in which the secondary and additional metastases permit sustained, exponential growth. The re-coalescence exhibited in the earlier lattice model does not occur simply because the individual micro-metastases in this model are explicitly assumed to be non-interacting: the exponential nature of this latter stage of growth is readily apparent, and

straightforward to measure.

The growth rate  $G$  of these ensembles depends on the probability of migration  $M$ . Furthermore,  $G$  seems to have a power-law-like dependence on  $M$ , so we can hypothesise that

$$G \approx cM^p \quad (2.51)$$

where  $c$  and  $p$  are parameters to be determined.

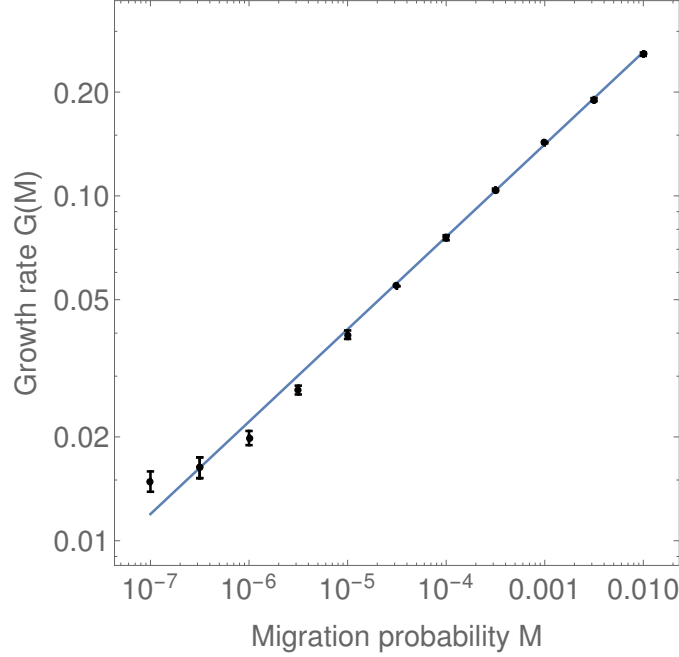


**Figure 2.13** A plot to show the power law dependence of the exponential growth rate  $G$  of an ensemble of metastatic tumours on the migration probability  $M$  for the Eden-like lattice model with instantaneous migration, showing data from simulations (blue points and bars) alongside the curve of best fit,  $G = cM^p$  with  $c = 0.898 \pm 0.007$  and  $p = 0.268 \pm 0.001$ . Parameter values for the simulations were division rate  $b = 1.0 \text{ day}^{-1}$ , death rate  $d = 0$ : there were no other free parameters in this minimalistic model. Finite size effects become visible at the lowest values of  $M$ .

We elaborate on this in more detail in chapter 3, but a qualitative argument as to why this should be the case is due to Prof. M.E. Cates is as follows:

If growth is sustained and exponential, it must be determined by the average frequency with which new micro-metastases occur. If the growth of one lesion follows  $n(t)$ , and any new cell has a probability  $M$  to escape and found a new lesion, the expected number of new lesions by time  $t$  is  $Mn(t)$ . The frequency  $G$  with which new lesions appear will scale as  $G \sim T^{-1}$  with the time  $T$  between these occurring: so  $Mn(G^{-1}) \approx 1$ . For spheroids which expand cubically in time as  $n(t) \propto t^3$ , this implies  $G \propto M^{1/3}$ . Although this argument (and the more detailed analytical models which support it) does not precisely fix the value of the exponent  $p$ , it does demonstrate how the power-law dependence emerges from geometrically constrained growth: other growth curves will presumably entail other dependencies, which will require a more rigorous derivation to characterise (see chapter 3).

The situation in actual simulations is of course a little more complicated: the exponent  $p$  is significantly lower at around  $p = 0.26(6)$ . The underlying reason why this differs from  $1/3$  is surface roughness: only new cells present on the surface are able to escape, so the rate at which

motile cells escape is proportional to the surface area. If the surface is very rough, the number  $n_S$  of cells on the surface will scale approximately as

$$n_S \sim n^q \quad (2.52)$$

with  $q > 2/3$ . Given  $n \propto t^3$ , the expected number of lesions present after a time  $t$  will then be  $\propto \int M n_S dt \propto M t^{3q+1}$ . By similar arguments to above, the growth rate  $G$  should follow

$$G = cM^{\frac{1}{3q+1}} \quad (2.53)$$

with  $2/3 < q < 1$ : the exponent  $p$  should therefore take values in between  $1/4$  and  $1/3$ , consistent with the results of simulations.

An interesting point to note is that the proportion  $M$  of cells that escape to form new micro-lesions is closely related to the frequency of EMT in the previous model. A simple argument inspired by chemical kinetic arguments as to why this should be is that since the reverse rate of switching  $k_{MET} \gg k_{EMT}$ , the rate at which motile cells are released and switch back to non-motile types should be determined by  $k_{EMT} n_{surf}$ , where  $n_{surf}$  is the number of cells on the surface: given that in this set of models, the rate at which new metastases occur will also be proportional to the number of cells on the surface, around  $M b n_{surf}$ .

So, to the extent that  $k_{MET} \gg k_{EMT}$ , we have

$$k_{EMT} n_{surf} \approx M b n_{surf} \quad (2.54)$$

so

$$M \approx k_{EMT} / b. \quad (2.55)$$

There are several things that this crude analysis does not take into account: effects of the finiteness of  $k_{MET}$ , and the delays in founding of new lesions, are two of these. However, the basic conclusions that the speed of cell movement does not strongly affect growth rates, and that  $k_{EMT}$  and  $M$  are the strongest determinants of  $G$  in both models are both supported.

As has already been observed, the growth rate  $G$  has a different dependence on  $M$  in the two models: although a power law provides a decent approximation in both cases, the exponent is not the same. For the model with instant fixation, the exponent is very close to  $1/3$ , whereas in the earlier model with explicit spatial structure and non-instantaneous migration, it was closer to  $0.21(8)^4$ , significantly lower. This may be a finite-size effect: tumour sizes were limited by constraints on computational resources to around  $10^8$ . However, it may also be explained by the occurrence of migration from deep inside solid tumours: the Eden model simulations also showed a considerably lower exponent when cell death and migration occurred throughout the volume of the tumour, and not only at the surface, so it may also be the case that due to roughness and porosity of tumours, cells are able to escape from much deeper into tumours than is immediately obvious.

What is especially interesting about the observed importance of the rates of EMT and MET is that these dynamics have not seen as drastic degrees of simplification as have the mechanics, motility and spatial structure of cells in the course of progressive abstraction from the off-lattice mechanical model up to this point. Although, the description of phenotypic plasticity is already much simplified in the underlying model, and the extent to which this level of simplification is justified is a subject of active research [53].

## 2.5 Concluding remarks

We established that the elastic stiffness of migrating cells could affect the speed with which they can migrate through epithelial monolayers. (see figure 2.4) This is potentially relevant to treatments which target the cell's cytoskeleton, as these may have knock-on effects on the cell's elastic stiffness [4, 49].

We also established that the rates at which cells switched between invasive, mesenchymal types and static, epithelial types controlled how quickly tumours could grow (see figures 2.9). In essence, the forward and reverse rates with which cells switched between the different types controlled how many invasive cells were present, and how long it took them to form new lesions. Furthermore, the growth of tumours was also affected by the speed with which invasive cells move. We have not arrived at a satisfying explanation for this latter observation.

Finally, more coarse-grained simulations supported the idea that exponential growth could be enabled by migration (see figure 2.13). But only as long as this migration resulted in new lesions that were essentially non-interacting, and grew independently of their primaries and of each other. This raised a number of interesting questions about how this exponential growth could be related to how frequently migration occurred which could not be easily answered. To address these, and bridge the gap between abstract microscopic models and macroscopic tumours, we will need to develop new analytical tools.

## Chapter 3

# Structured population models of clonal selection

### 3.1 Introduction

In the previous and following chapters, we explore how lattice models of evolution and invasion in cancer could be used to make predictions about the rate of growth and of the accumulation of advantageous drivers, and also what forms of growth and resistance are observed in clinical settings. In this chapter, we will develop a theoretical approach which makes as few assumptions about the underlying model as necessary, and which enables us to draw connections between the large-scale behaviour of the computational models and the observables of the experimental studies.

The main phenomenon we want to capture here is the feedback between growth and migration that enables metastatic cascades: growing tumours produce new tumours, which begin new growth, and produce more new tumours in an accelerating process.

Computational models have recently been proposed [40, 78, 79] in which cancerous tumours are conglomerates which consist of one large primary tumour with many surrounding microscopic lesions, presumed to form when cancer cells detach from the primary lesion, migrate or are passively advected through intervening tissue, and resume growth at an adjacent site. This process is similar to metastasis - the ability to invade form new micro-lesions elsewhere in the body - which is arguably the defining characteristic of cancer: however, these models [40, 78, 79] are also applicable to short-range invasiveness, perhaps as short as a few micrometers from the edge of the primary lesion. The presence or absence of cancer cells in a narrow region surrounding the primary tumour called the surgical margin has in fact long been used as a predictor of recurrence and indicator of the success or failure of surgical excision of solid tumours, and is a standard histological practice [45, 77].

The movement of cells in these models is usually understood to be caused by cells undergoing epithelial-to-mesenchymal transition and local invasion [80], but may also possibly be due to “sprouting” caused by mechanical instability [58, 81]: nonetheless, the models tend to be neutral as to the precise underlying mechanism. Having left the primary lesion, cells may enjoy better access to nutrients and oxygen and can proliferate faster. The tumour has a complex structure which can enable faster expansion than if it were made of a homogeneous and simple cluster of cells [82, 83].

In this chapter, we study a simplified, mathematical counterpart of the models in previous chapters and [40, 78, 79] which can be solved exactly and used to make predictions about the accumulation of drivers and the growth curves of the conglomerate tumours.

To this end, we will begin by studying a stochastic model which abstracts away the behaviour of individual cells and treats individual micro-lesions as continuous masses, whose growth and dynamics over time are determined by their geometry and size. The underlying growth dynamics is thus deterministic rather than stochastic as in the case of the lattice models, and in this model only migration is a stochastic process. The underlying motivation for this was the hypothesis that migration was relatively rare compared to division and death, otherwise tumours would be rather diffuse.

The entire tumour is modelled as a collections of micro-lesions made of cancer cells. Distinct micro-lesions do not interact with one another: this is key to the analytic solubility of the model. This rather strong assumption could possibly be justified by interpreting micro-lesions as spatially-separated metastases, but even if micro-lesions are fragments of the same primary tumour, numerical simulations indicate that as long as micro-lesions are separated by normal tissue, their growth rate is minimally affected by these interactions, [40], and data from the lattice simulations with detailed cell motility (chapter 2) support the conclusion that interactions only become significant once the tumour has become much larger than the average run distance.

One plausible scenario in which lesions will typically be separated by normal tissue is in the case of ductal carcinomas. In these cases, the primary tumour forms deep within a duct, and secondary tumours in the same gland will tend to be separated by some amount of distorted basement membrane and supporting extracellular matrix (see figure 2.1).

This stochastic model will be compared to an analytical treatment of its average or expected behaviour, and the degree of disagreement quantified and tentatively explained. The expected behaviour will be analysed by means of interpreting the rates of the stochastic model as parameters in a set of differential equations governing a frequency distribution in the number of lesions: the average behaviour thus results in yet another even more abstract model which is entirely deterministic, and which will be shown to be exactly solvable in a few important special cases.

This latter, entirely deterministic model belongs to the class of age-structured population models, which originate from population ecology and epidemiology [84, 85], but which have since also been applied to modelling metastasis in cancer with some degree of empirical success [82, 86].

These two contrasting approaches, the simplified stochastic model and the averaged-out deterministic model, nonetheless both make predictions regarding the total volume of the entire tumour burden, and of the relative frequencies of mutant strains with some increasing relative selective advantages. We will use these two quantities to compare the predictions of the averaged, deterministic model to both the simplified stochastic model with deterministic growth, and later to the fully stochastic lattice models. This is done with a view to gauging the predictive power of the deterministic model, and the various quantities that can be extracted with a few powerful analytical methods, but also to attempt to better understand phenomena which are qualitatively striking in the lattice model: in particular, the possibility of sustained exponential growth of the entire tumour even when individual micro-lesions grow much slower than exponentially, and if this phenomenon depends on the sustained growth of these individual micro-lesions or not.

## 3.2 Stochastic model

Let us begin by recalling some qualitative observations of the previous computational models, which can be easily verified visually (see figure 2.11).

In both the Eden-type lattice model with instantaneous, distant migration, and in the lattice model with local migration, distinct micro-lesions were approximately spherical. The growth of each of these micro-lesions was slower than exponential after an initial burst of fast, well-mixed growth: contact and spatial exclusion of cells meant that only cells near the surface of the spheres could grow, and the spheres' diameters increased linearly in time. This can be expressed equally

accurately by stating that each spheroid expanded with some characteristic speed.

In the local migration model and in the off-lattice mechanical model, some proportion of the cells in any given lesion were motile, and moved with some characteristic speed, in the former case faster than the expansion speed of the lesion they were in. These cells could stochastically switch back to a non-motile type which could divide and produce additional offspring.

In the instant migration model, this corresponded to a process in which any individual cell on the surface could escape and found a new micro-lesion instantaneously, with some probability  $M$  per time step of doing so.

In all models, there was initially only one cancer cell: one cell which had accumulated just enough genetic damage to decisively out-compete surrounding tissue, and to propagate in an uncontrolled manner. This is a well-established hypothesis in the experimental literature.

Finally, in the instant migration model, there was some probability per division that each daughter cell could gain a new mutation. This mutation could either be neutral, or give some advantage to the daughter cells: cells with advantageous mutations could divide faster overall (that is, not necessarily absolutely faster: this could equally result from dying less before having the chance to divide) and would typically form an expanding sector in spheroidal micro-lesions which grew at a faster rate than the surrounding cells without these mutations.

These qualitative observations about the geometry, and the stochastic processes which govern rare but important events in the growth of individual spheroids, can be captured in a simple model.

At any given time, the state of each micro-lesion is fully characterized by two numbers: its age  $a$ , and its sub-line  $n$  which reflects the genetic make-up of the lesion and for simplicity is taken to be equal to the number of driver mutations in the cell which initiated that lesion. This convention doesn't require all micro-lesions to be genetically identical: in fact, we should expect a large number of selectively neutral passenger mutations to be present in all micro-lesions, many of which will be unique to lineages present in single lesions. But as these passenger mutations are selectively neutral, they should not effect the growth dynamics at all, and only the driver mutations should affect growth. We shall study only the case in which the total number of driver mutations affects fitness: more complex functional dependencies are of course possible, but are not our object of study at this early stage.

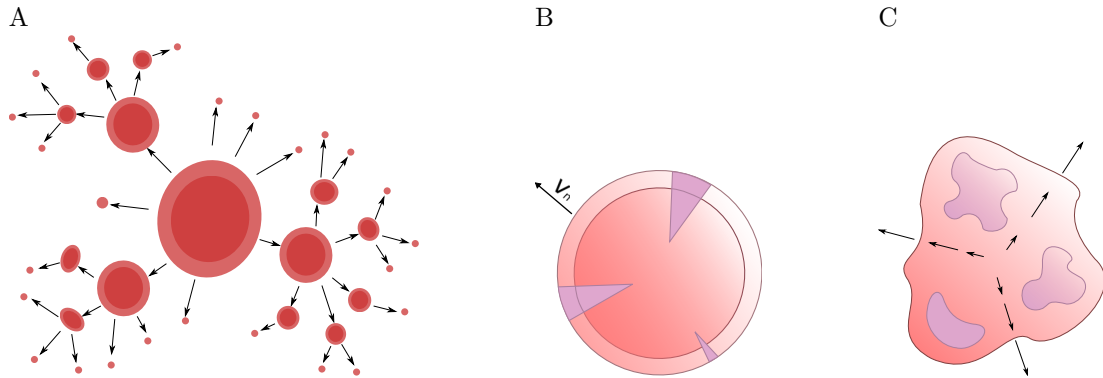


**Figure 3.1** *A: The model assumes that the tumour is made of discrete micro-lesions. Cells migrate from micro-lesions (arrows) and establish new microscopic lesions. All lesions increase in size over time. B,C: two different growth models of individual micro-lesions. In the surface growth model (B), cells replicate only in a narrow layer of constant thickness near the surface, and the radius of the lesion increases with velocity  $v_n$ . In the volumetric growth model (C), replication occurs everywhere and the micro-lesion grows exponentially which causes the whole lesion to “inflate”. Arrows show the expansion velocity which is small close to the centre and increases towards the surface. Purple areas correspond to new mutations.*

In the following, we will also assume that any lesion  $n, a$  contains at most two different genotypes:  $n$  and  $n + 1$ , with relative abundances among those cells that can migrate (a distinction whose relevance which shortly become clear) of  $r_n(a)$  and  $1 - r_n(a)$  respectively. Note that individual cells are not modelled explicitly: only the aggregate behaviour of these microscopic lesions is studied, and these may contain thousands or even millions of individual cells.

The following processes are accounted for:

- Lesions grow in a deterministic way: their volume and area increase with their age (the time since the lesion was founded).
- Cells rarely gain benign mutations: most cells in any given lesion will have the same number of driver mutations as the cell which founded the lesion, and some fraction near the surface have one additional driver.
- Cells escape from the surface of these lesions stochastically: the rate at which new lesions appear is proportional to the area of the lesion they were seeded by.
- All cells in the tumour descend from one originating clone.

In this scheme, the common process of cell division and growth in the underlying models occurs relatively frequently, and is abstracted to a deterministic trend. The rare processes of cell mutation and migration occur much less frequently: although, since mutation has a relatively large effect when it does produce an advantageous strain, this is summarised as a deterministic process by which an increasing proportion of cells escaping from the surface are mutants, and all of the randomness in this model falls into the rate at which migration happens.

These assumptions may be expressed with some convenient notation:

- *Growth.* Lesions' growth is determined by the number of driver mutations in the founding cell,  $n$ , and their age,  $a$ : their volume is denoted  $V_n(a)$ , their surface area  $S_n(a)$ , and their radius  $\rho_n(a)$  increases as  $\rho_n(a) = v_n a$ . The spatial character of the model manifests itself in our choice of these functions:  $V_n(a)$  is very different for three-dimensional, spatially constrained growth in which replication can occur only on the surface of growing spheroids, than it is for "well-mixed" growth in which growth may occur throughout the entire volume and all cells may replicate with identical rates.
- *Driver accumulation.* New lesions of type  $n$  are produced by other lesions: lesions of type  $n$  and age  $a$  produce micro-lesions of the same type with probability  $r_n(a)$ , and lesions of type  $n + 1$  with probability  $1 - r_n(a)$ .
- *Migration.* The production of new lesions via the escape and re-settlement of tumour cells occurs in a inhomogeneous Poisson process. The rate with which new lesions of either type are produced by a lesion of type  $n$  and age  $a$  may be denoted  $\phi_n(a)$ , and is proportional to the instantaneous rate of growth of these lesions,  $\phi_n \propto \dot{V}_n$ .
- *Initial conditions.* There is initially one lesion of type  $n = 1$  and age  $a = 0$ .

We will later examine other forms of growth than expanding spheres, such as plateaus or well-mixed exponential ("volumetric") growth.

The precise fitness landscape, and what advantage is actually imparted by each additional driver, is a matter of what the precise form each of these functions takes: in particular, if the advantage manifests through a more rapid net growth rate, through the form of  $v_n$ .

By "fitness", we mean

$$s = \frac{b_{n+1}}{b_n} - 1 \quad (3.1)$$

with  $s$  the relative advantage imparted by the  $n + 1^{\text{th}}$  driver over the  $n^{\text{th}}$ .

Several such landscapes may be investigated: of particular interest are landscapes with a continuous increase in fitness, in which one expects to see straightforward selection for fitter drivers, and landscapes in which only a few specific drivers carry a substantial advantage.

Two distinct possibilities for the case in which additional drivers monotonically increase fitness are the case in which  $v_n$  increases exponentially with  $n$  (i.e. having a constant relative advantage) and the case in which  $v_n$  increases linearly in  $n$  (i.e. having a diminishing relative advantage) [18, 41].

There are many imaginable cases in which only the first few drivers after tumorigenesis increase fitness and growth rate further, as might be expected if tumours have already accumulated sufficient mutations to out-compete surrounding normal tissue, but there are still remaining opportunities for further adaptation, such as to new environmental niches in the body, or to adverse conditions (such as therapy). For simplicity, we will investigate here the cases in which only the first two additional drivers increased  $v_n$  substantially, in our cases by increasing it rapidly and linearly at first, and any additional drivers after these impart only a small advantage.

### 3.2.1 Basic algorithm

In the following, we will use  $n$  to index the number of driver mutations present instead of the population of cells in the tumour or lesion. The size of the tumour will be expressed in terms of its volume,  $V_{\text{tot}}$ .

The rules of the model can be straightforwardly simulated once  $v_n$  and corresponding parameter values are specified.

The basic algorithm is as follows:

1. One tumour with  $\rho = 0$  and  $n = 1$  is initialised: this is stored in a data structure *lesions* with all other tumours and micro-lesions.
2. Each time step: every tumour in *lesions* grows, its radius  $\rho$  is incremented by  $v_n dt$ . Its area  $S_n$  and fraction of mutants on the surface  $1 - r_n$  are recalculated.
3. The number of escaping cells both of type  $n$  and  $n + 1$  are calculated. These are both Poisson-distributed random variables  $dN_n$  and  $dN_{n+1}$  with means  $r_n \phi_n dt = M r_n v_n S_n dt$  and  $(1 - r_n) \phi_n = M(1 - r_n) v_n S_n dt$  respectively. After these Poisson-distributed random variables are calculated,  $dN_n$  and  $dN_{n+1}$  new lesions are initialised with  $\rho = 0$  of types  $n$  and  $n + 1$  respectively.
4. Time advances by  $dt$ .

The total volume of all tumours, the volume of tumours of each type, and the average number of drivers present in the entire ensemble may then be calculated and recorded.

The following forms were assumed for the geometry, migration rate  $\phi_n$ , the expansion speed  $v_n$  and the non-mutant surface function  $r_n$  as functions of age  $a$ :

- A tumour is a sphere with radius  $\rho = v_n a$ . Consequently, the surface area  $S_n = 4\pi v_n^2 a^2$ , and the volume  $V_n = 4\pi v_n^3 a^3 / 3$ .

- New lesions are established with rate  $\phi_n = 4\pi M v_n^3 a^2$ . Of these,  $r_n = \exp(-\mu a)$  are of type  $n$ , the same as the originating lesion, and  $1 - r_n = 1 - \exp(-\mu a)$  are of type  $n + 1$ , carrying one additional driver mutation.
- Only the first three driver mutations carried a substantial selective advantage. As such,  $v_n = n v_1$  for  $n \leq 3$ , and  $v_n = 3 v_3 + (n - 3) \epsilon v_3$  for  $n > 3$ .

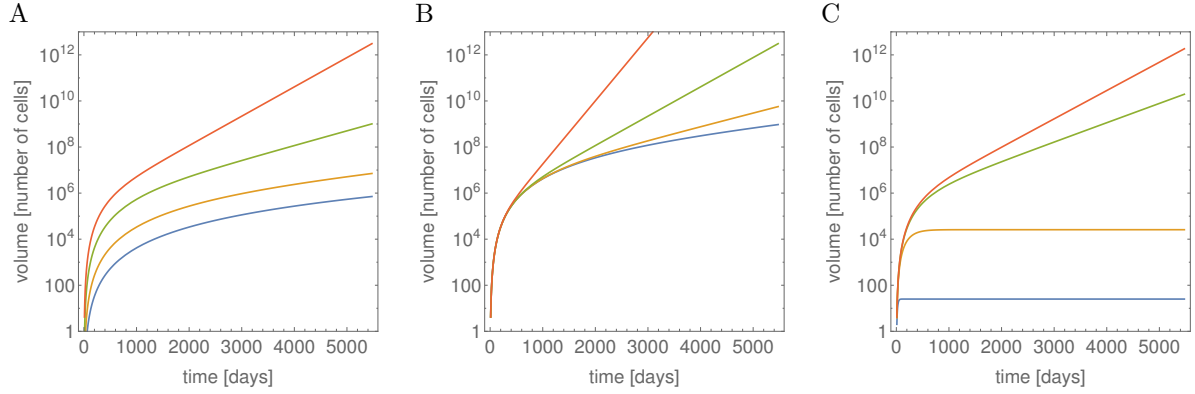


**Figure 3.2** *A: total tumour volume  $V_{\text{tot}}(t)$  versus time for different single-lesion expansion velocities  $v = 0.01$  (blue),  $v = 0.02$  (yellow),  $v = 0.05$  (green) and  $v = 0.1$  (red), and the same migration probability  $M = 10^{-6}$ . B:  $V_{\text{tot}}(t)$  for  $v = 0.1$  and four different  $M = 10^{-8}, 10^{-7}, 10^{-6}, 10^{-5}$  (blue, yellow, green and red, respectively). C:  $V_{\text{tot}}(t)$  for the slow-down model,  $M = 10^{-6}$ ,  $v = 0.1$  and four different  $\lambda = 0.1, 0.01, 10^{-3}, 10^{-4}$  (blue, yellow, green and red).*

Some basic phenomena are readily apparent from figure 3.2: in simulations with no mutation (and only one driver, the first), after an initial phase of growth in which metastases and new micro-lesions are infrequent and the primary lesion forms most of the mass of the tumour, the cloud of micro-metastases increases in frequency and mass exponentially, despite the sub-exponential growth of individual lesions. With some mutation rate incorporated via  $r_n(a) = \exp(-\mu a)$ , this exponential growth is accelerated to super-exponential, driven by an exponential accumulation of driver mutations.

An extended discussion of these phenomena, an analytical theory of what determines them, and a detailed comparison of the two can be found in section 3.4.1.

The questions that our analytical theory has to address are several: how can the growth of the ensemble be exponential whilst the growth of individual components is considerably slower? What determines the precise form of the accumulation of driver mutations? Can these be related to quantitative determinants of the microscopic behaviour?

The cumulative frequency distribution of the resulting lesions' ages can also be calculated: by this, we understand the number of lesions of a given type  $n$  which are younger than a certain age  $a$ . An empirical cumulative age distribution can be calculated in any given realisation of the model, and the proportion of cells younger than a given age will clearly increase with age: this distribution, denoted  $\text{CDF}_n(a, t)$ , is simply the number of lesions which are younger than  $a$ , and will therefore start from zero

$$\text{CDF}_n(a, t) = 0 \parallel a \leq 0 \quad (3.2)$$

since there are no lesions with negative age, and will flatten out at the total number of type- $n$  lesions present at any given time,  $N_n$ ,

$$\text{CDF}_n(a, t) = N_n \parallel a > t \quad (3.3)$$

since there are no lesions older than the oldest lesion, whose age is always equal to the total elapsed time.

This is primarily an auxiliary quantity: useful in order to define other distributions. It is nonetheless relatively easy to calculate for both this stochastic model and other analytical models we will later analyse, and as such provides a way to compare the two approaches meaningfully.

### 3.3 Analytical methods

#### 3.3.1 Definitions and exact results

The mean behaviour of the stochastic model can be readily analysed in terms of the expected distribution of the number of lesions of a given type and age: by “mean” and “expected” in the following, we understand these means and expectations to be over realisations of the underlying stochastic process. A smooth, expected distribution can be given which is governed by a system of differential equations in age and time.

The stochastic process of escape and self-metastasis is replaced with a deterministic drift term, with a rate equal to the rate of the underlying Poisson process. The average number of new metastases to appear stochastically in a short interval will consequently agree with the number (or weight) of new metastases that appear in the model of the lesion size distribution. Since this process accounts for all stochasticity in the underlying model, the evolution of the expected lesion size distribution is purely deterministic.

It is important to note that the underlying model, as well as most simulations of the lattice models, exhibits exponential growth enabled by the migration of escaping cells. It is therefore reasonable to expect to observe exponential growth.

The dynamics of the model can be expressed in terms of the distribution of lesions’ ages and types  $n$ : in this deterministic model, the cumulative distribution of lesion ages and types will be expected to have a smooth, analytic appearance rather than a jagged and noisy appearance, but will nonetheless follow the same obvious tendency of increasing from zero to the total number of lesions  $N_n$  of type  $n$  at a given time.

From this function, one can define an age distribution function as the density or mass function corresponding to  $\text{CDF}_n$ :

$$f_n(a, t) = \partial_a \text{CDF}_n(a, t) \quad (3.4)$$

which, as lesions are assumed to grow deterministically and are not removed, will evolve in a very simple manner for  $a \neq 0, t \neq 0$

$$\partial_t f_n(a, t) + \partial_a f_n(a, t) = 0, \quad (3.5)$$

so that if we wait for any time interval  $\epsilon$ , the distribution  $f_n$  will “age” to  $f_n(a, t + \epsilon) = f_n(a - \epsilon, t)$ . This ageing process corresponds to the underlying growth dynamics of each individual tumour, and given the function  $V_n(a)$  the total size can be calculated to be

$$V_n(t) = \int_0^\infty V_n(a) f_n(a, t) da . \quad (3.6)$$

The processes of local invasion and self-metastatic seeding corresponding to migration and driver accumulation are represented as a boundary condition

$$f_n(0, t) = \int_0^\infty [r_n(a) \phi_n(a) f_n(a, t) + (1 - r_{n-1}(a)) \phi_{n-1}(a) f_{n-1}(a, t)] da \quad (3.7)$$

for  $n > 1$ , which represents the production of new lesions of type  $n$  from both other type  $n$  lesions (first term in integral) and from mutations in type- $n - 1$  lesions (second term in integral). Since we start numbering lesions at  $n = 1$  in this model, there are no lesions of type 0, and the equivalent of equation (3.7) is just

$$f_1(0, t) = \int_0^\infty r_1(a) \phi_1(a) f_1(a, t) da . \quad (3.8)$$

The initial condition that there is one micro-lesion of type- $n$  and age  $a = 0$  is simply

$$f_n(a, 0) = \delta_{n,1} \delta(a) . \quad (3.9)$$

The growth of individual lesions over time, encoded in the functions  $V_n(a)$  and  $S_n(a)$ , do not directly appear in these equations, which are expressed entirely in terms of time and lesion age, is nonetheless implicitly present. The rate of metastasis  $\phi_n(a)$  is directly proportional to  $S_n(a)$ , as before,

$$\phi_n(a) = M v_n S_n(a), \quad (3.10)$$

and the volume of individual tumours appears both in expressions for the total volume of tumours of type- $n$ ,

$$V_{\text{tot},n} = \int_0^\infty f_n(a, t) V_n(a) da ; \quad (3.11)$$

for the total volume of the tumour,

$$V_{\text{tot}} = \sum_n V_{\text{tot},n} = \sum_n \int_0^\infty f_n(a, t) V_n(a) da ; \quad (3.12)$$

and for the average number of drivers per cell,

$$\langle n(t) \rangle = \frac{1}{V_{\text{tot}}(t)} \sum_{n=1}^\infty n \int_0^\infty f_n(a, t) V_n(a) da . \quad (3.13)$$

Despite the generality of the equations (3.5) and (3.7), the infinite genome approximation enforces a strict hierarchical structure on them: lesions of type  $n$  can only produce micro-lesions of type  $n + 1$ , never the reverse [87]. In addition to this — crucially — the growth of individual lesions is assumed to be independent. These two properties of the underlying stochastic model carry

over into equations equation (3.5)-equation (3.8), ensuring that they are linear in age and time, and that they form a strict hierarchy which can be closed once we solve for the type-1 lesion size distribution  $f_1(a, t)$ . This last case should be possible as no other distribution  $f_n$  should appear in equation (3.8).

### 3.3.2 Only one driver

Since only  $f_1$  appears in equation (3.8), it is essential to analyse the case in which there is only one strain, with no mutations. Without loss of generality, let us take  $r_n = 1$  at all ages  $a$ . Three special cases will be considered after the general formal solution is found.

In this case, the governing equations reduce to McKendrick-von Foerster equation without removal [85],

$$\partial_t f_1(a, t) + \partial_a f_1(a, t) = 0 \quad (3.14)$$

$$f_1(0, t) = \int_0^\infty \phi_1(a) f_1(a, t) da \quad (3.15)$$

for  $t \neq a$ , and  $f_1(a, 0) = \delta(a)$ .

This set of equations are better known as the McKendrick-von Foerster, or age-structured population equations, well-known in demography, epidemiology, and mathematical ecology: here, the ages do not correspond to individual organisms, but rather to individual cancerous micro-lesions in a diffuse cancerous tumour composed of a conglomerate of such micro-lesions.

The first equation, equation (3.14), implies that  $f_1(a, t)$  can be written as a simpler function

$$f_1(a, t) = F_1(t - a) \quad (3.16)$$

which should consist of some smooth part, corresponding to a diffuse mass of secondary and tertiary micro-lesions (and so on), and a non-smooth Dirac delta corresponding to the presence of the initial, primary lesion,

$$F_1(t - a) = F_1^{\text{sm.}}(t - a)\Theta(t - a) + \delta(t - a) \quad (3.17)$$

with  $F_1^{\text{sm.}}$  the smooth part of  $F_1$ . This means that the Laplace transforms of  $F_1$  and  $F_1^{\text{sm.}}$  are related by

$$\tilde{F}_1 = \tilde{F}_1^{\text{sm.}} + 1. \quad (3.18)$$

Since at  $t > 0$ , the non-smooth part of  $F_1$  will drop out of the left side of equation (3.15), it can then be written

$$F_1^{\text{sm.}}(t) = \int_0^t \phi_1(a)(F_1^{\text{sm.}}(t - a) + \delta(t - a))da. \quad (3.19)$$

This equation may be Laplace-transformed in time to yield

$$\tilde{F}_1^{\text{sm.}}(s) = \frac{\tilde{\phi}_1(s)}{1 - \tilde{\phi}_1(s)} \quad (3.20)$$

so that (3.18) implies

$$\tilde{F}_1(s) = \frac{\tilde{\phi}_1(s)}{1 - \tilde{\phi}_1(s)} + 1 = \frac{1}{1 - \tilde{\phi}_1(s)} . \quad (3.21)$$

Providing that the shedding rate  $\phi_1(a)$  has a sufficiently tractable Laplace transform (that is, meromorphic in  $s$ ), the lesion age distribution  $F_1(a, t)$  can be given explicitly, not merely as a formal exact solution. This is the case for several important special cases that will be discussed shortly.

However, even if the full distribution cannot be obtained this way, Eq. equation (3.21) can still provide us with a means to infer qualitative insight into the large- $t$  behaviour of  $f_1(a, t)$ . Note that  $\tilde{F}_1(s)$  in the general solution equation (3.21) becomes singular wherever  $\tilde{\phi}_1(s) = 1$ : near any of the roots of this equation, which can equivalently be written

$$\int_0^\infty \phi_1(a) e^{-Ga} da = 1 , \quad (3.22)$$

the Laplace transform of the distribution has a pole, and goes as  $\tilde{F}_1 \sim 1/(s - G)$ . The inverse of this Laplace transform will therefore be of the form

$$F_1(t - a) \propto \exp(G(t - a)) + \dots \quad (3.23)$$

and contain as many exponential terms as there are distinct poles of  $\tilde{F}_1(s)$ : or equivalently, roots of equation (3.22).

Not only should exponential growth be a *generic* feature – one which is enabled by migration regardless of the specific form of the seeding rate  $\phi_1(a)$  or even the lesion volume  $V_1(a)$  – equation (3.22) provides a direct link between the rate at which new lesions are seeded and the growth rate of the ensemble. This could also go a long way to explaining why so many of the underlying models showed a sudden, qualitative change to their growth curves once any model of migration was incorporated. This is a really remarkable result!

Equation (3.22) is better known as the Euler-Lotka equation [84, 85], previously discovered by both Euler and Alfredo Lotka in the context of quite different of ecological models, and has been independently rediscovered a number of times [36]. The importance of this remarkable result is that it shows how populations and ensembles of individuals can grow exponentially even while individuals themselves grow much slower than exponentially (or not at all), and enables the growth rate of the population as a whole to be determined in terms of the mean rates at which new individuals (in our case, new micro-lesions) are created.

This result is so useful that its generalization in section 3.3.3 and related techniques is very much the keystone for all subsequent mathematical results in this chapter.

If one can think of the Laplace transform as being, roughly speaking, the representation of a function in terms of frequency rather than time or space, this growth rate can be thought of as the average *frequency* with which new micro-lesions appear.

Alternatively, as  $\phi_n$  represents the rate of a stochastic process, the Laplace transform of this rate gives the number of expected events at a given frequency. If the number of expected events at

the growth rate  $G$  is 1, then this equation can also be interpreted as telling us that the growth rate of a population corresponds to how often one individual in the population produces one more individual in the population.

This is a process of positive feedback: larger, mature lesions produce new, small lesions, which in turn grow into larger, mature lesions and go through a similar process again. The overall mechanism is very similar to the growth of animal populations, or the spread of infectious diseases, in the context of which closely related models have been proposed [84].

The total number of lesions  $N_1(t)$  and the total volume of these lesions  $V_{\text{tot}}(t)$  also show very similar behaviour:

$$N_1(t) = \int_0^\infty f(a, t) da \propto e^{Gt} \quad (3.24)$$

and

$$V_{\text{tot}}(t) = \int_0^\infty f(a, t) V(a) da \propto e^{Gt} . \quad (3.25)$$

We can now use these general results to investigate three special cases of the growth of individual tumours and the effect of these variations on the growth of the ensemble of tumours.

### 3.3.2.1 Surface growth

As before, we assume that micro-lesions are spherically symmetric, and that all growth can occur only on the surface. The centre of the lesion is static in this case: it does not contribute to growth at all.

Let the volume of the lesion increase as it grows as

$$V(a) = \frac{4\pi}{3} (v_1 a)^3 \quad (3.26)$$

where  $v_1$  is the speed with which the radius of this lesion expands in time. The rate of migration  $\phi_1$  should, as before, be proportional to the surface area,

$$\phi_1(a) = M v_1 (4\pi v_1^2 a^2) = 4\pi M v_1^3 a^2 \quad (3.27)$$

The above method for deriving exact, formal solutions can be applied here, yielding

$$\tilde{F}_1(s) = \frac{s^3}{s^3 - 8\pi M v_1^3} \quad (3.28)$$

which can be inverted using Mellin's inverse formula

$$F_1(z) = \mathcal{L}^{-1}\{\tilde{F}_1\} = \frac{1}{2\pi i} \oint_\Gamma e^{sz} \tilde{F}_1(s) ds , \quad (3.29)$$

where the contour  $\Gamma$  encircles all poles of  $\tilde{F}_1(s)$  anticlockwise. The residue theorem then yields

$$F_1(z) = \delta(z) + \frac{1}{3}Ge^{-\frac{Gz}{2}} \left[ e^{\frac{3Gz}{2}} - \sqrt{3} \sin\left(\frac{\sqrt{3}}{2}Gz\right) - \cos\left(\frac{\sqrt{3}}{2}Gz\right) \right] \Theta(z) \quad (3.30)$$

where

$$G = 2\pi^{1/3}M^{1/3}v \quad (3.31)$$

from equation (3.22).

This allows expressions for the total number  $N(t)$  and volume  $V_1(t)$  to be derived by substituting equation (3.30) and equation (3.26) into equation (3.12) and equation (3.13),

$$N(t) = \int_0^t F(t-a)da = \frac{1}{3} \left[ e^{Gt} + 2e^{-\frac{Gt}{2}} \cos\left(\frac{\sqrt{3}}{2}Gt\right) \right] \quad (3.32)$$

and

$$V_{tot}(t) = \frac{1}{3M}e^{Gt} + \frac{2}{3M}e^{-\frac{Gt}{2}} \cos\left(\frac{\sqrt{3}}{2}Gt\right) - \frac{1}{M}. \quad (3.33)$$

both of which increase exponentially in time after an initial period during which the growth predominantly consists of the originating primary tumour.

For the tumour to grow to a size typical of those that have been detected and warrant treatment, say  $10\text{cm}^3 - 100\text{cm}^3$  after a long period of progression prior to intervention of 15 years,  $V_{tot}$  should be  $10^{11} - 10^{12}$  cells, and it follows that  $M$  and  $v$  must be sufficiently large. However,  $M$  and  $v$  only have to be  $10^{-6}$  and 0.1 cells/day respectively for the tumour burden to reach macroscopic sizes and continue to expand exponentially in this time frame.

However, individual spheroidal lesions can't be expected to expand indefinitely: there are a number of factors which act to constrain their growth, such as limited diffusion and availability of oxygen and glucose, or mechanical pressure from surrounding tissue. As a result, many tumours never reach clinically detectable sizes, and can remain undetected and asymptomatic for many years [88, 89].

### 3.3.2.2 Surface growth with slow-down

As a simple but somewhat artificial case, consider a scenario in which the volume undergoes an initial burst of growth before slowing down. One model which will show this behaviour, but which will also bear a close resemblance to the case we previously studied, is if the volume follows

$$\dot{V}(a) = 4\pi v^3 a^2 e^{-\lambda a} \quad (3.34)$$

where  $\lambda > 0$  is the time-scale after which the growth rate decreases. Consequently,

$$V(a) = \frac{8\pi v^3}{\lambda^3} \left( 1 - \left( 1 + \lambda a + \frac{(\lambda a)^2}{2} \right) e^{-\lambda a} \right). \quad (3.35)$$

At first glance, this does not look like it generalises equation (3.26). But it can be verified by performing a Taylor expansion of equation (3.35) that it is in fact cubic in age  $a$  to leading order, as is equation (3.26).

This function has a sigmoidal shape, and saturates at the volume  $V(\infty) = 8\pi v^3 \lambda^3$ . Finally, if we also assume that the rate of migration  $\phi$  also declines exponentially after the same characteristic time-scale, so that

$$\phi(a) = 4\pi M v^3 a^2 e^{-\lambda a} \quad (3.36)$$

one can easily see that these formulas reduce to equations equation (3.27) for  $\lambda = 0$ .  $\tilde{F}_1(s)$  is easily calculated through the above method to be

$$\tilde{F}_1(s) = \frac{(s + \lambda)^3}{(s + \lambda)^3 - 8\pi M v^3} \quad (3.37)$$

which corresponds to

$$F_1(z) = \delta(z) + \frac{G + 3\lambda}{3} e^{-\frac{G+\lambda}{2}z} \left[ e^{\frac{3(G+\lambda)}{2}z} - \sqrt{3} \sin\left(\frac{\sqrt{3}}{2}(G + \lambda)z\right) - \cos\left(\frac{\sqrt{3}}{2}(G + \lambda)z\right) \right] \Theta(z) \quad (3.38)$$

where  $z = t - a$ , and

$$G = 2\pi^{1/3} M^{1/3} v - \lambda \quad (3.39)$$

which corresponds to the long-term exponential growth or decline rate of the tumour.

### 3.3.2.3 Volumetric growth

Finally, one can consider the almost trivial case in which all cells from the lesion are able to replicate and migrate, not only those on the surface, and that all lesions increase in size exponentially. If the rate with which calls replicate is  $b$  and the rate at which they migrate is  $m$ , then

$$V(a) = \exp[(b - m)a] \quad (3.40)$$

$$\phi(a) = mV(a) \quad (3.41)$$

and as might be expected, the ensemble of all micro-lesions comprising the tumour grows exponentially in time with rate

$$G = b. \quad (3.42)$$

### 3.3.3 Multiple driver mutations

These results can be extended in a more-or-less straightforward manner to the case in which there are arbitrarily many cell lines, denoted by the number of drivers in their founding clone,  $n$ . The underlying reason for the ease of this extension is the conjunction of two assumptions regarding growth and mutation: that individual lesions do not affect one another's growth, and that mutation is an essentially irreversible event. The latter assumption is reasonably uncontroversial, although as previously discussed there are several important criticisms that can be made of the former, and several justifications of it.

The key additional ingredient in the mix in the case of many driver mutations is, of course, the mutant surface fraction  $1 - r_n$ . Some obvious constraints can be put on it: there should initially be no mutants on the surface at all, so  $r_n(0) = 1$ , and since the new mutant strains we are interested in carry active, driver mutations, they will eventually take over the lesion in which they appear, so  $\lim_{a \rightarrow \infty} (r_n) = 0$ . Beyond this, there are no specific forms which appear especially likely for all models *a priori*, and no specific forms suggested by experiment at this time, as the dynamics of the emergence and expansion of driver mutations and their sub-lines within tumours is as extremely difficult object of study at present given that there are few ways to identify specific driver mutations and their frequencies within actual tumours.

Nonetheless, several forms of  $r_n$  can be investigated that do show some reasonable decline, with determining parameters which can be tentatively connected to experimental observables for individual cells, but which can nonetheless be used for tractable mathematical calculations due to their simple form. This will be the case for any form of  $r_n$  which falls off exponentially in lesion age or faster.

For most of the following results and analysis, we will use an exponentially decreasing surface fraction

$$r_n(a) = \exp(-\mu a) \quad (3.43)$$

because it declines sufficiently quickly and has a simple Laplace transform that is easily invertible (roughly speaking, meromorphic). There are a few possible physiological and geometrical justifications that can be made for this choice, but it is primarily for convenience.

This form for  $r_n(a)$  be rationalized by assuming that cells on the surface of the lesion with  $n + 1$  drivers appear with some small rate  $\mu$  and that their selective advantage can be neglected, so that the dynamics is effectively neutral and dominated by drift and geometrical effects. A mutant sector that arose at time  $a_0$  will then have on the order of  $(a/a_0)^2$  cells on the surface, and the fraction of mutant cells  $1 - r_n(a)$  then obeys

$$\frac{\int_0^a 4\pi a_0^2 \mu r_n(a_0) (a/a_0)^2 da_0}{4\pi a^2} = 1 - r_n(a) \quad (3.44)$$

which given  $r_n(0) = 1$ , implies that  $r_n(a) = \exp(-\mu a)$ .

Other than affecting  $r_n$ , a problem which we will revisit later, the effect of these driver mutations will be encapsulated by specifying  $v_n$ , the expansion speed of lesions with  $n$  drivers. We will investigate several such cases: a continuous, steady increase in fitness, consisting of linear and exponential increases of  $v_n$  with  $n$ , and the case in which only a few additional mutations  $n$  carry substantial advantages, after which their effect is small.

However, for the assumed  $v_n = nv_1$ , the selective advantage carried by novel driver mutations is  $(n + 1)/n - 1 = 1/n > 0$  and the assumption that population dynamics are mostly neutral is explicitly not true for small  $n$ . The dynamics of non-neutral mutant sectors in spatial models is

complex [41, 90] and leads to formulae for  $\phi_n r_n$  whose Laplace transforms are not analytically tractable. We will therefore use the simpler and admittedly less realistic formula for now.

The effect of these driver mutations should in general be to accelerate the expansion of lesions: lesions with additional advantageous mutations should obviously grow faster than lesions without, at least under conditions in which these mutations are advantageous. We will not consider the accumulation of mutations which are ordinarily not advantageous but become so under certain conditions: that is, mutations which confer some resistance to specific therapies but which otherwise slow down cell division or obstruct cell survival before a cell has a chance to divide. Under the conditions of long, steady growth prior to discovery and clinical intervention, these mutations can only accumulate by genetic drift, rather than by clonal selection, and this stochastic process is not what we are interested in studying.

The effect of each new driver mutation is therefore assumed to be an increase in the expansion speed of the micro-lesion in which it is present. The main motivation for this is that replication and death should balance exactly in normal tissue in the absence of wounds and suchlike in order to maintain homeostasis. A driver mutation increases the rate of cell division, or decreases the rate of cell death, and hence the growth rate becomes more positive [32]. In the case of lesions which can grow only on their surfaces due to inefficient perfusion or spatial constraints this is assumed to translate into a change in the radial expansion rate  $v_n$ .

Let us recall equation (3.5)

$$\partial_t f_n(a, t) + \partial_a f_n(a, t) = 0, \quad (3.45)$$

and its boundary conditions

$$f_n(0, t) = \int_0^\infty [(r_n(a)\phi_n(a))f_n(a, t) + (1 - r_{n-1}(a))\phi_{n-1}(a)f_{n-1}(a, t)] da \quad (3.46)$$

for  $n > 1$ , and

$$f_1(0, t) = \int_0^\infty r_1(a)\phi_1(a)f_1(a, t)da \quad (3.47)$$

for  $n = 1$ , and

$$f_n(a, 0) = \delta_{n,1}\delta(a). \quad (3.48)$$

The method for solving these in full generality follows that for the case in which there is only one strain quite closely: in particular, the solution for  $f_1$  is formally identical,

$$\tilde{F}_1(s) = \frac{1}{1 - \mathcal{L}[r_1\phi_1](s)} \quad (3.49)$$

Equation (3.5) implies that  $f_n$  can be written

$$f_n(a, t) = F_n(t - a) \quad (3.50)$$

for some  $F_n$  to be determined. The Laplace transform of the corresponding boundary condition then reads

$$\tilde{F}_n(s) = \mathcal{L}[r_n \phi_n](s) \tilde{F}_n(s) + \mathcal{L}[(1 - r_{n-1}) \phi_{n-1}](s) \tilde{F}_{n-1}(s) \quad (3.51)$$

for  $n > 1$ , or

$$\tilde{F}_n(s) = \frac{\mathcal{L}[(1 - r_{n-1}) \phi_{n-1}](s)}{1 - \mathcal{L}[r_n \phi_n](s)} \tilde{F}_{n-1} \quad (3.52)$$

from which one can determine  $\tilde{F}_n$  for arbitrary  $n$  recursively, given that  $\tilde{F}_1$  is known, closing the hierarchy.

Explicitly,

$$\tilde{F}_n(s) = \frac{1}{1 - \mathcal{L}[r_1 \phi_1](s)} \prod_{m=2}^n \frac{\mathcal{L}[(1 - r_{m-1}) \phi_{m-1}](s)}{1 - \mathcal{L}[r_m \phi_m](s)}. \quad (3.53)$$

This general solution clearly has poles at every  $s = G_m$  which satisfies

$$\int_0^\infty r_m(a) \phi_m(a) e^{-G_m a} da = 1 \quad (3.54)$$

which is a generalised version of the classical Euler-Lotka equation for structured population models, holding for each strain  $m$ . At sufficiently long times, those for which  $G_m t \gg 1$  or once the mass of secondary and tertiary micro-lesions is substantial, the number of micro-lesions of any type  $n$  will increase exponentially. The rate of this exponential growth corresponds to the largest real root in the set  $G_j$  with  $1 \leq j \leq n$ : this is distinct from the real root  $G_n$  only when  $v_n$  is less than or equal to some other  $v_j$  of a previous strain.

In the more likely and interesting case that each additional driver increases the net replication rate of cells in the lesion, the number and mass of micro-lesions of type  $n$  will increase exponentially with rate  $G_n$ .

### 3.3.3.1 Linear increase in fitness

**3.3.3.1.1 Surface growth** First, we study the case in which each new driver contributes the same advantage to an individual cell, and  $v_n = nv_1$ : that is, each additional driver after tumorigenesis increases cell survival and division by the same amount as the last driver during tumorigenesis. In this case,

$$V_n(a) = \frac{4\pi}{3} (nv_1 a)^3 \quad (3.55)$$

and

$$\phi_n(a) = 4\pi M (nv_1)^3 a^2 \quad (3.56)$$

with an exponentially declining  $r_n(a) = \exp(-\mu a)$  as discussed previously.

These can be substituted into equations (3.5) and equation (3.53), and several important features of this class of models thus determined.

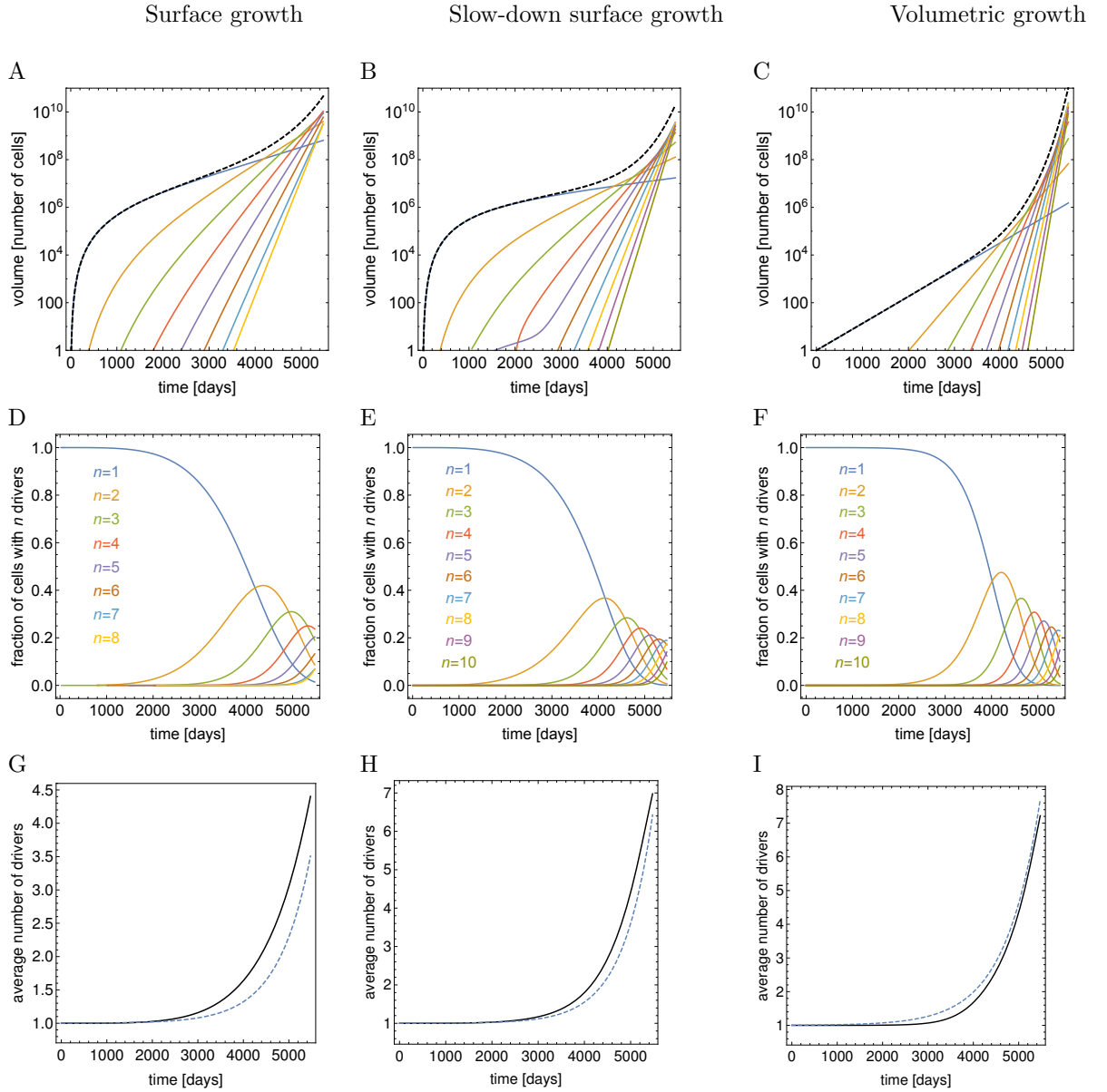


**Figure 3.3** Plots of different quantities (rows of panels) characterizing the tumour as a function of time (days), for different growth scenarios (columns of panels). A,B,C: the total volume (number of cells) of micro-lesions with  $n$  driver mutations (coloured curves) and the total volume  $V_{\text{tot}}$  of the whole tumour (black dashed curve). D,E,F: the fraction of cells with  $n = 1, 2, 3, \dots$  driver mutations in the whole tumour (colours as in A,B,C). G,H,I: the average number of drivers  $\langle n(t) \rangle$ : exact calculation (black) and asymptotic formula (dashed blue). The columns are as follows. Panels A,D,G: from the section on the “Surface growth” model with parameters  $v_1 = 0.0475$ ,  $M = 10^{-6}$ ,  $\mu = 2 \cdot 10^{-5}$  (all rates in units  $[\text{day}]^{-1}$ ). The parameters  $v_1, M$  have been chosen such that the tumour reaches about  $10^{11}$  cells in 15 years ( $\sim 5500$  days) and accumulates 3–4 drivers,  $\mu$  was assumed to be the same as in Ref. [18]. Black dashed curve in A is the total volume  $V_{\text{tot}}$  derived from Eqs. (3.12) and (3.53) with  $F_n(z)$  given by (3.57). Solid black curve in G is the exact analytical calculation from Eqs. equation (3.13) and equation (3.57), blue curve the asymptotic approximation equation (3.97). Panels B,E,H: corresponding to the section on the “Surface growth with decreasing replication rate” model) for  $v_1 = 0.053$ ,  $M = 10^{-6}$ ,  $\mu = 2 \times 10^{-5}$ ,  $\lambda = 10^{-3}$ . Blue curve in panel H is the asymptotic approximation equation (3.101). Panels C,F,I: volumetric growth for  $b = 0.0026$ ,  $M = 10^{-5}$ ,  $\mu = 2 \cdot 10^{-5}$ . Solid black curve is the exact analytical calculation derived from Eqs. equation (3.12) and equation (3.53) with  $F_n(z)$  given by (3.78). Blue curve is the asymptotic approximation derived from equation (3.106).

An expression for the Laplace transformed distribution  $\tilde{F}_n(s)$  can be determined straightforwardly, and then inverted to find the direct formula for  $F_n(z)$  to be

$$F_n(z) = \sum_{j=1}^{3n} A_j \exp(G_{n,j}z) + \sum_{j=0}^{3n-4} B_j z^j \quad (3.57)$$

where  $G_{n,j}$  is the  $j$ -th root of equation (3.54) for a given number of drivers  $n$ , namely

$$G_{n,j} = G_n \exp(2\pi i j / 3) \quad (3.58)$$

where  $i$  is the imaginary unit, and the coefficients  $a_j$  and  $b_j$  depend on  $v_1, M, \mu$  and of course  $n$  and  $j$ : in general, as they are the coefficients of the poles of  $\tilde{F}_n$ , they can be determined from the residues

$$A_j = \lim_{s \rightarrow G_{n,j}} \left( (s - G_{n,j}) \tilde{F}_n(s) \right) \quad (3.59)$$

and

$$B_j = \lim_{s \rightarrow 0} \left( \frac{s^{j+1}}{j!} \tilde{F}_n(s) \right). \quad (3.60)$$

The precise form of the exponential growth rate of the number of micro-lesions with  $n$  drivers follows

$$G_n = (8\pi M)^{1/3} n v_1 - \mu = G_1 + (G_1 + \mu)(n - 1), \quad (3.61)$$

where  $G_1 = (8\pi M)^{1/3} v_1 - \mu$ . The growth rate can thus become negative for sufficiently large mutation rates  $\mu$ . This effect is similar to what was found in subsection 3.3.4.1.2. However, in contrast to this earlier result in which replication slowed down over time, resulting in fewer cells able to migrate and establish new micro-lesions, here the cells only change their type while their replication and migration is not affected. The total number of cells thus increases over time; we shall show this explicitly later in this section. A negative  $G_n$  only means that a subpopulation of type  $n$  cannot grow exponentially at long times: once a strain with  $G_n > 0$  emerges, it rapidly dominates the population.

The number of micro-lesions of type  $n$  can be expressed in terms of these functions

$$N_n(t) = \sum_{j=1}^{3n} a_j \frac{\exp(G_{n,j}t) - 1}{G_{n,j}} + \sum_{j=1}^{3n-3} \frac{b_j}{j} t^j \quad (3.62)$$

as can the total volume of cells of type  $n$

$$V_{\text{tot},n} = \sum_{j=1}^{3n} a_j \frac{8\pi v_n^3}{G_{n,j}^4} \left[ e^{G_{n,j}t} - \left( 1 + G_{n,j}t + \frac{(G_{n,j}t)^2}{2} + \frac{(G_{n,j}t)^3}{6} \right) \right] + \mathcal{O}(1). \quad (3.63)$$

In order to gain some useful insight into how rapidly drivers accumulate, we can either calculate  $\langle n \rangle$  directly from our analytical expressions (as is done above), or we can make some approximations

in order to study the qualitative dynamics of  $\langle n \rangle$ . We will proceed to do both, and to compare the results.

To accomplish this in a systematic and transparent way, consider the behaviour of the function  $\tilde{F}_n(s)$  around  $s = G_n$ : from equation (3.53) it follows that  $\tilde{F}_n(s)$  is dominated by a pole of the form

$$\tilde{F}_n(s) \cong \frac{A_n}{s - G_n} , \quad (3.64)$$

and so from equation (3.59),

$$A_n = \frac{(n-1)!^3 (G_n + \mu) \left[ \left(1 + \frac{\mu}{G_n}\right)^3 - 1 \right]^{n-1}}{3 \prod_{m=1}^{n-1} [n^3 - m^3]} , \quad (3.65)$$

from which it can be seen from an inverse Laplace transform of equation (3.64) that  $F_n(z) \cong A_n \exp(G_n z)$ .

These formulae for the age distribution are sufficient to specify the age distribution for type- $n$  lesions: further exact results are not especially enlightening, and so a comparison of these formulae to both simulations of the corresponding stochastic model and approximate formulae derived from these exact results (see chapter 3.3.4) are discussed in detail in 3.4.1.

**3.3.3.1.2 Surface growth with slow-down** It is not possible for a lesion to grow constantly. Due to spatial constraints and limited supplies of nutrients and oxygen, growth is eventually inhibited, often stopping before tumours reach detectable sizes [88, 89].

As an extension of the previous case which remains consistent in the limit that the characteristic time-scale of growth rate decrease approaches zero, suppose that the initial expansion speed of lesions with slow-down growth obeys the same linear increase as before, so that

$$v_n = n v_1 \quad (3.66)$$

with

$$V_n(a) = \frac{8\pi v_n^3}{\lambda^3} \left( 1 - \left( 1 + \lambda a + \frac{(\lambda a)^2}{2} \right) e^{-\lambda a} \right) , \quad (3.67)$$

$$\phi_n(a) = 4\pi M v_n^3 a^2 e^{-\lambda a} . \quad (3.68)$$

These formulae may be substituted into the exact explicit hierarchy equation (3.53) to obtain

$$\tilde{F}_n(s) = \frac{(s + \mu + \lambda)^3}{(s + \mu + \lambda)^3 - 8\pi M v_0^3} \cdot \prod_{j=2}^n \frac{8\pi M v_{j-1}^3 \left[ \left(1 + \frac{\mu}{s+\lambda}\right)^3 - 1 \right]}{(s + \mu + \lambda)^3 - 8\pi M v_j^3} \quad (3.69)$$

the poles of which clearly occur around  $s = G_n$ , as is generically the case, where

$$G_n = (8\pi M)^{1/3} v_n - \mu - \lambda = (8\pi M)^{1/3} n v_1 - \mu - \lambda. \quad (3.70)$$

The equivalent expression to equation (3.57), concerning the prefactors of the series

$$F_n(z) = \sum_{j=1}^n A_j \exp(G_j z) + \text{other terms} \quad (3.71)$$

may be found from equation (3.59),

$$A_n = \frac{(n-1)!^3 (G_n + \mu + \lambda) \left[ \left( 1 + \frac{\mu}{G_n + \lambda} \right)^3 - 1 \right]^{n-1}}{3 \prod_{m=1}^{n-1} [n^3 - m^3]}. \quad (3.72)$$

**3.3.3.1.3 Volumetric growth** A linear increase in net growth rate must be parametrised differently for the volumetric growth rate, and there is no well-defined surface and as such no characteristic speed. We will use

$$b_n = nb. \quad (3.73)$$

We also have

$$V_n(a) = \exp[(b_n - M)a] \quad (3.74)$$

$$\phi_n(a) = M V_n(a) \quad (3.75)$$

We also assume that all  $r_n(a) = \exp(-\mu a)$  as before. This formula can only describe the fraction of cells that may become invasive correctly only if cells of type- $n+1$  have a negligible selective advantage over cells of type- $n$ , which cannot actually be the case here: this can therefore only be approximately correct, and the limits of this approximation are discussed in section 3.4.1.

The Laplace-transformed lesion age distribution from equation (3.53) can be given explicitly in this case and has the form

$$\tilde{F}_n(s) = (M\mu)^{n-1} \frac{s + M - nb}{\prod_{j=1}^n (s - jb) \prod_{j=1}^{n-1} (s - jb + M + \mu)} \quad (3.76)$$

which clearly has simple poles at every  $s = kb$  for  $1 \leq k \leq n$  and  $s = kb - M - \mu$  for every  $1 \leq k \leq n-1$ . Consequently, the real age distribution  $F_n(z)$  can be expressed exactly by an inverse Laplace transform of equation (3.76), so

$$F_n(z) = \left[ \sum_{k=1}^n A_{n,k} e^{kbz} + \sum_{k=1}^{n-1} B_{n,k} e^{(kb - M - \mu)z} \right] \Theta(z) + \delta_{n,1} \delta(z) \quad (3.77)$$

which implies that the total volume of cells with  $n$  drivers is

$$V_{\text{tot},n}(t) = \delta_{n,1}e^{(b-M)t} + \sum_{k=1}^n \frac{A_{n,k}}{(n-k)b-M} \left( e^{(nb-M)t} - e^{kbt} \right) + \sum_{k=1}^{n-1} \frac{B_{n,k}}{(n-k)b+\mu} \left( e^{(nb-M)t} - e^{(kb-M-\mu)t} \right) \quad (3.78)$$

where the coefficients  $A_{n,k}$  and  $B_{n,k}$ , derived from equation (3.59) are

$$A_{n,k} = \left( \frac{M\mu}{b^2} \right)^{n-1} (-1)^{n-k+1} \frac{(n-k)b-M}{(k-1)!(n-k)! \prod_{j=1}^{n-1} (k-j + \frac{M+\mu}{b})}, \quad (3.79)$$

$$B_{n,k} = \left( \frac{M\mu}{b^2} \right)^{n-1} (-1)^{n-k} \frac{(n-k)b+\mu}{(k-1)!(n-k-1)! \prod_{j=1}^n (k-j - \frac{M+\mu}{b})}. \quad (3.80)$$

Although the above formulae are exact, they are rather complex, and the asymptotic behaviour of  $V_{\text{tot},n}$  is not immediately apparent. These formulae may nonetheless be used to plot and compare  $V_{\text{tot},n}$  numerically to simulations, as in section 3.4.1: a fruitful approximate approach is detailed in section 3.3.4.

### 3.3.3.2 Fitness increase with rapid plateau

In all previous cases, all drivers carried an increasing selective advantage over one another with an identical relative strength, meaning that cells with  $n = 3$  driver mutations had a net growth rate three times that of cells with  $n = 1$ . It is not possible for this pattern to continue indefinitely, as there is an upper limit to how quickly cells can progress through the cell cycle (detailed in chapter 1), and increases in this net growth rate presumably occur by reductions in the rate of cell death by apoptosis in addition to modest increases in the rate of division induced by self-signalling. A linear increase cannot continue past the point at which there is no cell death, and cells divide as rapidly as possible, and can at best be a rough approximation of the truth.

Linear increases in fitness also imply that drivers accumulate exponentially (see section 3.3.4), which would imply in turn that the majority of drivers emerge at a very late stage in the progression of the tumour, for which there is very limited evidence.

In this section, we will study the case in which the selective advantage of the first few drivers is much larger than that of any subsequent driver. The first additional driver mutation can substantially increase the net replication rate, to double the net growth rate of cells in the primary lesion, and this linear increase may continue until up to the third, after which point additional drivers have only a very weak effect. That is, for the underlying net replication rate we will take

$$b_2 = 2b_1 \quad (3.81)$$

$$b_3 = 3b_1 \quad (3.82)$$

$$b_n = 3b_1 + (n-3)\epsilon b_1 | n > 3 \quad (3.83)$$

for the volumetric growth model and for the lattice model simulations, and for the surface growth model we will take

$$v_2 = 2v_1 \quad (3.84)$$

$$v_3 = 3v_1 \quad (3.85)$$

$$v_n = 3v_1 + (n-3)\epsilon v_1 | n > 3 \quad (3.86)$$

with some  $b_1 \propto v_1$ , with a constant of proportionality fixed by comparing the measured total volume in a set of Eden model simulations without mutation or migration to the simple geometrical expansion  $V(t) = 4\pi v_1^3 t^3 / 3$ .

Statistical evidence of cancer incidence rates suggest that having a restricted number of early driver mutations which make a large contribution to the net replication rate of a given cell line is indeed the case for some lung and colorectal cancers [91].

All cancer cells in this subset of models are assumed to initially have one driver, which enables them to outgrow surrounding tissue, and the “additional drivers” we talk about here should be taken to mean the second driver overall, and then the third, and so on.

We will study both cases in which only the first two additional drivers substantially increase the net replication rate: there is little to be gained from studying analytical approximations in this case, so we will restrict ourselves to analysing a few exact formulae, and then comparing the results of direct calculation from these to the results of simulations with the corresponding underlying fitness landscape.

From figure 3.5, one can see that the average number of drivers per cell accumulates roughly sigmoidally, before the tumour reaches a detectable size ( $V_{\text{tot}} > 10^9$ ), and consequently most drivers will emerge and accumulate relatively early in the tumour’s development. This implies that the final tumour is much less heterogeneous upon treatment because almost all cells have the same underlying set of driver mutations. Moreover, the total volume grows approximately exponentially after the appearance and accumulation of these drivers, rather than super-exponentially as in previous models: one can clearly observe a gradual transition between the early and late exponential growth rates in both the exact analytics and the simulations, as evidenced in figure 3.5. These results are in broad agreement with recent experimental evidence on intra-tumour heterogeneity in colorectal cancer [35].

### 3.3.4 The generating function technique

The exact results of the previous section can already be used to calculate relevant quantities such as the total tumour burden and the mean number of drivers present per cell, a calculation which can be meaningfully compared to the same quantities obtained from the stochastic model. However, this procedure is rather opaque, and it is difficult to obtain qualitative insights into the effect of different fitness landscapes or underlying growth models for individual micro-lesions in this way.

To derive expressions for the total volume and mean number of drivers from equation (3.53), equation (3.26) and equation (3.12) more easily, and to allow asymptotic behaviour of both of these to be studied, it would be useful to develop an approach to systematically extract  $V_{\text{tot}}$  and  $\langle n \rangle$  from the exact expressions.

First, we can notice that both the total volume and mean number of drivers depend on expressions for the total volume of lesions of each type  $n$  like so

$$V_{\text{tot}}(t) = \sum_n V_{\text{tot},n}(t) \quad (3.87)$$

$$\langle n \rangle(t) = \frac{\sum_n n V_{\text{tot},n}}{\sum_n V_{\text{tot},n}} \quad (3.88)$$

both of which are entirely determined by the sequence of functions  $\{V_{\text{tot},n}\}$ . As a result, they can be expressed in terms of the behaviour of another function in a dummy variable  $q$  which encodes all the relevant information in the series  $\{V_{\text{tot},n}\}$ . We will call this function the generating function

$Z(t, q)$  for consistency with other literature in which closely related techniques are used. We define  $Z(t, q)$  as

$$Z(t, q) := \sum_n e^{qn} V_{\text{tot}, n} \quad (3.89)$$

from which several interesting quantities can be calculated: in particular,

$$V_{\text{tot}} = Z(t, 0) \quad (3.90)$$

and

$$\langle n(t) \rangle = \left[ \frac{\partial \log Z(t, q)}{\partial q} \right]_{q=0}. \quad (3.91)$$

Other, higher-order moments and cumulants such as the variance in the number of mutations  $\sigma^2(n)$  may also be calculated by taking higher order derivatives of  $Z$ , but are not interesting to us at this time.

This approach is especially useful for cases in which the precise form of  $V_n$  and  $F_n$  are such that  $Z(t, q)$  is an analytic function in the dummy variable  $q$ . Approximations of  $Z$  make the asymptotic behaviour of  $\langle n \rangle$  and  $V_{\text{tot}}$  much easier to investigate, as features of both may be determined significantly faster than their calculation from the exact series derived in the previous section.

### 3.3.4.1 Linear increase in fitness

**3.3.4.1.1 Surface growth** For human cancer cells, the mutation rate  $\mu$  is considerably less than the net growth rate  $G_1$  and other  $G_n$ , simply because the appearance of any new mutation at a specific locus is very unlikely in any given cell division event. Equation (3.65) simplifies in the relevant limit  $\mu/G_1 \ll 1$  to

$$A_n \approx \frac{(n-1)!^3}{3n^{n-1} \prod_{m=1}^{n-1} [n^3 - m^3]} \left( \frac{3\mu}{G_1} \right)^{n-1} \quad (3.92)$$

so the  $Z$  from (3.89) is asymptotically

$$\begin{aligned} Z(t, q) &\cong \sum_{n=1}^{\infty} e^{qn} A_n \int_0^{\infty} e^{G_n(t-a)} \frac{4\pi}{3} v_0^3 n^3 a^3 da \cong \text{const} \cdot \sum_{n=1}^{\infty} e^{qn+G_1 nt} \frac{A_n}{n} \\ &\cong \text{const} \cdot e^{G_1 t} \sum_{n=1}^{\infty} \left( \frac{3\mu}{G_1} e^{q+G_1 t} \right)^n \frac{(n-1)!^3}{3n^n \prod_{m=1}^{n-1} [n^3 - m^3]}. \end{aligned} \quad (3.93)$$

The complicated numerical prefactor in this equation can be approximated for large  $n$  as

$$\frac{(n-1)!^3}{3n^n \prod_{m=1}^{n-1} [n^3 - m^3]} \cong \text{const} \cdot \frac{1}{(n-1)!} \exp \left[ -n \left( \frac{\pi}{2\sqrt{3}} + \frac{3 \ln 3}{2} + 1 \right) \right] \quad (3.94)$$

from Stirling's approximation. Given this, it can be obtained from equation (3.93) that

$$Z(t, q) \approx C \exp \left[ G_1 t + q + \frac{\mu e^{G_1 t + q - \frac{\pi}{2\sqrt{3}} - 1}}{\sqrt{3}G_1} \right] \quad (3.95)$$

and finally, using equation (3.91), it follows that

$$V_{\text{tot}}(t) = Z(t, 0) \propto \exp \left[ G_1 t + \frac{\mu e^{G_1 t - \frac{\pi}{2\sqrt{3}} - 1}}{\sqrt{3}G_1} \right], \quad (3.96)$$

and

$$\langle n(t) \rangle \cong 1 + \frac{\mu e^{-1 - \frac{\pi}{2\sqrt{3}}}}{\sqrt{3}G_1} e^{G_1 t}, \quad (3.97)$$

so that the total volume is seen to increase faster than exponentially in this case, driven by an exponential increase in the average number of drivers  $\langle n \rangle$ .

**3.3.4.1.2 Surface growth with slow-down** In the biologically relevant limit, mutations should occur only rarely in any given cell division event. As the probability of any type of mutation occurring in any given cell division event should be proportional to the ratio  $\mu/G_n$ , barring possibly some factors regarding turnover and ploidy, it makes sense to ask what happens to the exact formulae in the limit that  $\mu/G_1 \ll 1$ .

The prefactors from equation (3.72) reduce to

$$A_n \cong \frac{(n-1)!^3}{3n^{n-1} \prod_{m=1}^{n-1} [n^3 - m^3]} \left( \frac{3\mu}{G_1 + \lambda} \right)^{n-1}. \quad (3.98)$$

This allows us to write

$$Z(t, q) \cong \text{const} \cdot \exp \left[ G_1 t + q + \frac{\mu e^{(G_1 + \lambda)t + q - \frac{\pi}{2\sqrt{3}} - 1}}{\sqrt{3}(G_1 + \lambda)} \right] \quad (3.99)$$

which implies

$$V_{\text{tot}}(t) \cong \text{const} \cdot \exp \left[ G_1 t + \frac{\mu e^{(G_1 + \lambda)t - \frac{\pi}{2\sqrt{3}} - 1}}{\sqrt{3}(G_1 + \lambda)} \right] \quad (3.100)$$

$$\langle n \rangle(t) \cong 1 + \frac{\mu e^{(G_1 + \lambda)t - \frac{\pi}{2\sqrt{3}} - 1}}{\sqrt{3}(G_1 + \lambda)} \quad (3.101)$$

and the total volume can be seen to increase faster than exponentially once again, being driven by an exponential increase in the average number of drivers.

In both cases, linear fitness landscapes give rise to faster-than-exponential growth. We are not aware of any serious proposals to use such super-exponential growth curves to successfully model the growth of actual tumours, which motivates a look at fitness landscapes which gradually tail off later on in this chapter.

Curiously, the average number of drivers is independent of  $\lambda$ . Every appearance of  $\lambda$  in the above formula is exactly cancelled out by a corresponding  $-\lambda$  term arising from the explicit expression of  $G_1$ . I have not found any intuitive arguments as to why this should be the case.

**3.3.4.1.3 Volumetric growth** To obtain simpler expressions for the total volume and number of drivers, we can first note that in real tumours migration is relatively rare, and so the replication rate must be much larger than the migration rate, or else cells would only move around in a diffuse mass without replicating, so that  $b \gg M$ . As beneficial mutations are also very rare events, the rate  $\mu$  must also be much smaller than  $b$ .

As a consequence,  $V_{\text{tot},n}(z)$  will be dominated by the term proportional to  $A_{n,n}$  from (3.80) as long as  $bt \gg 1$ : i.e. for sufficiently long times (much longer than the individual lesion's doubling time),  $e^{bt} \gg 1$ .

We can furthermore approximate  $A_{n,n}$  as

$$A_{n,n} \cong \left(\frac{M\mu}{b^2}\right)^{n-1} \frac{M}{n!^2} \left(1 + \mathcal{O}\left(\frac{M}{b}\right)\right) \quad (3.102)$$

whereupon the generating function  $Z(t, q)$  becomes

$$Z(t, q) \cong \frac{M}{M - \mu} e^{bt+q} (e^{-\mu t} - e^{-Mt}) \sum_{n=0}^{\infty} \frac{1}{n!^2} \left(\frac{M\mu}{b^2} e^{bt+q}\right)^n \quad (3.103)$$

$$= \frac{M}{M - \mu} e^{bt+q} (e^{-\mu t} - e^{-Mt}) I_0 \left( \frac{2\sqrt{M\mu}}{b} e^{(bt+q)/2} \right) \quad (3.104)$$

where  $I_0(x)$  is a modified Bessel function of the first kind. This immediately allows us to write

$$V_{\text{tot}}(t) = Z(t, 0) \propto e^{bt} I_0 \left( \frac{2\sqrt{M\mu}}{b} e^{bt/2} \right) \quad (3.105)$$

$$\langle n \rangle(t) \cong 1 + \frac{e^{bt/2} \sqrt{M\mu} I_1 \left( \frac{2\sqrt{M\mu}}{b} e^{bt/2} \right)}{b I_0 \left( \frac{2\sqrt{M\mu}}{b} e^{bt/2} \right)} \cong 1 + \frac{\sqrt{M\mu}}{b} e^{bt/2} \quad (3.106)$$

so that the total volume can again be seen to increase faster than exponentially, whilst drivers accumulate exponentially, both phenomena which are also exhibited in the surface growth models. This therefore seems to be a generic feature of having a linear increase in fitness with the number of drivers: an exponential accumulation of driver mutations drives a super-exponential increase in tumour burden.

Note that for this model to reach the same size as in the surface growth model (around  $10^{11}$  cells) in a reasonable time frame as well as having accumulated a similar number of drivers (more than two), the actual increment  $b$  of the growth rate per driver has to be very small, and so this model is of limited applicability.

## 3.4 Comparison to simulations

We compared the results obtained in section 3.3 with numerical simulations of both the stochastic model defined in section 3.1 and the lattice model defined in chapter 2. In the simplified stochastic

model, growth and the appearance of lineages carrying additional driver mutations were both deterministic, whereas migration was left as a stochastic process. This was intended to reflect the fact that despite the relative complexity of all processes, migration is a relatively rare event compared to growth.

In the Eden-like lattice model based on that from [40], all processes were stochastic, but with different rates that depended on a cell's surrounding environment. It was never the case that a cell totally surrounded by others could migrate and found new lesions, for instance, and so the rates of both migration and of individual lesions' growth were found to be asymptotically proportional to their surface area.

All models attempted to make predictions for at least the total tumour burden, denoted  $V_{\text{tot}}$ , and for the relative frequencies of different lineages with different numbers of accumulated driver mutations, the populations of which are denoted  $V_{\text{tot},n}$ . These can both be used to calculate the mean number of additional driver mutations per cell,  $\langle n \rangle$ , and other statistical measures of genetic diversity.

### 3.4.1 Comparison of stochastic minimal model and analytics

We performed numerical simulations of the surface growth model described in section 3.2.1, and treated individual lesions of age  $a$  as balls of volume  $4\pi(v_n a)^3/3$ . New lesions were founded with rate  $\phi_n = 4\pi M v_n^3 a^2$ , a fraction  $r_n(a) = \exp(-\mu a)$  of these had the same number of driver mutations  $n$  in their founding cell, and a complementary fraction  $1 - r_n(a)$  of which had  $n + 1$ .

Mutations in these simulations consisted of three initial strong drivers, and a very small fitness advantage  $\epsilon$  for any additional driver after this point. This fitness advantage was non-zero, so that additional driver mutations did indeed carry some selective advantage (and must by definition), but was in practice too small to strongly affect growth on clinically relevant timescales. The expansion speeds  $v_n$  were thus given by 3.86.

In each simulation, we measured the total volume  $V_{\text{tot}}$ , the mean number of drivers per cell  $\langle n \rangle$ , the volume  $V_{\text{tot},n}$  of cells with a specific number of mutations  $n$ , and the fraction of cells with  $n$  mutations  $w_n = V_{\text{tot},n}/V_{\text{tot}}$ . These quantities were averaged over 500 simulations with the same underlying parameters. Figures 3.4 and 3.5 demonstrate remarkable agreement between simulations and the formulae derived from our analytical theory at early times: some deviation from the analytical prediction appears at small values of  $M$ , which may be a finite-size effect. The analytical formulae also seem to overestimate the frequency of mutant strains, which can be seen in figure 3.5.

We believe that this deviation is caused by the way in which we neglect fluctuations in the derivation of equation (3.5): while the neglect of fluctuations in growth rates and mutation clearly do not have a significant effect on the primary tumour and its cloud of secondary micro-lesions, the effect becomes increasingly pronounced with increasing number of driver mutations  $n$ . The deterministic model of equation (3.5) overestimates the frequency of mutants of a given age and  $n$  at most times, but nonetheless predicts the growth rate of each strain with remarkable accuracy.

The effect of fluctuations must therefore be to suppress the growth of secondary micro-lesions when they are very small. One may well ask how this is possible, as fluctuations are, by definition, deviations from expected behaviour, and should not have an effect on the mean overall. This may be explained by multiplicative noise (see section 3.4.1.1).

Other substantial disagreement, which is even present between different calculations of what are superficially identical quantities, result from more subtle statistical issues and properties of the distribution of mutant proportions  $w_n$ .

If we first calculate the average number of drivers  $\langle n \rangle$  using the measured distribution  $w_n$ , calling

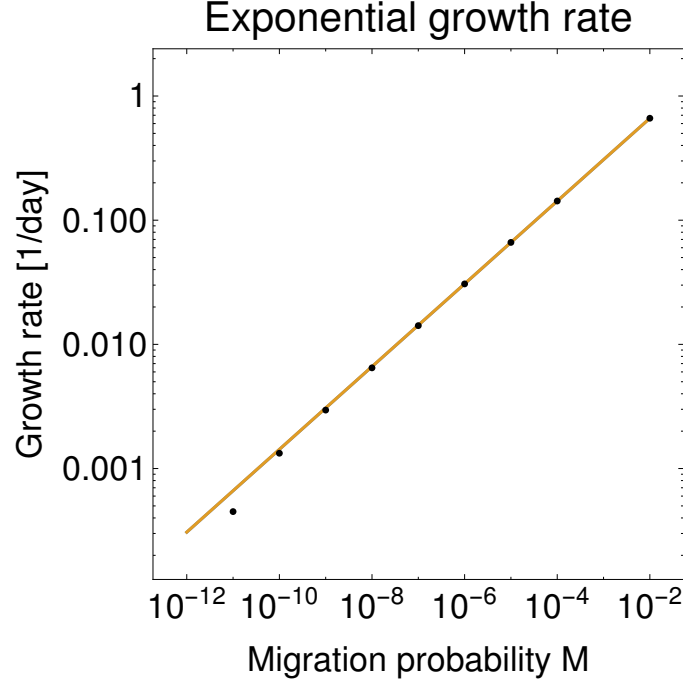


**Figure 3.4** Plot showing the measured growth rate of the diffuse collection of micro-lesions in the ensemble model versus migration rate  $M$ . Parameter values were expansion speed  $v = 1.05$ , with  $M$  varied between two extreme values. This plot confirms the power-law dependence with an exponent of  $1/3$ .

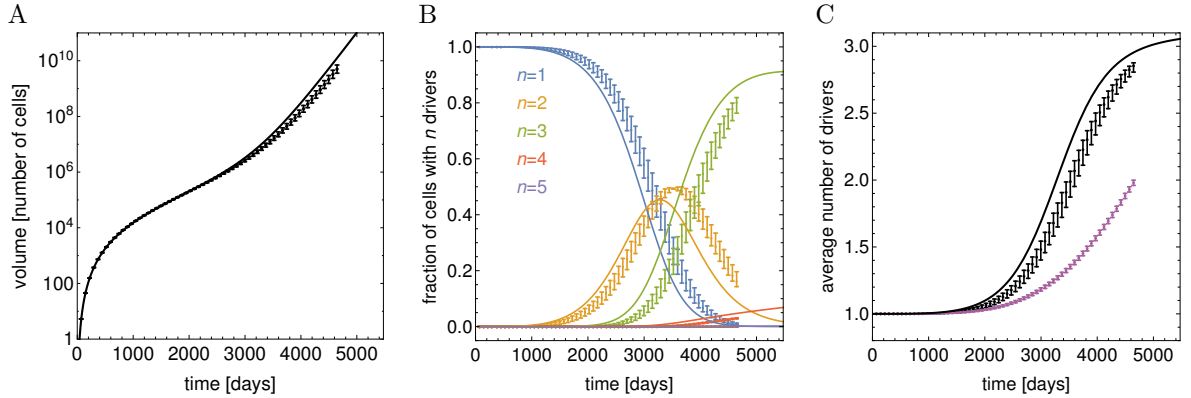


**Figure 3.5** The model with three strong drivers as in Eqs. equation (3.86). A: The total volume of the whole tumour (black curve). B: the fraction of drivers with  $n$  mutations. C: the average number of drivers (black curve). In all cases  $v_1 = 0.015$ ,  $M = 10^{-4}$ ,  $\mu = 2 \cdot 10^{-5}$ ,  $\epsilon = 0.01$ . Data points with error bars in all panels come from stochastic simulations of the original model (Section 3.2.1, for which 500 replicates were performed). In panel C, two sets of data points are presented. Purple points have been obtained by calculating the average number of drivers for each simulated tumour and then taking the average over many tumours. Black points represent averaging the fractions of cells with  $n$  drivers over many tumours (as in panel B), and using this to calculate the average  $n$ .

this quantity  $\langle n \rangle_{w_n}$ , and find the average this quantity with respect to many replicates of our simulations, we find the quantity  $\langle \langle n \rangle_{w_n} \rangle_{\text{repl.}}$ , which deviates strikingly from the analytical curve for  $\langle n \rangle$  (purple points in figure 3.5): call this “Method 1”.

However, if we calculate volumes  $V_n$  of cells of type  $n$  for each simulation, average this quantity over many replicates  $\langle V_n \rangle_{\text{repl.}}$ , and then calculate the average number of drivers  $\langle n \rangle$  via  $\langle n \rangle_{\langle w_n \rangle_{\text{repl.}}} = \sum_n n \langle V_n \rangle_{\text{repl.}} / \langle V_{\text{tot}} \rangle_{\text{repl.}}$  (“Method 2”), we obtain a much better agreement (black point in figure 3.5). In that the second method corresponds to averaging out randomness before calculating  $\langle n \rangle$ , it is arguably closer in spirit to what we do in our analytical calculations, but there is a more fundamental cause of the disagreement here.

Since driver mutations act to accelerate growth, in any given simulation we can readily observe that the average number of mutations per cell is strongly correlated with size. If we average out the proportions of cells of each type  $n$  before averaging over replicates, we treat those simulations with relatively few drivers and corresponding *much* smaller sizes with equal weight to simulations with many drivers and enormous sizes. This acts to bias the calculation of  $\langle n \rangle$  downwards. If we average the volumes  $V_n$  before calculating proportions  $w_n$  and  $\langle n \rangle$ , the contribution of these smaller tumours with fewer drivers is proportional to their relatively small size, and we see that the calculated  $\langle n \rangle$  is consequently higher.

### 3.4.1.1 The effect of multiplicative noise

In rare cases, fluctuations may not exactly average out when considering mean behaviour of growth processes with multiplicative noise, and may act to suppress growth. Depending on whether or not noise is interpreted in an Ito or a Stratonovich sense, variations in the amplitude of stochastic noise with  $n$  can have significant confounding effects, even on apparently large systems.

As a very simple illustrative model, consider the growth process

$$\dot{n} = bn + \sigma \xi \quad (3.107)$$

with  $\xi$  standard white noise and  $\sigma$  the scale of the fluctuations. If, as in our stochastic model, growth occurs in something like a Poisson process, with the mean number of new cells per time step equal to  $bn \, dt$ , then the variance  $\sigma^2$  of this process will be equal to the mean,  $\sigma^2 = bn \, dt$ , as the mean and variance have the same scale for all Poisson-distributed random variables. Our growth process therefore has the form

$$\dot{n} = bn + \sqrt{bn} \xi . \quad (3.108)$$

Our neglect of fluctuations amounts to immediately taking the noise term to zero, as  $\langle \xi \rangle = 0$ , so that

$$\langle \dot{n} \rangle \approx b \langle n \rangle \quad (3.109)$$

However, it is not necessarily true that  $\langle n^{1/2} \xi \rangle = 0$ . In fact, if we rigorously derive a Fokker-Planck equation from equation (3.108) *without* conditioning the probability distribution on survival, we instead recover

$$\langle \dot{n} \rangle = b \langle n \rangle - \frac{b}{2} \quad (3.110)$$

with an extra  $-b/2$  term representing extinction due to stochastic fluctuations. For identical initial conditions, say  $\langle n \rangle(0) = 1$ , the long-term behaviour of solutions to equation (3.110) is found to be lower than solutions to equation (3.109), although the growth rate is identical in both cases.

Intuitively, this means that the (Stratonovich) noise gradient has a much larger effect on small populations than large populations. Small populations will be dominated by the random fluctuations of noise, and can only begin a stage of steady exponential growth once they “escape” the noisy area of state space: but this escape can only happen due to the stochastic dynamics of the system itself. Eventually, the system will fluctuate out of having a small unstable population (or else die out), so a typical history will involve some delay before exponential growth gets underway.

This is just a heuristic argument: fluctuations which scale in the same way as our growth rate fluctuations in a simple well-mixed can suppress growth without changing the exponential growth *rate*, but this is a simple well-mixed model, and our above model is considerably more sophisticated with regards to spatial structure. It may be the case that the same argument does not hold once one carries out a fully rigorous analysis of the effect of fluctuations on the system of partial differential equations equation (3.5) and their corresponding Fokker-Planck equations: due to the mathematical complexity of this task and time constraints, we cannot say for sure that the observed disagreement is certainly due to multiplicative noise.

## 3.5 Discussion

In this chapter we studied models of cancer evolution which were all based on three processes: replications of cancer cells, driver mutations which resulted in differential increases in the net rate of replication and survival of these cells, and local migration which caused cells to disperse. The latter process results in a picture of tumours in which they are formed of a large primary and a conglomerate of micro-lesions surrounding it. The dispersal of cells in this way has been recognized as a process by which tumours [78, 92] and other populations of motile cells [93] can speed up their growth. Although our model was motivated by the process of local migration, it is neutral to the precise details of the underlying mechanism of cell dispersal and migration, and is potentially applicable to long-range invasion characteristic of late-stage metastatic cancers [2].

The spatial structure and position of these secondary micro-lesions is not explicitly dealt with at any stage in our formalism, and the conglomerate we describe can be straightforwardly re-interpreted as an abstract distribution of lesions, including distant metastases [82].

One of the strengths of the approach developed in this chapter lies in the ease with which the average behaviour of the minimal stochastic model can be obtained and analysed analytically, and the degree of agreement between the minimal stochastic model, the structured population model, and the fully stochastic lattice models. Remarkably, the inclusion of migration results in a model which is easier to exactly solve than many spatial models of individual tumours: as long as interactions between lesions are negligible, migration has the effect of “smearing out” spatial structure, and in permitting populations to grow exponentially, results in behaviour which is qualitatively similar to that of well-mixed models.

Analytical solubility means that the model works for tumours of arbitrary size, including both large masses that warrant surgical removal and undetectable micro-lesions, and can be used to model cancer progression over a range of timescales. The most important implications of the model deal with two aspects of cancer evolution: growth laws, and genetic heterogeneity.

*Tumour growth.* In the absence of new driver mutations and assuming sufficient migration, our model predicts that long-time growth is exponential. This is also true when individual micro-lesions grow sub-exponentially, and even if their growth slows down over time. Given that most tumours contain avascular areas where the lack of oxygen and glucose inhibits proliferation [94, 95], our model provides a plausible explanation how the growth of an entire tumour can still be exponential,

as often observed experimentally for intermediate-size tumours. This phenomenon does not require postulating any novel or previously unknown mechanism, but relies only on short-range migration of cancer cells, a process that certainly occurs in nature, informs standard histological procedures, and is a subject of active research [45, 96].

If all new driver mutations carry a significant fitness advantage, and steadily accumulate during tumour development, our theory predicts super-exponential growth. The acceleration does not have to be large, and may arise only in tumours that are too big to arise on clinically relevant timescales, but nonetheless we are unaware of any evidence that super-exponential growth of this type has ever been observed in human cancer.

Exponential or faster growth is obviously unrealistic for very large tumours for which spatial constraints and other inhibitors of growth become important. Many models of tumour growth have been proposed that account for the sigmoidal growth curve of many tumours [30]. The majority of these models are phenomenological, and are not based on the microscopic dynamics of cancer cells as ours is. It would be highly instructive to learn what minimal changes would be required to our model in order to reproduce sigmoidal growth, or if these models which do exhibit sigmoidal growth are appropriate for tumours once local invasion or metastasis are taken into account.

*Genetic heterogeneity of tumours.* Experimental evidence gathered by a number of different groups over the last decade strongly suggests that cancerous masses show some degree of genetic heterogeneity, although the precise amount and its possible importance are still a subject of debate [33, 34, 97]. In this chapter, we explored this heterogeneity by calculating the size of clonal cell lines with differing numbers of driver mutations, and showed that these cell lines increase in population at an exponential rate. At first, only one driver predominates, until becoming replaced by a mixture of clones with two, three, and more drivers. The coexistence of multiple genetically distinct cell lines in this way means that the evolution is not well represented as being a simple counting process, in which one cell line forms the majority of the population until a new mutant emerges and rapidly takes over after a long time. The time to reach some average number of drivers is not a simple sum of waiting times for consecutive mutants to emerge, and a number of distinct cell lines are present simultaneously.

We have also shown that if each new driver increases the selective advantage of cancer cells in comparison to normal cells, the average number of driver mutations predicted by our model increases exponentially in time for all considered scenarios. This means that most drivers would accumulate late during cancer progression. There is limited evidence [34, 35] that this is not true. On the other hand, if only a few first drivers have significant fitness advantage, these drivers will accumulate early during growth and the tumour will become much more homogeneous. An interesting application of our model would be to predict how strong the selective advantage of new drivers can be that would still be consistent with recently postulated neutral evolution in tumours [34].

There are several ways our model could be revised and extended. We have not analysed the spatial distribution of drivers: it may not be feasible to do this analytically, but as the model proposed here is easily simulated (see section 3.4.1), it may be practical to extend it to include locations of micro-lesions and draw out some meaningful predictions.

Another interesting extension would be to attempt to incorporate phenotypic plasticity and the presence of cancer stem cells, and asking what would result if only some small fraction of cells could replicate indefinitely, whilst the majority of cells can only undergo a few rounds of replication, as in Ref. [98]. This would affect the net replication rate, and the rate at which mutations accumulate in a single lesion  $r_n$ .

The analytical formulae also seem to overestimate  $F_n$  and  $V_n$ , which we believe is related to multiplicative noise. How this may affect equations (3.5) is a question which beyond the scope of this thesis at this time, but which has the potential to resolve the remaining discrepancies

between the analytics and simulations.

Finally, since the separability of the deterministic governing equations equation (3.5) only depends on the validity of the infinite genome approximation and the non-interaction of distinct lesions, it seems very likely that this approach is extensible to evolution in more complex landscapes than the linear chain of driver mutations that we have studied. Particularly interesting questions surround the effect of epistatic interactions between driver and passenger mutations [99], and the statistical behaviour of the model in the context of random fitness landscapes is another open question [15].

### 3.5.1 Relevance to open questions in the field

In the introduction, we described two broad open problems in the field of cancer evolution and treatment: what growth curves accurately describe complex, growing cancers and more importantly their physiological interpretation; and how quickly cancers evolve. Our interest in these two problems consists of how these two aspects of cancer can be modelled in such a way that they can be related to microscopic cell-scale determinants in a flexible, yet minimalistic and intelligible theoretical framework.

We have found in this chapter that the total volume of many independent lesions that constitute a cancerous ensemble can grow exponentially: when genotypes of differing fitness are accounted for, we find that the frequencies of each cell line grow exponentially as well, with an exponential growth rate determined by the migration rate  $\phi_n$  of solid tumours dominated by a given cell line.

The total tumour burden in these cases is therefore a sum of multiple exponential growth curves, despite the fact that none of the distinct lesions in the ensemble grow exponentially.

The widespread usage of exponential growth as an heuristic by clinicians and a simple basis for other models by applied mathematicians may not, as a result, be totally baseless: at least in the case of metastatic cancer for a limited period of time, the paradoxical popularity of these models may not be paradoxical at all, but the simplest workable model in the context of a metastatic cascade.

On the second point, the “speed” of evolution has been shown to be related to the effective fitness landscape generated by the differential growth and invasion of lesions comprised of different cell lines. Quantified by the average number of drivers  $\langle n \rangle$  present in a cell picked at random from the ensemble of tumours, steady linear increases in additive fitness were found to correspond to accelerating, super-exponential growth and an exponential increase in mean number of drivers  $\langle n \rangle$ . Linear increases in fitness of underlying cells, whether this is quantified in terms of expansion speed for solid spheroids or simply growth rate for well mixed lesions, all correspond to accelerating growth and accelerating selection: this corresponds with the “late sweep” class of models described in the introduction.

Given that super-exponential growth has not (to the best of our knowledge) been observed in actual clinical studies of metastatic cancers, this rather generic finding warrants a look at other underlying landscapes.

If the fitness is bounded from above, say by physiological constraints on how rapidly cells can divide, then a plausible alternative would be for only the first few drivers to carry a substantial advantage, followed by a mostly-flat plateau. In this case, we found that after an initial burst of growth and selection, the metastatic ensemble underwent an extended phase of exponential growth. The growth rate of this extended phase may be quite slow, as it is determined by the frequency of migration rather than the underlying cell division time. The average number of drivers increased sigmoidally, before settling down to a much slower rate of increase for an extended length of time.

This scenario displays more realistic growth curves than the simple linear increase popular with modellers, but also predicts that most selection occurs in an early burst: this early set of selective

sweeps still occurs after initiation, and is driven by migration, in contrast to “Big Bang” like models. This more realistic scenario of fitness landscapes with a plateau therefore correspond to an intermittent acceleration and deceleration of evolution by selection, and an “early sweep”.

Finally, in all cases multiple drivers were found to be present at any one time, which meant that the simplifying assumption of a succession of hard sweeps such as in the work of I. Božič *et al.* was not valid in general, resulting in slightly different growth rates of  $\langle n \rangle(t)$  for the same underlying fitness function (among other less important details). The most plausible set of parameters we have looked at in this chapter therefore seem to point to an early selective sweep.

### 3.5.2 Future work

A number of simplifying assumptions have made our research tractable, but limited its application. Evolution does not occur on linear landscapes, comprised of a simple succession of drivers: there are multiple, branching pathways available, and epistasis (roughness in the fitness function) can strongly affect dynamics.

In addition, we have noted the effect of noise on our growing structured populations, but a fully stochastic development of structured population models is rather beyond the scope of this thesis. Some initial attempts at formulating such stochastic models [100] and providing a means of building solutions have been attempted, but are not yet at the stage that useful conclusions can be drawn from analytics alone. The effect of stochastic fluctuations on the expected behaviour of structured population models is therefore one area of research that may prove relevant and fruitful in the future.

There are also a number of interesting experimental issues. The actual detection and timing of selective sweeps is strongly frustrated by the lack of dynamical data in most cases, which raises the question of how the occurrence of selection can be reliably detected in real tumours. One serious proposal for gaining useful dynamical data is the use of neutral mutations in a lesion as a molecular clock: if these occur at a constant rate, the number of expected drivers can be related to the number of passengers. This could be a potentially useful proxy for the missing dynamical information. One attempt to do this, and use neutral passenger mutations as an indirect measure of time, assumes that cell divisions occur at a constant rate, with some given expected number of passenger mutations occurring at each division event: the total expected number of passenger mutations  $n_p$  present after some time  $t$  is then

$$n_p = \nu t / T \quad (3.111)$$

where  $\nu$  is in essence the expected number of new neutral mutations per division, and  $T$  the average cell cycle time [18]. This formula could be used to express our results in terms of the number of passenger mutations, a more easily measurable quantity than time, in a similar way to earlier work. However, this assumes the rate of cell division is constant over time: if it varies continually in some way, equation (3.111) will not be valid. More generally, one can say that  $n_p$  should be proportional to the number of cell divisions  $n_D$ ,

$$n_p = \nu n_D(t) . \quad (3.112)$$

Although the precise form of  $n_D(t)$  is not known (and is an independent assumption from any made so far in our framework), the absolute lower bound is the minimum number of divisions needed to produce a total tumour size of  $V_{\text{tot}}$ : this minimum number of divisions is clearly  $\log_2(V_{\text{tot}})$ , so

$$n_p > \nu \log(V_{\text{tot}}) / \log(2) . \quad (3.113)$$

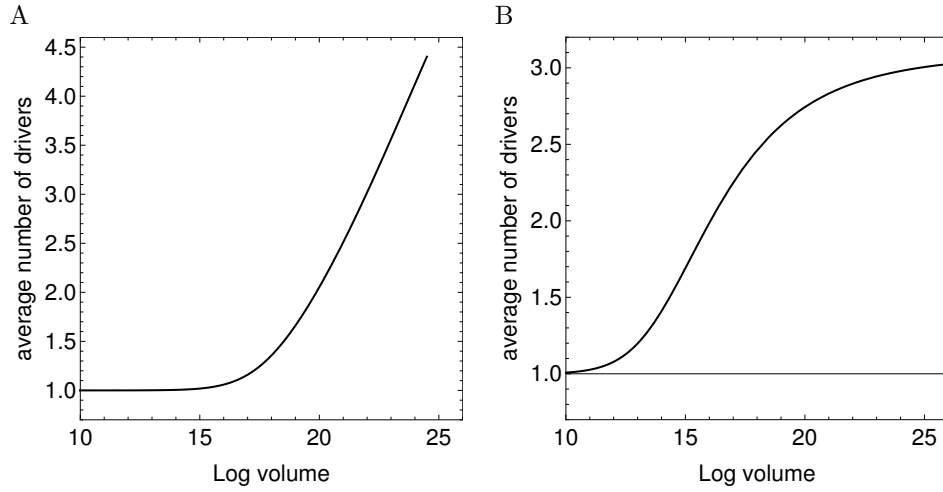


**Figure 3.6** *Figure showing qualitative differences in plots of the average number of drivers per cell  $\langle n \rangle$  versus the logarithm of the total tumour burden, demonstrating A. a clear convex curve for the late sweep model (gradualistic fitness landscape) and B. a warped sigmoidal curve for the soft sweep model (fitness landscape with plateau).*

The result of plotting the average number of drivers  $\langle n \rangle$  against  $\log(V_{\text{tot}})$ , which is related to the lower bound on  $n_p$  from equation (3.113) can be seen in 3.6.

In light of this, we can also use our above theory to produce parametric plots of average number of drivers against the logarithm of the population size: the latter quantity is a lower bound on the number of cell division events, and hence also on the number of potential passenger mutations. There is still a qualitative difference between the predicted curves for the linear fitness increase and the fitness increase with a sharp plateau: if selective sweeps occur late, we see a convex curve. If they occur early, we see a warped sigmoidal curve.

However, this approach has the problems that it leaves aside the actual detection of driver mutations themselves, and furthermore depends on assuming well-mixed models (which may be justified in some sense: see above) and a constant rate of appearance of passenger mutations as do most versions of molecular clocks and coalescent theory. Extensions of structured population models and the stochastic model underlying ours here are clearly necessary to make the connection to this experimental observable.

## Chapter 4

# Resistance to low-dose combination chemotherapy

### 4.1 Background

The main areas of interest in this thesis are simple models of population-level behaviour of evolving cancers. We have attempted to derive predictions for growth curves and the pace of evolution, especially from models which can be related to the biophysical properties of individual cells. In relation to this, the questions of how quickly cancers can evolve, and how this is affected by migration and invasion are needed to understand how quickly a metastatic cancer can gain a mutation which enables it to resist a specific type of therapy. One application and opportunity for testing our work can be found in clinical studies of the incidence of resistance to chemotherapy. We contributed analytical techniques and offered a number of possible interpretations of the results of a clinical study on the resistance to combined chemotherapy in pancreatic adenocarcinoma.

The usually accepted therapeutic regimen is the maximally tolerated dose concept: the highest possible non-lethal dose of a cytotoxic chemical is administered, the purpose being that since the cytotoxin is usually chosen to kill cells at the point of mitosis (division), it will have a disproportionately large effect on the cancer cells, which divide more often than normal cells. Administering the maximally tolerated dose attempts to kill off more of the cancer cells than normal cells, which are also inevitably affected. Of particular note are cells of the intestinal lining and some immune cells, which have an especially short cell cycle.

Although for many cancers, this treatment regimen has represented a significant advance in survival and recovery, pancreatic cancer has stubbornly resisted improvements in outlook after many attempts at devising an effective therapy. In large part, this is due to the location of the pancreas. Cancers of internal organs tend to have longer periods during which they are effectively asymptomatic before detection, and reach a stage at which they have several metastases by the time they are detected. Pancreatic cancers are usually inoperable by the time they are detected and diagnosed, and treatment is generally palliative [101]. The search for more effective treatments, and the twin search for the reasons for previous treatment regimens' shortcomings, is an area of intense research. Progress in the field has been slow, with extended periods in which no new treatment regimen showed any clinically significant improvement [102].

In the early 2010s, combinations of multiple drugs administered at maximally tolerated doses in the same course (megadose combination chemotherapy) were found to have better outcomes than single drug maximally tolerated dose (MTD) regimens, which constituted the first significant improvement in more than a decade [102]. However, this and subsequent improvements are still

ultimately palliative, and in most cases the disease ends in relapse and eventual failure. Median overall survival is rarely longer than a year [102, 103]. This resistance was hypothesised to be due to the presence of some small population of cells with some mutation which conferred resistance to the drug combinations that were explored. When the treatment was applied, there was a strong selective pressure for these subclones to expand, and outpace the susceptible population [104, 105]. In a straightforward evolutionary process, the cancer acquires resistance and regrows. If this hypothesis were true, it should be very unlikely that resistance to many different chemotherapeutic agents with different mechanisms of action could evolve by this mechanism. The chances that a single mutation could confer resistance to many different drugs at once are, at least in theory, very small [105].

To test this theory, a novel multi-drug therapy at lower doses than MTD or megadose combination chemotherapy was designed and tested by Dr. L.A. Diaz. We developed a simple mathematical model for observations of antigen concentrations, and measures of survival compared to the parameters of this mathematical model. In addition, and of particular relevance to this thesis, the inferred frequency of resistant subclones could also be analysed with this model, which was used to make some comments about the potential mechanism and suggestions for future research.

#### **4.1.1 Protocol and mechanisms of action**

Twenty-eight patients were administered the low dose combination therapy over a 21-day cycle, and a further ten patients were administered the same doses over a 28-day cycle. Four cytotoxic agents were administered in cyclical succession: gemcitabine, docetaxel, capecitabine, and cisplatin. The combination was selected due to the clinicians' previous experience with similar combinations in megadose therapy (gemcitabine, docetaxel and capecitabine) and for the heterogeneity of the combination of four. Both the mechanisms of action and chemical structures are, on the whole, very different, which should in theory minimise the chances of cross-resistance emerging. To see how, it is worthwhile to quickly review some of what is known about the pharmacology of the drugs in question.

Of the four drugs that were used, capecitabine and gemcitabine deserve some mention as having the most similar mechanisms of action as well as some structural similarities. Both chemicals interrupt the synthesis of DNA, in capecitabine's case by metabolism to the molecule 5-fluorouracil (5-FU), which also happens to be synthesised and administered as a distinct chemotherapeutic agent. After metabolism to 5-FU, the 5-FU binds to thymidilate synthase, which prevents it from carrying out its normal function of synthesising thymidine [106]. Thymidine is necessary to produce thymine, one of the base pairs and "building blocks" of DNA, and without it cells are unable to replicate, resulting in what is known as thymineless death [106]. Gemcitabine, on the other hand, is incorporated into the DNA strand during synthesis after being phosphorylated, which results in an irreversibly "broken" DNA strand being produced, and DNA synthesis is effectively "aborted" [107]. Both capecitabine and gemcitabine interfere with DNA replication, and are both fluoridated nucleoside analogues. They therefore both have similar uptake routes, being transported into the cell along the same pathways as nucleosides, such as hENT1 [108, 109]. Cross-resistance for these two would not be especially surprising.

Docetaxel, by contrast, binds to microtubules rather than interfering with DNA synthesis. Cell division cannot continue without replicated DNA and other components being separated into the new pair of daughter cells by microtubules, and so docetaxel blocks cell division [110]. Docetaxel is transported into cells across cell membranes by a number of distinct transmembrane transporter in the solute carrier family [111], and is structurally a taxane. It is a considerably larger molecule than capecitabine or gemcitabine [112].

Finally, cisplatin directly damages DNA, which triggers cell death by apoptosis as cells progress through the cell cycle [113]. As cancer cells progress through the cell cycle with fewer checks and balances on their activity, they are theoretically more strongly affected and killed more than normal

cells, in a similar statistical way to other chemotherapeutic agents. Cisplatin is a small molecule and an inorganic compound, in contrast to the other drugs in the combination which are as a rule organic. The molecule only becomes toxic as such when the chloride groups are replaced with water molecules (aquation), which happens essentially as soon as the molecule enters the cytoplasm, having been transported into the cell [113, 114]. Cisplatin is transported into cells via similar routes to other metal-based small molecules and ions, by the transmembrane pump copper transporter 1 [115]. Resistance to cisplatin in pancreatic cancer is quite common, with some fraction of the cancer cell population appearing to acquire resistance during the course of therapy, and many patients intrinsically resistant to cisplatin from the start [113]. Both of these observations will be returned to shortly, but it should be emphasised that the mechanism of action, uptake pathway, and chemistry of cisplatin are all quite distinct from any other drug in the combination.

With the possible exception of gemcitabine and capecitabine, these agents have widely different mechanisms of action and pharmacology. By design, just as the components of cellular machinery that interact with and are damaged by each drug have relatively little in common, mutations that alter one piece of this machinery are unlikely to have an effect on different components. In this way, the likelihood of cross-resistance emerging is supposed to be minimised. All of the patients were newly diagnosed and had had no previous treatment for the disease, and so there should be no selective pressure for resistance before their treatment. The drug combination was in evolutionary terms essentially novel, and pre-existing resistance should have been exceptionally unlikely.

## 4.2 Analysis

Over the course of the therapy, concentrations of the tumour marker CA19-9 in the bloodstream, an antigen associated with pancreatic tumour masses, were measured at 3 week intervals. CA19-9 is an antigen, a molecule that the immune system “recognises” and responds to [4], which is often used as an indicator of the sizes of tumours and the effect of therapy [116]. Measuring concentrations of a known molecule in the bloodstream only involves a blood test, rather than a medical imaging scan, which would be a more direct method of measuring tumour size, and can be performed more frequently and cheaply.

Our goal was to use the measurements of CA19-9 levels to infer the underlying tumour burden, and the proportion of resistant cells present at the onset of chemotherapy. But, as CA19-9 is not a direct measure of tumour size, but rather reflects something more akin to inflammation of the pancreas *due* to the tumour, there are some issues in interpreting CA19-9 levels that have to be addressed. One well-known problem with the use of CA19-9 as a marker is that while it is a highly sensitive indicator of tumour sizes in some cases, it is not very specific overall. Levels can be high when no cancerous cells are present, in cases such as pancreatitis, jaundice, and other inflammatory disorders of the pancreas; and a substantial minority of patients do not express CA19-9 at all [116–118]. The “signal” of tumour size carried by CA19-9 levels is therefore very noisy, and affected by natural variations and the complex inflammatory response of the immune system in ways that are difficult to quantify. Given that useful quantitative measurements of the strength of this “inflammatory noise” do not (to the best of our knowledge) exist, we had to devise some way of classifying the experimental data into sets where the levels could be meaningfully interpreted in terms of tumour burden and sets where the signal was apparently being swamped by noise or was otherwise on the threshold of detection.

### 4.2.1 Immunological noise and over-interpretation

We developed two four-parameter mathematical models, and fitted to the CA19-9 data. The first model was a simple sum of two exponentials,

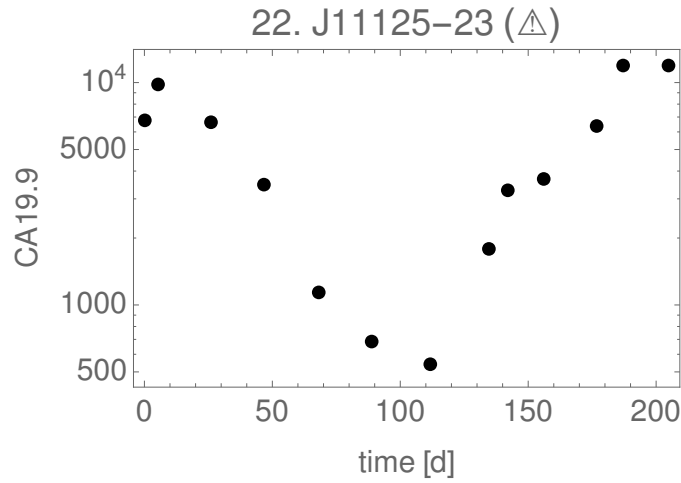


**Figure 4.1** *A plot of a typical CA19-9 concentration during the course of chemotherapy showing two characteristic phases: an initial decline followed by a rebound after a few months. The simplest interpretation of this is that the underlying burden of cancer cells declines, and then regrows. It is tempting to interpret this plot as representing a resistant and sensitive sub-population of cancer cells, but some care must be taken to account for the noisy and fluctuating nature of CA19-9 and its relationship to inflammation (see main text).*

$$c_{\text{exp.}}(t) = ae^{-dt} + ce^{bt} \quad (4.1)$$

which can be simply interpreted as representing the CA19-9 secretion of two sub-populations of tumour cells, one of which is sensitive to the therapy and dies off at some exponential rate  $d$ , and the other of which is resistant to the therapy for one reason or another and regrows at some rate  $b$ . We will henceforth refer to this as the “exponential model”.

This model has a number of plausible motivations. As discussed in Chapter 1, simple exponential growth is a very popular model with clinicians, essentially because it is the simplest possible model, and which in many cases does not disagree with actual observations. Despite the debate regarding which of the many postulated models is the most appropriate for real tumours, we have also seen in Chapters 2 and 3 that exponential growth can emerge even in scenarios when there are complex spatial constraints on the growth of tumours, and when individual lesions grow much slower than exponentially. This can be facilitated by cell migration and local invasion. The escape of cancer cells to distinct, nearby locations can lift constraints on growth that would otherwise force power-law or decelerating growth with some plateau, and permit exponential growth for an extended period of time.

These were all cases of late stage cancers, with several liver metastases visible on CT scans in most (about 80%) cases according to the interpretation of other clinicians working on this study. However, as these patients were all clinically naive, no prior treatments or surgeries had been attempted at this stage, and there was no record of whether or not a histologist had found the surgical margin to be clear, an important prognostic test that would have been performed following surgery and a smoking gun indicator for whether or not the type of local migration we set out to model in Chapters 2 and 3 was occurring [45].

The parameters  $a$  and  $c$  of the multiple exponential model have natural interpretations as proportional to the populations of the sensitive and resistant cell populations, and  $d$  and  $b$  their respective death and regrowth rates. One can calculate the inferred fraction of resistant cells  $f_R$ ,

$$f_R = \frac{c}{a + c} \quad (4.2)$$

and the approximate time-scale  $T$  needed for the tumour to regrow to some lethal size  $N$ ,

$$T = \frac{\ln(N/c)}{b} \quad (4.3)$$

which can be seen to be rather insensitive (in theory) to  $N$  and  $c$  and more sensitive to  $b$ , which is likely to be an important predictor of survival after recurrence.

This exponential model was fitted to each patient’s dataset, and the parameter values used to calculate values for the resistant fraction  $f_R$ . However, whether or not these parameters can actually be interpreted *meaningfully* for a given dataset depends on how “trustworthy” the CA19-9 data is in this case. In some cases, the levels were so low as to be on the threshold of detection, and in others fluctuated so widely that there was no obvious trend. As previously discussed, CA19-9 is associated with inflammation, and the effect of the complex dynamics of the immune system is very difficult to quantify (and quite beyond the scope of this thesis). Some test for how meaningful the signal extracted by fitting the multiple exponential model is necessary, but the exact dynamics of noise are not known, so this test should ideally be independent of specified “noise levels” or detailed postulates about the dynamics of CA19-9 in the absence of cancer (as we are ignorant about both of these). What we want is a relatively systematic way of avoiding over-interpreting data which is known to include some highly complicated confounding processes.

The simple test that we arrived at was to compare the performance of the relatively well-motivated multiple exponential model to a null model with the same number of parameters. If the exponential model had a worse fit to the model than the null model, this was interpreted as it failing to extract meaningful information in this case. Only cases in which the multiple exponential model did better than the null model would be considered as having meaningful interpretations.

The second model, or “null model”, was defined by

$$c_{\text{null}}(t) = \exp(a + bt + ct^2 + dt^3) \quad (4.4)$$

and by design has no meaningful interpretation nor correspondence with other proposed models of tumour growth outlined in chapter 1. It has the same number of parameters as the multiple exponential model, but there is no reason to believe that such a form would be a good model of anything on either an empirical or *a priori* basis.

Cubic polynomials have the property that they minimize the amount of “bending” in a curve or surface, and arise naturally in Euler-Bernoulli beam theory and engineering [65, 119]. Their use as splines, for interpolation between points in a dataset, derives directly from the use of flexible beams (the original meaning of “spline”) to model smooth, mechanically stable curves in shipbuilding [120]. There is no simple mechanism for motivating (4.4) in this way. Perhaps some complex chemical kinetics can turn up something of the correct form after some abuse, but this is more of a post-hoc rationalization than a genuine motivation in the absence of a compelling underlying mechanism.

But it isn’t too difficult to motivate (4.4) without reference to splines. The idea is that higher-order polynomials will provide progressively better models for  $\log c$ . A polynomial will be on equal footing with a more mechanistic model when it has the same number of parameters, so a cubic polynomial is the natural null choice for comparing to a four-parameter mechanistic model.

As there is no reason to expect this model to accurately reflect the data except coincidence, any dataset to which the null model had a better fit than the multiple exponential model (as quantified

by reduced chi-squared statistic) was considered to be swamped by immunological “noise” or else was on the threshold of detection. We consider datasets to be swamped by this noise if

$$\chi_r^2(\text{exp.}) \leq \chi_r^2(\text{null}) \quad (4.5)$$

and are therefore over-interpreted by the exponential model, thus “failing”, and otherwise are considered to “pass”. We should emphasise that this is a test of how plausible and trustworthy the exponential model is for a given dataset, and not a test for noise in the underlying data itself.

This difference-in- $\chi_r^2$  test came the closest of several candidate tests to being independent of quantitative thresholds, which due to empirical ignorance would necessarily be arbitrary. This allowed us to comment on which datasets were “reliable” and which were over-interpreted by the multiple exponential model.

#### 4.2.2 Theoretical fraction of resistant cells

The theory that motivated the therapy and allowed relatively precise estimates of the probability that multi-drug resistance could emerge by cells’ acquiring several independent neutral mutations, was developed by I. Božič, T. Antal *et al.*. It is formulated in terms of branching processes, and is essentially a generalization of the Luria-Delbrück model of evolution to include cell death, which is an important complication in the case of cancer cells [105, 121, 122].

From the theory of branching processes, the fraction of resistant cells that appear before therapy (while these mutations are neutral)  $f_R$  depends on the point mutation rate  $p_\mu \approx 10^{-9}$  (for most cancers [105]), on the number of different mutations that can result in resistance to a given drug  $n_i$  or to several drugs simultaneously  $n_{ij\dots}$ , and (weakly) on the size of the tumour at the start of therapy  $N$ . In the case of two drugs, labelled 1 and 2, for which there are  $n_1$  and  $n_2$  possible mutations that cause resistance to each alone and  $n_{12} = 0$  (no possible mutations that cause cross-resistance), the expected fraction of resistant cells at the start of therapy  $f_R$  is on the order of

$$f_R \approx (\log(N))^2 n_1 n_2 p_\mu^2 \quad (4.6)$$

neglecting other pre-factors of order 1 that arise in the detailed theory [105]. When there are  $n_{12}$  mutations that can cause cross-resistance,  $f_R$  is instead

$$f_R \approx \log(N) n_{12} p_\mu \quad (4.7)$$

which is much larger. Suppose upon the start of treatment that a tumour consists of  $10^{10}$  cells, and only 1 mutation can confer resistance to each drug, but there is no cross-resistance mutations:  $f_R$  is then  $\approx 5 \times 10^{-16}$ , a fraction so small that we should never see cross-resistance emerge in this way. If instead there is one mutation that can confer cross-resistance,  $n_{12} = 1$ , then  $f_R \approx 2 \times 10^{-8}$ , and we can expect around 100 cross-resistant cells to be present in the tumour.

Even if some cross-resistance, in particular between capecitabine and gemcitabine, could plausibly be granted by one mutation, the therapy still makes use of three distinct classes of drugs which are heterogeneous enough that no single mutation should grant cross-resistance. In theory,  $n_{1234} = 0$ , calling gemcitabine and capecitabine drugs 3 and 4, let  $n_1 = n_2 = 1$  and  $n_{34} = 1$ , and we have

$$f_R \approx (\log(N))^3 n_1 n_2 n_{34} p_\mu^3 \approx 10^{-23} \quad (4.8)$$

so that, again, cross-resistance should essentially never happen. Really, the different numbers of possible mutations  $n_i$  are not precisely known, and may well be much larger than 1. Pessimistically, if  $n_1 = n_2 = n_{34} = 1000$ , then

$$f_R \approx 10^{-14} \quad (4.9)$$

which is still so low compared to the number of cells present that it should - in principle - never be observed.

Let us summarise the working hypothesis underlying low-dose combination chemotherapy in simple terms: if there are no mutations which confer cross-resistance to all 4 drugs simultaneously, and all relevant mutations are selectively neutral prior to therapy, and resistance can only be acquired by the appearance of genetic mutations, then  $f_R$  should be unmeasurably small. If it is not unmeasurably small, at least one of these postulates has to be wrong.

## 4.3 Results and discussion

### 4.3.1 Inferred fraction of resistant cells

Out of all 38 datasets analysed, 19 were rejected: about half. This is what we might expect if both models had equally bad fits to datasets with a very low “signal-to-noise ratio”. However, there are qualitative differences in the shape of datasets which show a clear decline and regrowth phase, and those with CA19-9 concentrations so low as to be on the verge of detectability (such as patients 3, 5, 10 and 33, figures 4.2 and 4.3). Many of the datasets which were rejected as noisy by the difference-in- $\chi_r^2$  test were indeed qualitatively noisy, or had flat CA19-9 concentrations on the lower limit of detectability. On the other hand, some datasets that we expected to pass the test did not, such as patients 7 and 8 (see figure 4.2). This difference between the qualitative shape and results of the quantitative test may be due to the fact that the null model can more easily fit wildly varying large concentrations than the exponential model, and more datasets are rejected than would be under a more specific test. However, some advances in dynamical models of inflammatory responses are required before a well-founded test to distinguish immunological noise can be developed.

The median length of time that patients survived before succumbing to their recurrent cancer, or median overall survival, was 13 months. Individual overall survival was found to be closely correlated to the relapse time calculated from equation (4.3) having set the unknown “tumour size at relapse”  $N$  to be equal to the initial CA19-9 concentration  $a + c$ . The time to relapse is closely related to the regrowth rate  $b$ , but not very sensitive to the tumour size at relapse  $N$ , depending on it only logarithmically. That equation (4.3) should be a decent predictor of the actually observed relapse time is not especially surprising from a mathematical perspective, but bears mentioning as the clinicians on the study found this to be practically useful.

Although the clinicians who participated in the study found the multiple exponential model’s measurement of the regrowth rate  $b$  very useful, the applied mathematicians and biophysicists were more interested in the inferred fraction of resistant cells,  $f_R$ . Since one of the motivations for this combination was to minimise the likelihood of cross-resistance, the inferred fraction of resistant cells is an indicator of the proportion of cells that are cross-resistant at the start of therapy, and measurement of  $f_R$  can provide a stringent test of the working hypothesis that cross-resistance arises from purely evolutionary means. That is, it is acquired by novel genetic mutations and requires several distinct genetic mutations (to the different pathways relevant to the distinct mechanisms of action of each drug).

The inferred fraction of resistant cells  $f_R$  varies substantially between patients (see figure 4.4), but

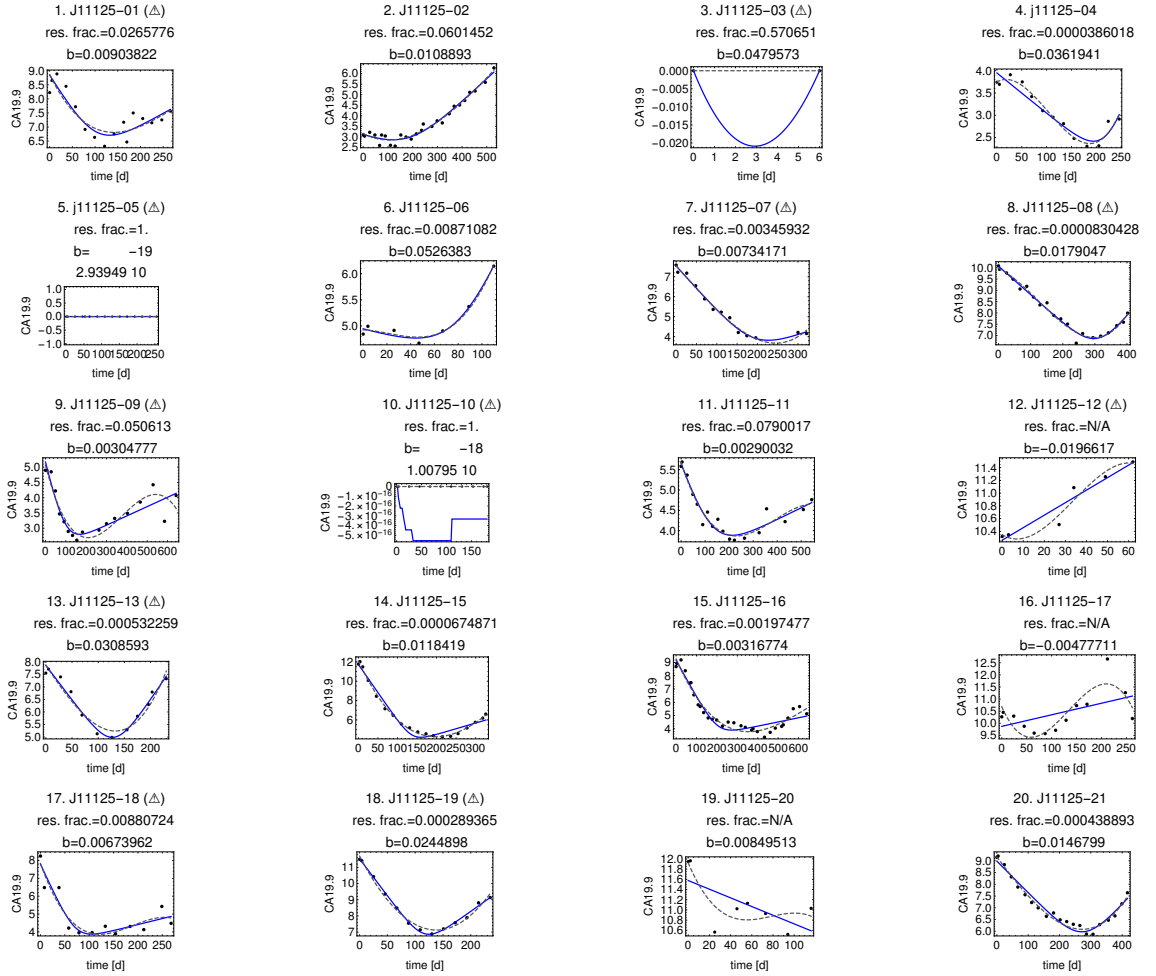


**Figure 4.2** *Plots of CA19-9 levels in patients 1 — 20, showing the best fit for the multiple exponential model (blue curve) along with the inferred resistant fraction  $f_R$  and regrowth rate  $b$ , and the best fit for the null model (grey dashed curve). Cases in which the multiple exponential model had a worse fit than the null model (failing our test for over-interpretation) are labelled with warning signs.*

in all cases was many orders of magnitude higher than theoretically expected. The lowest value observed was  $3.4 \times 10^{-7}$  (patient 25, see figure 4.4, and 4.3), while the highest values were 1 (i.e. all cells seemed to be resistant, patients 12, 25 and 26), although we should point out that for many of these particularly high values, the multiple exponential model fails our test for over-interpretation. The highest value of  $f_R$  for which the multiple exponential model was considered meaningful was  $7.9 \times 10^{-2}$  (patient 11, see figure 4.2), which is still many orders of magnitude higher than was theoretically expected. Median values of  $f_R$  and  $b$  were  $2.98 \times 10^{-3}$  and  $1.44 \times 10^{-2} \text{ day}^{-1}$  respectively. If we restrict this analysis to the datasets for which the multiple exponential model did not fail our test for over-interpretation of noise, we instead find  $3.99 \times 10^{-4}$  and  $2.46 \times 10^{-3} \text{ day}^{-1}$ .

Other research on multi-drug resistance also estimates  $f_R$  to be much higher than what one would expect on the basis of the above working hypothesis, in the range  $5 \times 10^{-5}$  to  $3 \times 10^{-4}$ , consistent with our inferences from the best-fit model parameters above [123]. However, it is important to note that this study analysed resistance to two drugs only, erlotinib and crizotinib, two protein kinase inhibitors which have very different mechanisms of action to any in the combination studied here. In fact, these drugs target specific signalling proteins, whereas the combination chemotherapy analysed here is much less selective.

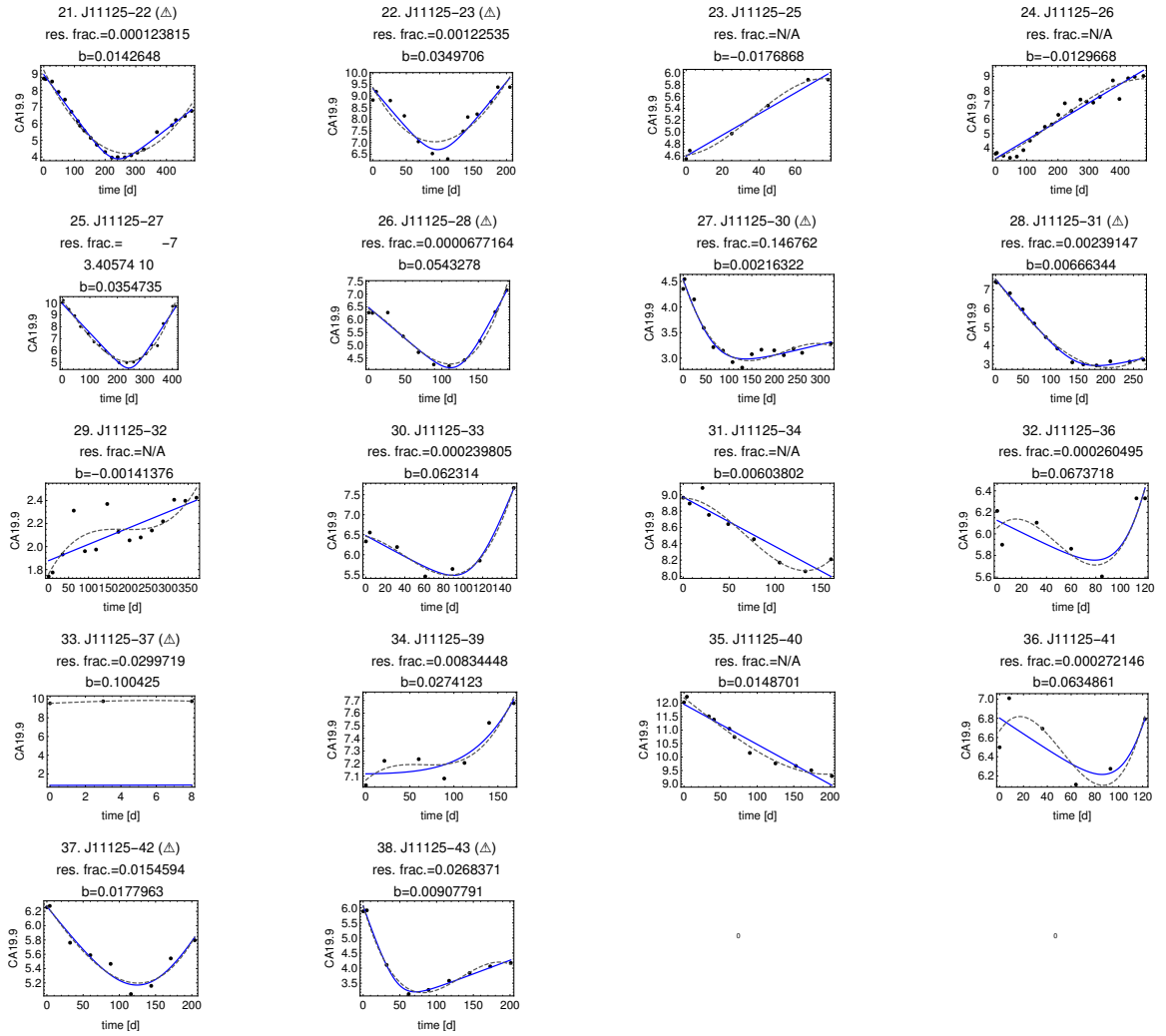


**Figure 4.3** Plots of CA19-9 levels in patients 21 — 38, showing the best fit for the multiple exponential model (blue curve) along with the inferred resistant fraction  $f_R$  and regrowth rate  $b$ , and the best fit for the null model (grey dashed curve). Cases in which the multiple exponential model had a worse fit than the null model (failing our test for over-interpretation) are labelled with warning signs.

As  $f_R$  was clearly not unmeasurably small, and the disease recurred in a resistant form in the majority of cases, it must be the case that at least one of the postulates underlying the working hypothesis behind the therapy is wrong. Either there *is* in fact a mutation which can confer resistance to all four drugs simultaneously, the relevant single-drug resistance mutations are not selectively neutral prior to therapy, or cells can become resistant without having acquired genetic mutations, or some combination of the above. We shall explore each of this possibilities in turn.

### 4.3.2 Molecular mechanisms of single-drug resistance

Before considering possible mechanisms of multi-drug resistance that can arise from a single mutation, let's review some of what is known about mechanisms of single-drug resistance, as it is a simpler case which can inform and constrain our discussion of the possible mechanisms of cross-resistance. As cisplatin resistance is very common when used in isolation [113], and cisplatin is the best studied of the drugs in the combination, we will focus primarily on the mechanisms of

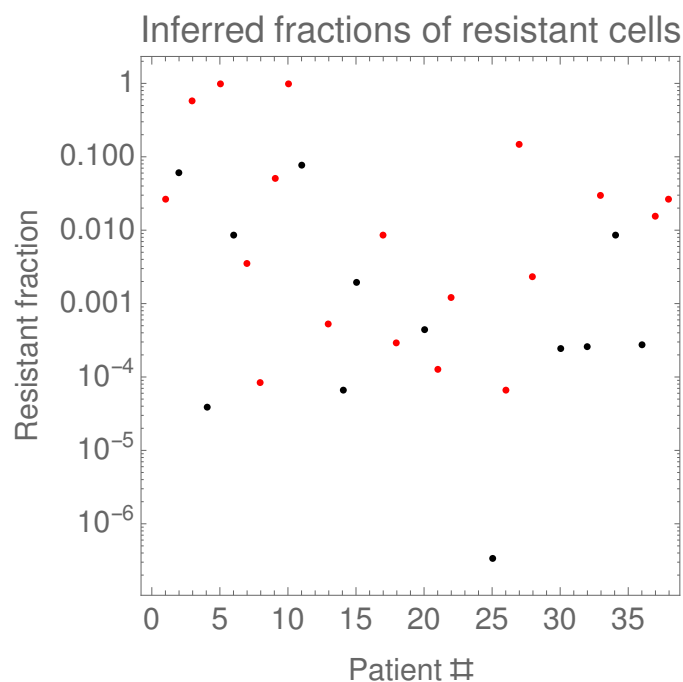


**Figure 4.4** *A plot of the inferred fractions of resistant cells for each patient. Only those datasets for which  $f_R$  was well-defined were plotted. Fits which failed our test for over-interpretation are represented by red points, fits that passed are represented with black points. Note the logarithmic scale: the range of observed values spans several orders of magnitude.*

action and transport into and out of the cell.

Cisplatin’s primary mechanism of action as an anticancer agent is by damaging DNA. This triggers a DNA damage response in the cell’s signalling pathways, inducing apoptosis (programmed cell death) [113]. Before any damage can be done by cisplatin’s reaction with the DNA itself, it must be present in the nucleus of the cell [114]. It is also only activated by a reaction with the cytoplasm [114]. It therefore has to have been transported into the cell sufficiently quickly (and out sufficiently slowly) that it has an appreciable concentration inside the cell [115]. Examples of uptake and efflux pathways are via copper transporter 1 (CTR1) and MRP2, one of the ATP-binding cassette (“ABC”) transporters [113, 115]. Resistance to cisplatin can therefore consist of a reduced response to DNA damage, decreased activation of the cisplatin complex by aquation, and lower concentrations of cisplatin inside the cell by modified uptake and efflux [113, 115].

Changes in efflux mediated by the ABC transporters like MRP2 have been studied for some time, due to the potential importance of these transporters as markers for responsiveness to therapy and as potential targets of new drugs [124]. At one time, they were even thought to be almost exclusively responsible for the emergence of multi-drug resistance [125]. However, although inhibitors of ABC transporters do reduce chemoresistance to a degree, they do not have a very strong affect with regards to restoring cells’ sensitivity to cisplatin. As a result, it is suspected that other factors must be involved in the development of cisplatin resistance. Either other efflux pumps insensitive to the inhibitors tested, or changes in uptake and action in the cell [126].

Evidence for CTR1’s role in cisplatin uptake seems more straightforward, and includes:

- Mice in which the transmembrane pump CTR1 has been knocked out are much more resistant to the cytotoxic effects of cisplatin [127].
- Cells with higher than normal copper concentrations (copper shares an uptake pathway with

cisplatin, CTR1) are more resistant to cisplatin [128].

- Cells with lowered copper concentrations are more sensitive to cisplatin [129].

All of which seems to indicate that CTR1 transports cisplatin into the cell, and less cisplatin is transported when CTR1 is absent or busy.

Finally, changes in signal transduction pathways could provide a way for cancer cells to continue to survive and divide even in the presence of high concentrations of cisplatin. Out of a preponderance of partially understood mechanisms, the ability of cells to divide in the presence of DNA damage by inhibiting apoptosis [113] and the ability of all cells to break down and recycle individual damaged components, autophagy, bear particular mention [130]. A mutation in one of the protein kinases that triggers apoptosis (programmed cell death) could plausibly result in a line of cancer cells which doggedly divide even with cisplatin-damaged DNA, although we should note that this mechanism of resistance is specific to cisplatin's mode of action. Autophagy, on the other hand, is a non-specific response to stress that is latent even in normal cells, and though its relevance to cisplatin resistance is not well understood, there are results which indicate that there is an inverse relationship between cisplatin resistance and the inhibition of autophagy [113, 130].

To summarise, proposed mechanisms that may contribute to cisplatin resistance include increased efflux and cisplatin removal from the cell, decreased uptake of cisplatin into the cell, and weakened cellular response to DNA damage and toxicity.

### 4.3.3 Possible mechanisms of cross-resistance

As this is the first time that this specific combination has been tested clinically, and consequently the first time that cross-resistance to the four agents involved has been observed, the mechanism behind this resistance is basically unknown and as a result we can at present only speculate as to its true nature. On the basis of the stochastic theory of Antal, Božič and others, the cross-resistance is extremely unlikely to be due to cells' acquiring multiple independent mutations by virtue of the heterogeneity of the drugs' mechanisms of action [105, 121]. However, the anomalously high fractions of resistant cells  $f_R$  can be explained in principle by there being many different mutations which can provide resistance to individual drugs, with  $n_i$  on the order of  $10^4$ . Given present uncertainties about the mechanism of action of several of these drugs, this possibility cannot be conclusively ruled out at this time.

Besides invoking such high values of  $n_i$ , the alternatives to the working hypotheses underlying this prediction can be tentatively sorted into two groups: mechanisms which involve cross-resistance being *acquired* by one (or very few) novel mutation, and mechanisms in which a sub-population of cells in which a latent *intrinsic* resistance is activated without requiring new genetic alterations as such. The heterogeneity in structure, transport pathways, and mechanisms of action between the drugs in the combination makes it unlikely that a mutation affecting one transport protein, or indeed any one of the specific mechanisms or cellular responses to each drug will result in resistance to others in the combination. A mutation that allows cells to avoid apoptosis triggered by cisplatin's damage of cellular DNA seems unlikely to have any relevance to the formation of microtubules blocked by docetaxel, for example. This presents a difficult puzzle to attempts to explain the observed frequencies of cross-resistance in terms of either acquired single mutations or intrinsic cellular responses. We will first discuss possible mechanisms of *acquired* cross-resistance (caused by mutations), and then discuss different mechanisms of *intrinsic* cross-resistance (not caused by mutations as such).

**4.3.3.0.1 Acquired resistance** One possibility for cross-resistance to be acquired by a single mutation is if there were a protein kinase that interacted with every drug's uptake and efflux pumps, perhaps downregulating the uptake pumps and upregulating the efflux pumps, acting as

part of a signal transduction pathway that is activated during a relatively non-specific cellular response to toxicity and stress. When this protein kinase was activated by another above it in the pathway, the effect of its simultaneously closing many intake transporters and opening many efflux transporters would be a kind of emergency evacuation of cytotoxins from the cell, as though an alarm had been sounded. A mutation which caused this kinase to take on its active conformation all the time would lead to broad changes in membrane transport, which would be consistent with cross-resistance. This hypothetical “alarm kinase”, if it exists at all, may be some undiscovered molecule yet to be characterised, or may simply be a hitherto obscure function of a protein that has already been partially characterised in the literature. In either case, there are some simple criteria that this protein kinase would have to meet:

- It should be sensitive to cytotoxic stress on the cell (possibly associated with inflammation, autophagy or the heat shock response)
- It should interact with many different pump and transporter proteins or should be “upstream” of them in many distinct signalling pathways
- The mutated protein should lose the specificity to stress but interact with transport proteins similarly

The existence of such an alarm kinase could provide one mechanism for cells to acquire broad cross-resistance with a single mutation. This single mutation would plausibly be neutral in the absence of combination chemotherapy, as there would be no selective advantage associated with excluding high concentrations of cytotoxins in this case. We should emphasise, nonetheless, that this is speculative. A single neutral mutation could arise through chance as in the branching process theory developed by Antal et al. detailed above in section 4.2.2, or else could arise as a genetic hitch-hiker [121].

While we are not aware of any one protein kinase that definitely satisfies all of the above criteria, after surveying the literature the best educated guess as to the identity of this alarm kinase that we were not able to conclusively rule out was JNK1 (also known as MAPK8). JNK1 is a signalling protein which is associated with stress and inflammation, interacts with several distinct signalling pathways, and there are results suggesting that activation of JNK1 is associated with drug resistance and conversely that inhibition of JNK1 is associated with reversal of resistance [131, 132]. Furthermore, JNK inhibition also results in P-glycoprotein (or MDR1), an important efflux pump, being downregulated, which sensitizes some lines of cancer cells to cisplatin, one of the drugs in the combination [133]. However, these results should be interpreted cautiously, as there is at least one contrary experimental result in the literature, and it may be the case that the specific cancers and cell lines studied are not representative of the specific type of cancer in our own study [134]. We are also not aware of any results regarding common mutated forms of JNK1, in particular whether or not mutants are permanently in the “active” conformation: continual failure to identify any single mutant protein kinase associated with cross-resistance would strongly suggest that the alarm kinase hypothesis was false.

While there are other conceivable ways that multi-drug responses can arise without such an alarm kinase, it does provide a simple explanation for the non-specific (in that several very different drugs are involved) but unified (in that they are all cytotoxic and resisted by the cell *somehow*) response observed in this study.

Alternatively, it may be the case that several distinct mutations are indeed required, but for some unknown reason are not neutral before the therapy is applied. This would throw out the framework in section 4.2.2 and fractions of resistant cells may be much higher, perhaps approaching fixation (that is,  $f_R \approx 1$ ). While it seems unlikely to us at first glance that alterations in the specific mechanisms of uptake, efflux and the targets of four specific drugs should also have some adaptive selective advantage in the absence of these drugs, enough is unknown about them that this cannot be conclusively ruled out — for example, modified efflux pump activity could be a side-effect of

an advantageous mutation controlling proliferation via some complex gene-gene or protein-protein interactions. Furthermore, this explanation does not need hypothetical uncharacterised functions of protein kinases to be invoked.

Either hypothesis - that resistance is acquired through the mutation of a single alarm kinase, or several independent drivers - would be conclusively falsified by demonstrating that cross-resistance could be induced in a line of cancer (or indeed normal) cells without any additional mutations. This would indicate that cross-resistance was an intrinsic response, rather than acquired.

**4.3.3.0.2 Intrinsic resistance** It may also be the case that resistance to several drugs at once can be induced in otherwise genetically normal cells, or simply that the drugs fail to have an effect for reasons unrelated to genetic alterations. This class of possible mechanisms attempt to explain the anomalously high resistant fractions in terms of intrinsic resistance. Cells resist the effect of the drug combination without inheriting the ability to do so as such, due to differences in regulation of normal genes or in their microenvironment.

Perhaps the simplest way in which this kind of apparent “resistance” can come about is by poor vascularization. If there is very poor penetration of the tumour by capillaries, drugs present in the bloodstream will find it difficult to reach high concentrations in the tumour cells by diffusion from the bloodstream alone. Poor vascularization, and the associated depletion of oxygen around these areas of the tumour, is known to be a factor in multi-drug resistance, but may be mediated by more complex cellular responses (e.g. involving ABC transporters) rather than the simple fact that less agent will be present [125].

Another way that cells could develop resistance to the combination of drugs is if there were a latent response to exclude cytotoxins from the cell by altering membrane transport, and this latent response was activated by signals from other cells. This generic response to cytotoxicity could possibly be triggered by the activation of an “alarm kinase”, but the possibility of this being controlled by a less centralised pathway cannot be ruled out. This class of mechanisms could work in concert with acquired resistance. The effective number of resistant cells can be amplified substantially, and one resistant cell could “shield” a number of other sensitive cells from the effects of the therapy by activating a latent intrinsic response.

It would be desirable to make some quantitative predictions as to how many sensitive cells could be shielded by one resistant cell by such a mechanism. The observed  $f_R$  of around  $10^{-4}$  would then be determined by the product of the underlying tiny core population of truly resistant cells  $f_R^*$  and this shielding ratio,  $S$ . The tiny resistant core  $f_R^*$  could take on some small value consistent with T. Antal and I. Božić’s theory based on branching processes, say  $f_R^*$  in the range  $10^{-14} - 10^{-8}$ , and since

$$f_R = f_R^* S , \quad (4.10)$$

then values of  $S$ , the number of sensitive cells shielded by one cell in the resistant core population, would then have to be at least  $10^4$  or larger to account for clinical observations. To understand whether or not this is an achievable value of  $S$ , we will have to look at more explicit models of signalling mechanisms.

First, consider the case that this latent resistance is activated by the diffusion of a small molecule such as a cytokine. The molecule is produced by the core resistant population, diffuses through the surrounding sensitive cells, triggering their latent intrinsic resistance program, and gradually breaks down over time (see figure 4.5 for an illustration). If this molecule is only produced by core resistant cells, is not transported actively, having a diffusion coefficient  $D_c$ , and has a degradation rate  $\lambda$ , then its steady-state concentration in the tumour  $\rho_c$  obeys the simple differential equation

$$D_c \Delta \rho_c - \lambda_c \rho_c = 0 \quad (4.11)$$

outside the core population of cells from which it is released. While one can explicitly solve this equation analytically in a few cases (such as one dimension, spherical symmetry, *et cetera*), we won't reproduce exact solutions here. Instead, we will be satisfied to observe that solutions of equation (4.11) have a characteristic length scale  $L_c$

$$L_c = \sqrt{\frac{D_c}{\lambda_c}} \quad (4.12)$$

which can be interpreted as the effective distance that the signalling molecule can travel before breaking down. A single resistant cell can then shield sensitive cells in a volume on the order of  $L_c^3$ , and so if a typical cell has size  $d_{\text{cell}} = 10 \mu\text{m}$ , the shielding ratio  $S$  will be

$$S = \left( \frac{L_c}{d_{\text{cell}}} \right)^3. \quad (4.13)$$

Many cytokines have diffusion coefficients on the order of  $10^{-6} \text{ cm}^2\text{s}^{-1}$ , and degradation rates on the order of  $10^{-3} \text{ s}^{-1}$ , which correspond to  $L_c \approx 300 \mu\text{m}$  [135, 136]. Via equation (4.13), given a cell size of around  $10 \mu\text{m}$ , this corresponds to a shielding ratio of  $S \approx 3 \times 10^4$ , the correct order of magnitude for this to be a viable explanation. While far more research would have to be done to exclude other explanations, this simple argument shows that shielding of sensitive cells by resistant cells is not ruled out by what is currently known about the dynamics of cell signalling.

The hypothesis that cytokine signalling could result in cross-resistance, which is at first glance compatible with current experimental knowledge, could be ruled out by demonstrating the presence of cross-resistance in the absence of signalling by cytokines or other small molecules, perhaps with a knock-out or inhibition experiment (on mice) [137].

Larger shielding ratios can be achieved with other signalling mechanisms. Rather than being mediated by a small signalling molecule, cells are able to transmit signals by coming into biochemical contact with cells they are adjacent to. Conformational changes in receptors on the membranes of two adjacent cells can trigger signalling cascades when they come into adhesive contact [4] (see figure 4.6). A given signal can then propagate through a population of connected cells in a wavelike manner, with characteristic speeds, in which newly activated cells on the wavefront trigger a new front of cells in front of them. Wavelike phenomena in tissues are well-attested, and the activation patterns associated with them are readily monitored by tracking second messengers such as calcium [138, 139].

Shielding models based on wavelike propagation differ from models based on diffusion of a small molecule in the crucial regard that the distance the signal can travel is not limited by the degradation of a small molecule. It follows that the number of cells that can be shielded could be much larger. Naively, one might suspect that arbitrarily large volumes of tumour cells could be reached by the signal, but this is probably not the case. The propagation of calcium waves depends on a reliable response of the cells to activation, and occasional random failure of some of these cells due to variability in response (among other imaginable factors) will attenuate the signal.

Although the mechanism underlying the attenuation was not studied in detail, an experiment to measure the distance that calcium-dependent waves could travel before becoming attenuated to the point of undetectability put the attenuation distance at about 1 mm. We should note, however, that this was in a very different type of tissue than ductal pancreatic cancer, and may also be affected by geometry [140]. This places an experimental estimate on the upper limit of shielding range by this mechanism.

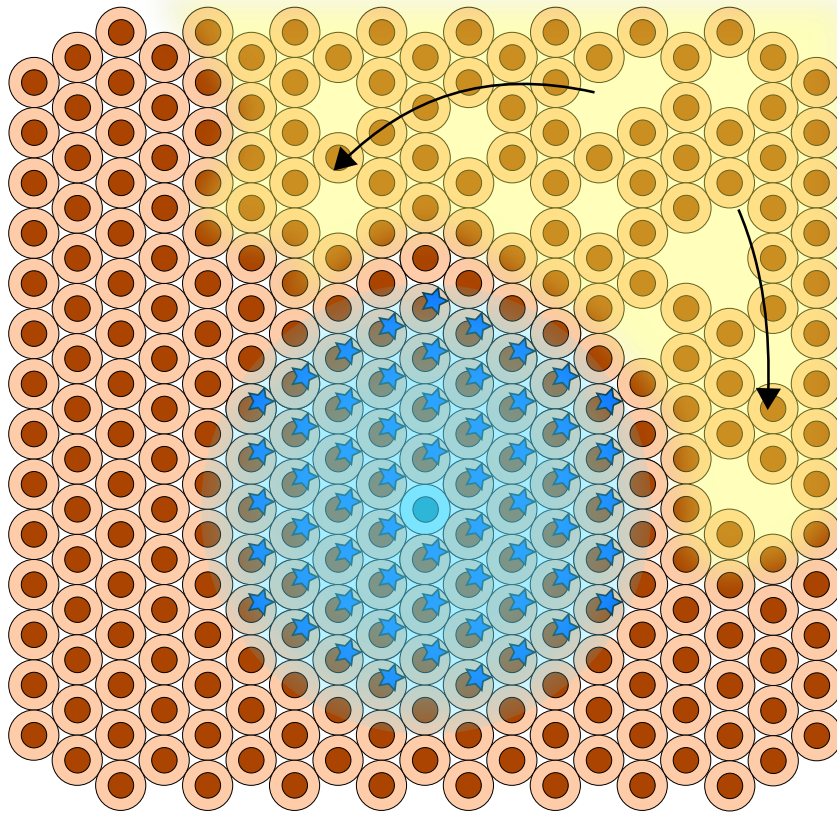


**Figure 4.5** *A diagram showing one possible mechanism by which the apparent number of resistant cells can be much larger than the true number of underlying resistant mutants. Resistant mutants “shield” sensitive cells by producing a small signalling molecule (represented by blue haze), which triggers sensitive cells to alter their transmembrane pump activity in response and slow their uptake of the cytotoxin diffusing across the tumour from top right (represented by yellow haze). The small molecule in question may be a cytokine, and the response related to inflammatory response in normal tissue: CA19-9 is also known to be elevated by inflammation. Resistant mutant cell in blue, sensitive cells with modified uptake/efflux tagged with blue stars.*

An attenuation distance of approximately 1 mm and a typical cell size of 10  $\mu\text{m}$  imply a shielding ratio

$$S \approx \left( \frac{1 \text{ mm}}{10 \mu\text{m}} \right)^3 = 10^6 \quad (4.14)$$

via equation (4.13). This is indeed much higher than in the small-molecule proposal.

In order to actually test this possibility, at least one candidate molecule and an interesting novel prediction are in order. The current experimental literature on calcium-dependent signalling in cancer seems to point to IP3R as another important second messenger in these pathways, but plays such diverse roles even in normal tissues that its presence wouldn't be specific to this proposed mechanism [141]. An alternative candidate, which transmitted signals from cell to cell via gap junctions, is Connexin-42. If it is the case that wavelike signalling is behind cross-resistance, then the fact that regions which can be reached by these waves must be spatially contiguous could be used to exclude this hypothesis. If only one spatially connected region of a tumour was found to have established multi-drug resistance, this would be consistent with the wavelike hypothesis; whereas if many distinct regions were found to have independently established cross-resistance or it was otherwise diffused throughout the tumour in a way not obviously related to space, this would effectively rule out wavelike signalling as responsible.

The fact that the resistant subpopulation regrows exponentially seems to suggest that well-mixed, and therefore spatially diffuse growth of the resistant subpopulation is occurring. However, it is not possible on the basis of our clinical data alone to rule out the possibility that this is due to the resistant population being well-perfused and growing exponentially albeit in a spatially limited region. An experiment which could detect cross-resistant regions and comment on their topology, perhaps via advances in medical imaging or analysis of tumour biopsies, could provide a stringent test of this hypothesis.

## 4.4 Concluding remarks

Despite positive remarks about our mathematical model's usefulness from practising clinicians who organised and carried out the experimental work of the study, the inferred fraction of resistant subclones  $f_R$  was several orders of magnitude higher than what was expected on the basis of a mathematically rigorous theory that assumed as little as possible about unknown biology. This inconsistency between the experimental result and the theoretical prediction indicates that at least one of the postulates of the underlying theory is wrong, a very surprising result which presents a major interpretative challenge.

The relevant postulates of the mathematical theory are that:

1. Resistance to chemotherapy is acquired by the accumulation of novel genetic mutations,
2. Several distinct mutations are required, as the mechanisms of action of the drugs do not overlap,
3. The relevant mutations are selectively neutral prior to the application of the therapy.

Different alternative mechanisms can be speculated about as explanations in each case, but much additional research would need to be done to exclude even a few of the abundance of possible explanations. Of particular interest is the possibility of poorly-characterised interactions between known protein kinases bringing about resistance to several agents simultaneously, whether this is by one of these mutating or a yet-to-be-discovered response to toxicity latent even in normal cells.

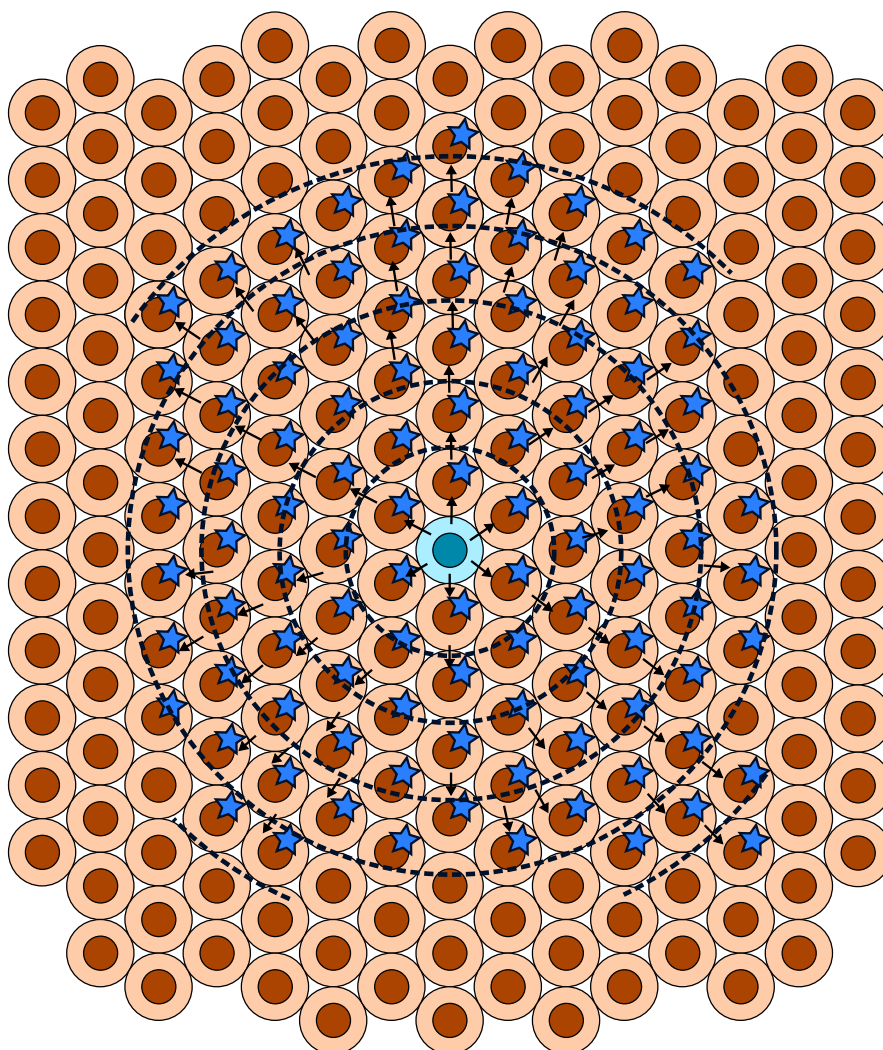


**Figure 4.6** *A diagram showing one possible mechanism by which a small number of resistant mutants can trigger a cascade of resistance in otherwise sensitive cells. A travelling wave of cell-to-cell signalling through transmembrane proteins and tight junctions triggers a change in transmembrane pump activity and slows the uptake of cytotoxin in cells. Candidate molecules that may be associated with this travelling wave are Connexin-42 and JNK1. Mutant cells in blue, sensitive cells with modified uptake/efflux tagged with blue stars, and the travelling wave of resistance to cytotoxin represented by successive wavefronts, dashed black line.*

Each of our proposed mechanisms to explain the anomalously high  $f_R$  can be clarified and made more concrete with educated guesses as to the identity of candidate molecules which may be involved. However, as many of our candidate molecules are known to have many different interactions, many of which are still poorly characterised, experimental evidence that one of them is correlated with cross-resistance does not in itself constitute evidence for our purported mechanism. More stringent tests that could specifically exclude each proposal, and ideally novel predictions of more rigorous quantitative formulations thereof, are necessary to clarify which if any are responsible for the unexpectedly high rates of cross-resistance observed. We have tried to put forward at least one way to experimentally falsify each proposal.

In conclusion, this analysis has highlighted very serious holes in the current understanding of multi-drug resistance in pancreatic cancer, in particular regarding the specificity of cellular responses to cytotoxins, and the possibility of overlapping mechanisms. While it may be the case that one yet-to-be-identified mutated protein can bring about resistance to drugs with widely different pharmacological properties and cellular transport mechanisms, there are a large number of other possible mechanisms by which intrinsic resistance could emerge which cannot be ruled out on the basis of current experimental knowledge, and would need to be ruled out by future research in order to shed light on the true mechanism of cross-resistance observed here.

## Chapter 5

# Conclusion

The main object of this thesis was to explore the relationships between cell motility, tumour growth, and evolution in advanced cancers. Although motility and invasion is known to be of critical importance for growth and clinical outcomes, there is a lack of research which is both precise, clinically applicable, and simple enough to be intelligible and transparent to ordinary humans. We intended to develop and apply a series of minimalistic models with a view to establishing how changes in migration could affect the speed at which cancers evolve, and furthermore we attempted to constrain and test these models' results empirically.

There are a number of more specific questions that we set out to address. What mechanical and kinetic properties determine the speed of cell migration, and the frequency with which motile cells are released by a tumour? What effect do the resulting changes in cell migration have on the growth curve of cancers? How do differences in growth rates and fitness determine the pace of evolution? And finally, how rapidly do cancers grow and evolve in reality?

To address how the mechanical properties of cancer cells affected how easily they could migrate through tissues, we performed simulations of how motile cells responded to applied forces while embedded in cellular monolayers. These simulations treated cells as isotropic elastic spheres, modelled the transition between different cell types as a stochastic process, and measured how quickly the cells moved when subjected to a constant traction force. The two cell types were treated as static, non-invasive epithelial cells and motile invasive mesenchymal type cells, with the invasive cells assigned a different elastic stiffness. The effect of adjusting the elastic stiffness was that more elastic and easily deformed cells could move faster through tissue, and stiffer cells moved slower through tissue: elastic stiffness therefore affects cells' drag coefficients, at least in cellular monolayers.

We also found that making invasive cells arbitrarily stiff did not result in an arbitrarily high resistance to motion. We interpreted this as representing the fact that even an ideally stiff sphere surrounded in a deformable medium would have its resistance to motion limited by the surrounding medium, similarly to the case of a very hard metal sphere falling through a viscous liquid.

These mechanistic simulations were very computationally intensive, so were not suitable for simulations of larger tumours. To examine the effect of changes in cell migration speed, changes in rates of type switching, and changes in cell division rate on the growth curves of large tumours, we developed a lattice model in which cells could transition between a non-motile type that stayed at one lattice site and divided with an adjustable stochastic rate, and a motile type which hopped between sites with a constant speed and randomly changed direction with some rate  $\alpha$ .

These simulations naturally showed how spheroidal tumours could emerge from a simple set of rules, and that migration enabled limited periods of exponential growth. They also demonstrated

that the rate of this exponential growth was not only affected by the rate at which cells switched to motile types, which was expected, but also by the rate at which they switched back to non-motile types, and furthermore by the migration speed. These latter two dependencies were unexpected and rather complex, but could be interpreted in terms of their effect on the proportion of motile cells present at any one time and the delay between a cell's escape and its founding of a new tumour.

Another lattice model was developed which abstracted cell migration entirely, treating migration events as instantaneous and extremely distant from the originating tumour. The new secondary lesions which were founded as a result of these events could therefore be thought of as developing independently of the originating primary. These simulations also included the appearance of new mutations, and treated cell division as a stochastic process. These simulations established that ensembles of tumours do indeed grow exponentially if the individual lesions' growth do not interfere with each other, and that the rate of this exponential growth can be related to the proportion of cells which migrate and found new lesions.

The roughness of the surfaces of the spheroids in this lattice model was also important, resulting in a more complex dependence between migration and growth rates and a slower speed at which new advantageous mutants can grow across the surface than previously estimated by other authors.

To understand how this last lattice model could support exponential growth and how the pace of evolution could be estimated, we developed a coarse-grained analytical theory which treated individual lesions as continuous "blobs" with pre-determined growth curves, and migration and mutation as stochastic events which occurred with some specified rates. The rationale for this was that invasion and new mutations occur much more rarely than cell division. Both numerical realisations of the stochastic process, and a mean-field approximation could be studied: they corroborated the idea that exponential growth could occur as long as individual lesions were isolated from each other, and showed how the accumulation of advantageous mutations could be related to the underlying growth curves of lesions of different genetic backgrounds. Some questions remain about the accuracy of the approximation scheme we used, and we were not able to answer them definitively.

Finally, we attempted to model how tumour size developed over time in pancreatic cancer patients during a new form chemotherapy designed to have very few possible mutations that could cause resistance. We found that in many cases a sum of two simple exponential functions provided a very good fit, but the inferred number of resistant cells was many orders of magnitude higher than predicted by other authors on the study. This revealed serious deficiencies in the current understanding of pancreatic cancer, as the prediction was made on the basis of a mathematical model which did not make any controversial assumptions with respect to the underlying biology, and we were forced to consider alternative hypotheses for the mechanisms by which resistance to chemotherapy emerges.

Although they weren't related in a strongly systematic way, we went to some effort to ensure that the conclusions of one model could inform the inputs of the following model. For example, the mechanistic simulation predicts cell motility speed, which is an important input to the run-and-tumble lattice model. This lattice model predicts growth curves of tumours, which were an important input to the analytical ensemble model, and the ensemble model made predictions for the proportion of advantageous mutants, which was one possible interpretation of the fraction of resistant cells observed in the clinical study. In this way, future work in a related area may be able to chain together improvements on our minimal models to estimate the effect of changing individual cell properties like elasticity on how rapidly new mutant strains emerge. We should emphasise that this is at this point rather speculative, and the number of possible factors affecting the macroscopic outcomes is probably much larger than the ones we have chosen to study in this thesis.

The usefulness of our approach, of making models that are "as simple as possible but no simpler", and of trying to connect our calculations to experimental observables, is not only that the resulting

mathematical models are open to experimental refutations, as is a prerequisite for all science, but also that the whole of our theoretical work can be understood and in principle reproduced by a single person. This is in contrast to many trends in current scientific work, which rely on models and analyses so complex that their reproduction requires cooperation between many different specialists on a wide scale.

Of course, the experimental study to which we contributed necessarily required a large collaboration, as the actual practical business of conducting it was intrinsically difficult. This does not mean, however, that theory should follow suit. I believe that we have demonstrated how theory which balances minimalism and empirical relevance still has the potential to give a unified picture of scientific knowledge where this is possible, and more importantly to reveal unexpected holes where this is not. If the point of science is to advance human understanding, then science cannot depend on black boxes.

# Bibliography

- [1] Steven I Hajdu. A note from history: landmarks in history of cancer, part 1. *Cancer*, 117(5):1097–1102, 2011.
- [2] Douglas Hanahan and Robert A Weinberg. The hallmarks of cancer. *Cell*, Vol. 100, 57-70, January 7, 2000, 2000.
- [3] Douglas Hanahan and Robert A Weinberg. Hallmarks of cancer: the next generation. *cell*, 144(5):646–674, 2011.
- [4] B. Alberts, D. Bray, J. Lewis, M. Raff, K. Roberts, and P. Walter. Molecular biology of the cell, 5th ed. 2008.
- [5] G. B. Pierce. Relationship between differentiation and carcinogenesis. *Journal of Toxicology and Environmental Health, Part A Current Issues*, 2(6), 1335-1342, 1977.
- [6] Cancer Research UK. Released under a Creative Commons share-alike license with attribution, <https://creativecommons.org/licenses/by-sa/4.0/deed.en>.
- [7] Sean J Morrison and Judith Kimble. Asymmetric and symmetric stem-cell divisions in development and cancer. *nature*, 441(7097):1068, 2006.
- [8] B. D. Simons and H. Clevers. Strategies for homeostatic stem cell self-renewal in adult tissues. *Cell*, 145(6), 851-862, 2011.
- [9] A. Wilson, E. Laurenti, G. Oser, R. C. van der Wath, W. Blanco-Bose, M. Jaworski, ..., and A. Trumpp. Hematopoietic stem cells reversibly switch from dormancy to self-renewal during homeostasis and repair. *Cell*, 135(6), 1118-1129, 2008.
- [10] Julia Frede, Philip Greulich, Tibor Nagy, Benjamin D Simons, and Philip H Jones. A single dividing cell population with imbalanced fate drives oesophageal tumour growth. 2016.
- [11] Maria P Alcolea, Philip Greulich, Agnieszka Wabik, Julia Frede, Benjamin D Simons, and Philip H Jones. Differentiation imbalance in single oesophageal progenitor cells causes clonal immortalization and field change. *Nature cell biology*, 16(6):615, 2014.
- [12] Peter C Nowell. The clonal evolution of tumor cell populations. *Science*, 194(4260):23–28, 1976.
- [13] Ben Vogelstein et al. Cancer genes and the pathways they control. *Nature Medicine* 10, 789-799, 2004.
- [14] B Vogelstein, N Papadopoulos, VE Velculescu, S Zhou, LA Diaz, and KW Kinzler. Cancer genome landscapes. *Science* 339 (6127): 1546-58, 2013.
- [15] R. Durrett, J. Foo, K. Leder, Mayberry J., and F. Michor. Evolutionary dynamics of tumor progression with random fitness values. *Theoretical Population Biology*, 78:54–66, 2010.
- [16] M.A. Nowak et al. The linear process of somatic evolution. *Proc. Natl Acad. Sci. USA*, 100, 1496614969, 2003.

- [17] Eric R Fearon, Bert Vogelstein, et al. A genetic model for colorectal tumorigenesis. *Cell*, 61(5):759–767, 1990.
- [18] Ivana Bozic, Antal, Hisashi Ohtsuki, Hannah Carter, Dewey Kim, Sining Chen, Rachel Karchin, Kenneth W Kinzler, Bert Vogelstein, and Martin A Nowak. Accumulation of driver and passenger mutations during tumor progression. *Proceedings of the National Academy of Sciences*, 107(43):18545–18550, 2010.
- [19] Luis A. Diaz Jr, Richard T. Williams, Jian Wu, Isaac Kinde, J. Randolph Hecht, Jordan Berlin, Benjamin Allen, Ivana Bozic, Johannes G. Reiter, Martin A. Nowak, Kenneth W. Kinzler, Kelly S. Oliner, and Bert Vogelstein. The molecular evolution of acquired resistance to targeted EGFR blockade in colorectal cancers. *Nature*, 486(7404):537–540, June 2012.
- [20] Gerard Manning, David B Whyte, Ricardo Martinez, Tony Hunter, and Sucha Sudarsanam. The protein kinase complement of the human genome. *Science*, 298(5600):1912–1934, 2002.
- [21] Piya Lahiry, Ali Torkamani, Nicholas J Schork, and Robert A Hegele. Kinase mutations in human disease: interpreting genotype-phenotype relationships. *Nature reviews. Genetics*, 11(1):60, 2010.
- [22] Erich A Nigg. Cyclin-dependent protein kinases: key regulators of the eukaryotic cell cycle. *Bioessays*, 17(6):471–480, 1995.
- [23] Ramsey A Foty, Gabor Forgacs, Cathie M Pflieger, and Malcolm S Steinberg. Liquid properties of embryonic tissues: measurement of interfacial tensions. *Physical review letters*, 72(14):2298, 1994.
- [24] Gabor Forgacs and Malcolm S Steinberg. Viscoelastic properties of living embryonic tissues: a quantitative study. *Biophysical Journal Volume 74* 22272234, May 1998.
- [25] Malcolm S Steinberg. Differential adhesion in morphogenesis: a modern view. *Current Opinion in Genetics & Development*, 17(4) 281286, August 2007.
- [26] Robert H Insall and Laura M Machesky. Actin dynamics at the leading edge: from simple machinery to complex networks. *Developmental cell*, 17(3):310–322, 2009.
- [27] Damijan Miklavčič, Tomaž Jarm, Rihard Karba, and Gregor Serša. Mathematical modelling of tumor growth in mice following electrotherapy and bleomycin treatment. *Mathematics and computers in simulation*, 39(5):597–602, 1995.
- [28] Andrew Stein, Daniel DeWoskin, Michael Higley, Kyle Lemoi, Ben Owens, Aminur Rahman, Horacio Rotstein, David Rumschitzki, Sumanth Swaminathan, Matthew Tanzy, et al. Dynamic models of metastatic tumor growth. In *Final Report of the 27th Annual Workshop on Mathematical Problems in Industry*, New Jersey Institute of Technology, 2011.
- [29] Sébastien Benzekry, Clare Lamont, Afshin Beheshti, Amanda Tracz, John M. L. Ebos, Lynn Hlatky, and Philip Hahnfeldt. Classical mathematical models for description and prediction of experimental tumor growth. *PLoS Comput Biol*, 10(8):e1003800, 08 2014.
- [30] I.A. Rodriguez-Brenes, N.L. Komarova, and D. Wodarz. Tumor growth dynamics: insights into evolutionary processes. *Trends in Ecology & Evolution*, 28:597–604, 2013.
- [31] Peter L Bonate. Modeling tumor growth in oncology. In *Pharmacokinetics in Drug Development*, pages 1–19. Springer, 2011.
- [32] R.A. Weinberg. *The Biology of Cancer*. Garland Science, 2007.
- [33] Shinichi Yachida, Sian Jones, Ivana Bozic, Antal, Rebecca Leary, Baojin Fu, Mihoko Kamiyama, Ralph H Hruban, James R Eshleman, Martin A Nowak, et al. Distant metastasis occurs late during the genetic evolution of pancreatic cancer. *Nature*, 467(7319):1114–1117, 2010.

- [34] S. Ling and et al. Extremely high genetic diversity in a single tumor points to prevalence of non-darwinian cell evolution. *Proceedings of the National Academy of Sciences*, 112:E6496–E6505, 2015.
- [35] A Sottoriva and et al. A big bang model of human colorectal tumor growth. *Nature Genetics*, 47:209–216, 2015.
- [36] James D Murray. *Mathematical Biology. II Spatial Models and Biomedical Applications*. Springer-Verlag New York Incorporated, 2001.
- [37] Ernst Mayr. *Systematics and the origin of species, from the viewpoint of a zoologist*. Harvard University Press, 1942.
- [38] Erik A. Martens, Rumen Kostadinov, Carlo C. Maley, and Oskar Hallatschek. Spatial structure increases the waiting time for cancer. *New journal of physics* 13(11), 115014, 2011.
- [39] O. Hallatschek, P. Hersen, S. Ramanathan, and D.R Nelson. Genetic drift at expanding frontiers promotes gene segregation. *Proceedings of the National Academy of Sciences*, 104(50):19926–30, 2007.
- [40] Bartłomiej Waclaw, Ivana Bozic, Meredith E. Pittman, Ralph H. Hruban, Bert Vogelstein, and Martin A. Nowak. A spatial model predicts that dispersal and cell turnover limit intratumour heterogeneity. *Nature*, 525(7568):261–264, September 2015.
- [41] Antal, PL Krapivsky, and MA Nowak. Spatial evolution of tumors with successive driver mutations. *Physical Review E*, 92, 2015.
- [42] Philip Greulich, Bartłomiej Waclaw, and Rosalind J Allen. Mutational pathway determines whether drug gradients accelerate evolution of drug-resistant cells. *Physical Review Letters*, 109(8):088101, 2012.
- [43] Stephen Jay Gould and Niles Eldredge. Punctuated equilibria: an alternative to phyletic gradualism. 1972.
- [44] Anne C Chiang and Joan Massagué. Molecular basis of metastasis. *New England Journal of Medicine*, 359(26):2814–2823, 2008.
- [45] Melanie C Smitt, Kent W Nowels, Mark J Zdeblick, Stefanie Jeffrey, Robert W Carlson, Frank E Stockdale, and Don R Gfnet. The importance of the lumpectomy surgical margin status in long term results of breast conservation. *Cancer*, 76:259–267, 1995.
- [46] Francesco Porpiglia, Cristian Fiori, Carlo Terrone, Enrico Bollito, Dario Fontana, and Roberto Mario Scarpa. Assessment of surgical margins in renal cell carcinoma after nephron sparing: a comparative study: laparoscopy vs open surgery. *The Journal of urology*, 173(4):1098–1101, 2005.
- [47] Jessica H Maxwell, Lester DR Thompson, Margaret S Brandwein-Gensler, Bernhard G Weiss, Martin Canis, Bibianna Purgina, Arpan V Prabhu, Chi Lai, Yongli Shuai, William R Carroll, et al. Early oral tongue squamous cell carcinoma: sampling of margins from tumor bed and worse local control. *JAMA Otolaryngology–Head & Neck Surgery*, 141(12):1104–1110, 2015.
- [48] LA Liotta, K Tryggvason, S Garbisa, Ian Hart, CM Foltz, and S Shafie. Metastatic potential correlates with enzymatic degradation of basement membrane collagen. *Nature*, 284(5751):67–68, 1980.
- [49] Miriam Schenk, Berk Aykut, Christian Teske, Nathalia A Giese, Juergen Weitz, and Thilo Welsch. Salinomycin inhibits growth of pancreatic cancer and cancer cell migration by disruption of actin stress fiber integrity. *Cancer letters*, 358(2):161–169, 2015.
- [50] Sir James Lighthill. *Mathematical biofluidynamics*. SIAM, 1975.

- [51] G Moreno-Bueno, F Portillo, and A Cano. Transcriptional regulation of cell polarity in emt and cancer. *Oncogene* 27, 6958-6969, 2008.
- [52] J. Yang, X. Du, G. Wang, Y. Sun, K. Chen, X. Zhu, ..., and W. Zhang. Mesenchymal to epithelial transition in sarcomas. *European Journal of Cancer*, 50(3), 593-601, 2014.
- [53] Piyush B. Gupta et al. Stochastic state transitions give rise to phenotypic equilibrium in populations of cancer cells. *Cell* 146(4), 633-644, 2011.
- [54] G John Ferguson, Laura Milne, Suhasini Kulkarni, Takehiko Sasaki, Simon Walker, Simon Andrews, Tom Crabbe, Peter Finan, Gareth Jones, Shaun Jackson, et al. Pi (3) k [gamma] has an important context-dependent role in neutrophil chemokinesis. *Nature cell biology*, 9(1):86, 2007.
- [55] Qiuhui Li, Kiera Rycaj, Xin Chen, and Dean G Tang. Cancer stem cells and cell size: A causal link? In *Seminars in cancer biology*, volume 35, pages 191–199. Elsevier, 2015.
- [56] Anh N Hoang, Caroline N Jones, Laurie Dimisko, Bashar Hamza, Joseph Martel, Nikola Kojic, and Daniel Irimia. Measuring neutrophil speed and directionality during chemotaxis, directly from a droplet of whole blood. *Technology*, 1(01):49–57, 2013.
- [57] M Lekka, P Laidler, D Gil, J Lekki, Z Stachura, and AZ Hryniewicz. Elasticity of normal and cancerous human bladder cells studied by scanning force microscopy. *European Biophysics Journal*, 28(4):312–316, 1999.
- [58] Dirk Drasdo. Buckling instabilities of one-layered growing tissues. *Physical review letters*, 84(18):4244, 2000.
- [59] Gernot Schaller and Michael Meyer-Hermann. Multicellular tumor spheroid in an off-lattice voronoi-delaunay cell model. *Physical Review E*, 71(5):051910, 2005.
- [60] Ramsey A Foty and Malcolm S Steinberg. The differential adhesion hypothesis: a direct evaluation. *Developmental biology*, 278(1):255–263, 2005.
- [61] Ramsey A Foty and Malcolm S Steinberg. Cadherin-mediated cell-cell adhesion and tissue segregation in relation to malignancy. *International Journal of Developmental Biology*, 48(5-6):397–409, 2004.
- [62] Gareth Wyn Jones and S Jonathan Chapman. Modeling growth in biological materials. *Siam review*, 54(1):52–118, 2012.
- [63] Jörg Galle, Markus Loeffler, and Dirk Drasdo. Modeling the effect of deregulated proliferation and apoptosis on the growth dynamics of epithelial cell populations in vitro. *Biophysical journal*, 88(1):62–75, 2005.
- [64] Dirk Drasdo and Stefan Höhme. A single-cell-based model of tumor growth in vitro: monolayers and spheroids. *Physical biology*, 2(3):133, 2005.
- [65] Lev D Landau and EM Lifshitz. Theory of elasticity, vol. 7. *Course of Theoretical Physics*, 3:109, 1986.
- [66] Remigiusz Kowalczyk. Preventing blow-up in a chemotaxis model. *Journal of Mathematical Analysis and Applications*, 305(2):566–588, 2005.
- [67] Tomasz Koziara and Nenad Bicanic. Bounding box collision detection. In *13th acme conference: university of sheffield*, 2005.
- [68] Hawa-Racine Thiam, Pablo Vargas, Nicolas Carpi, Carolina Lage Crespo, Matthew Raab, Emmanuel Terriac, Megan C King, Jordan Jacobelli, Arthur S Alberts, Theresia Stradal, et al. Perinuclear arp2/3-driven actin polymerization enables nuclear deformation to facilitate cell migration through complex environments. *Nature communications*, 7, 2016.

- [69] Matthew P Neilson, John A Mackenzie, Steven D Webb, and Robert H Insall. Modeling cell movement and chemotaxis using pseudopod-based feedback. *SIAM Journal on Scientific Computing*, 33(3):1035–1057, 2011.
- [70] Marco Scianna and Luigi Preziosi. Modeling the influence of nucleus elasticity on cell invasion in fiber networks and microchannels. *Journal of theoretical biology*, 317:394–406, 2013.
- [71] Murray Eden. A two-dimensional growth process. *Dynamics of fractal surfaces*, 4:223–239, 1961.
- [72] Luca Angelani. Run-and-tumble particles, telegraphers equation and absorption problems with partially reflecting boundaries. *Journal of Physics A: Mathematical and Theoretical*, 48(49):495003, 2015.
- [73] J Tailleur and ME Cates. Statistical mechanics of interacting run-and-tumble bacteria. *Physical review letters*, 100(21):218103, 2008.
- [74] Ron Breukelaar and Th Bäck. Using a genetic algorithm to evolve behavior in multi dimensional cellular automata: emergence of behavior. In *Proceedings of the 7th annual conference on Genetic and evolutionary computation*, pages 107–114. ACM, 2005.
- [75] Kurt Mehlhorn and Peter Sanders. Algorithms and data structures. 2007.
- [76] Sidney Goldstein. On diffusion by discontinuous movements, and on the telegraph equation. *The Quarterly Journal of Mechanics and Applied Mathematics*, 4(2):129–156, 1951.
- [77] M Suzuoki and et al. Impact of caveolin-1 expression on prognosis of pancreatic ductal adenocarcinoma. *British Journal of Cancer*, 87:1140–1144, 2002.
- [78] H Enderling, L Hlatky, and P Hahnfeldt. Migration rules: tumours are conglomerates of self-metastases. *British journal of cancer*, 100(12):1917–1925, 2009.
- [79] L Hanin, J Rose, and M Zaider. A stochastic model for the sizes of detectable metastases. *Journal of Theoretical Biology*, 243(3):407–417, 2006.
- [80] O G McDonald, H Wu, W Timp, and A Doi. Genome-scale epigenetic reprogramming during epithelial-to-mesenchymal transition. *Nature Structural & Molecular Biology*, 18:867–874, 2011.
- [81] Fabien Montel, Morgan Delarue, Jens Elgeti, Laurent Malaquin, Markus Basan, Thomas Risler, Bernard Cabane, Danijela Vignjevic, Jacques Prost, Giovanni Cappello, et al. Stress clamp experiments on multicellular tumor spheroids. *Physical review letters*, 107(18):188102, 2011.
- [82] K Iwata, K Kawasaki, and N Shigesada. A dynamical model for the growth and size distribution of multiple metastatic tumors. *Journal of theoretical biology*, 203(2):177–186, 2000.
- [83] F Michor, M A Nowak, and Y Iwasa. Stochastic dynamics of metastasis formation. *Journal of Theoretical Biology*, 240:521–530, 2006.
- [84] Barbara Lee Keyfitz and N Keyfitz. The mckendrick partial differential equation and its uses in epidemiology and population study. *Mathematical and Computer Modelling*, 26(6):1–9, 1997.
- [85] Benoît Perthame. *Transport equations in biology*. Springer, 2006.
- [86] E Baratchart and et al. Computational modelling of metastasis development in renal cell carcinoma. *PLoS Computational Biology*, 11:e1004626, 2015.
- [87] Motoo Kimura. The number of heterozygous nucleotide sites maintained in a finite population due to steady flux of mutations. *Genetics*, 61(4):893, 1969.

- [88] J Folkman. What is the evidence that tumors are angiogenesis dependent? *Journal of the National Cancer Institute*, 82:4–7, 1990.
- [89] G N Naumov, J Folkman, and O Straume. Tumor dormancy due to failure of angiogenesis: role of the microenvironment. *Clinical & Experimental Metastasis*, 26:51–60, 2008.
- [90] Maxim O Lavrentovich and David R Nelson. Survival probabilities at spherical frontiers. *Theoretical population biology*, 102:26–39, 2015.
- [91] C. Tomasetti, L. Marchionni, M. A. Nowak, G. Parmigiani, and B. Vogelstein. Only three driver gene mutations are required for the development of lung and colorectal cancers. *Proceedings of the National Academy of Sciences*, 112:118–123, 2015.
- [92] C.J. Thalhauser, J.S. Lowengrub, D. Stupack, and N.L. Komarova. Selection in spatial stochastic models of cancer: Migration as a key modulator of fitness. *Biol. Direct*, 5:21, 2010.
- [93] O. Hallatschek and D.S. Fisher. Acceleration of evolutionary spread by long-range dispersal. *Proceedings of the National Academy of Sciences*, 111:E4911–19, 2014.
- [94] P. Vaupel, F. Kallinowski, and P. Okunieff. Blood flow, oxygen, and nutrient supply, and metabolic microenvironment of human tumors: A review. *Cancer Research*, 49:6449–65, 1989.
- [95] S.K. Parks, Y. Cormerais, I. Marchiq, and J. Pouyssegur. Hypoxia optimises tumour growth by controlling nutrient import and acidic metabolite export. *Molecular Aspects of Medicine*, 47-48:3–14, 2016.
- [96] M. et al. Fokkelman. Cellular adhesome screen identifies critical modulators of focal adhesion dynamics, cellular traction forces and cell migration behaviour. *Scientific Reports*, 6:31707, 2016.
- [97] M. Gerlinger and et al. Intratumor heterogeneity and branch evolution revealed by multiregion sequencing. *New England Journal of Medicine*, 366:883–892, 2012.
- [98] B. Werner and et al. The cancer stem cell fraction in hierarchically organized tumors can be estimated using mathematical modeling and patient-specific treatment trajectories. *Cancer Research*, 76:1705, 2016.
- [99] B.J. Bauer, R. Sieberg, and A. Traulsen. Cancer initiation with epistatic interactions between driver and passenger mutations. *Journal of Theoretical Biology*, 358:52–60, 2014.
- [100] Chris D Greenman and Tom Chou. Kinetic theory of age-structured stochastic birth-death processes. *Physical Review E*, 93(1):012112, 2016.
- [101] Giles Bond-Smith, Neal Banga, Toby M Hammond, and Charles J Imber. Pancreatic adenocarcinoma. *Bmj*, 344(e2476), 2012.
- [102] Thierry Conroy, Françoise Desseigne, Marc Ychou, Olivier Bouché, Rosine Guimbaud, Yves Bécouarn, Antoine Adenis, Jean-Luc Raoul, Sophie Gourgou-Bourgade, Christelle de la Fouchardière, et al. Folfirinox versus gemcitabine for metastatic pancreatic cancer. *New England Journal of Medicine*, 364(19):1817–1825, 2011.
- [103] Daniel D Von Hoff, Ramesh K Ramanathan, Mitesh J Borad, Daniel A Laheru, Lon S Smith, Tina E Wood, Ronald L Korn, Neil Desai, Vuong Trieu, Jose L Iglesias, et al. Gemcitabine plus nab-paclitaxel is an active regimen in patients with advanced pancreatic cancer: a phase i/ii trial. *Journal of Clinical Oncology*, 29(34):4548–4554, 2011.
- [104] Mark Sausen, Jillian Phallen, Vilmos Adleff, Siân Jones, Rebecca J Leary, Michael T Barrett, Valsamo Anagnostou, Sonya Parpart-Li, Derek Murphy, Qing Kay Li, et al. Clinical implications of genomic alterations in the tumour and circulation of pancreatic cancer patients. *Nature communications*, 6:7686, 2015.

- [105] Ivana Bozic, Johannes G Reiter, Benjamin Allen, Tibor Antal, Krishnendu Chatterjee, Preya Shah, Yo Sup Moon, Amin Yaqubie, Nicole Kelly, Dung T Le, et al. Evolutionary dynamics of cancer in response to targeted combination therapy. *Elife*, 2:e00747, 2013.
- [106] Daniel B Longley, D Paul Harkin, and Patrick G Johnston. 5-fluorouracil: mechanisms of action and clinical strategies. *Nature Reviews Cancer*, 3(5):330–338, 2003.
- [107] E Mini, SFAU Nobili, BFAU Caciagli, I Landini, and T Mazzei. Cellular pharmacology of gemcitabine. *Annals of Oncology*, 17(suppl\_5):v7–v12, 2006.
- [108] CM Galmarini, JR Mackey, and C Dumontet. Nucleoside analogues: mechanisms of drug resistance and reversal strategies. *Leukemia*, 15(6):875, 2001.
- [109] Jing Zhang, Frank Visser, Karen M King, Stephen A Baldwin, James D Young, and Carol E Cass. The role of nucleoside transporters in cancer chemotherapy with nucleoside drugs. *Cancer and Metastasis Reviews*, 26(1):85–110, 2007.
- [110] Anne-Marie C Yvon, Patricia Wadsworth, and Mary Ann Jordan. Taxol suppresses dynamics of individual microtubules in living human tumor cells. *Molecular biology of the cell*, 10(4):947–959, 1999.
- [111] SD Baker, Jaap Verweij, GA Cusatis, RH Schaik, Steven Marsh, SJ Orwick, RM Franke, S Hu, EG Schuetz, V Lamba, et al. Pharmacogenetic pathway analysis of docetaxel elimination. *Clinical pharmacology & Therapeutics*, 85(2):155–163, 2009.
- [112] Donald Mastropaolo, Arthur Camerman, Yuogang Luo, Gary D Brayer, and Norman Camerman. Crystal and molecular structure of paclitaxel (taxol). *Proceedings of the National Academy of Sciences*, 92(15):6920–6924, 1995.
- [113] L Galluzzi, L Senovilla, I Vitale, J Michels, I Martins, O Kepp, M Castedo, and G Kroemer. Molecular mechanisms of cisplatin resistance. *Oncogene*, 31(15):1869–1883, 2012.
- [114] Mahmoud El-Khateeb, Trevor G Appleton, Lawrence R Gahan, Bruce G Charles, Susan J Berners-Price, and Ann-Maree Bolton. Reactions of cisplatin hydrolytes with methionine, cysteine, and plasma ultrafiltrate studied by a combination of hplc and nmr techniques. *Journal of inorganic biochemistry*, 77(1):13–21, 1999.
- [115] Fabio Arnesano, Maurizio Losacco, and Giovanni Natile. An updated view of cisplatin transport. *European journal of inorganic chemistry*, 2013(15):2701–2711, 2013.
- [116] XG Ni, XF Bai, YL Mao, YF Shao, JX Wu, Y Shan, CF Wang, J Wang, YT Tian, Q Liu, et al. The clinical value of serum cea, ca19-9, and ca242 in the diagnosis and prognosis of pancreatic cancer. *European Journal of Surgical Oncology (EJSO)*, 31(2):164–169, 2005.
- [117] Tomoko Ogawa, Hajime Yokoi, and Yoshifumi Kawarada. A case of inflammatory pseudotumor of the liver causing elevated serum ca19-9 levels. *The American journal of gastroenterology*, 93(12):2551–2555, 1998.
- [118] KS Goonetilleke and AK Siriwardena. Systematic review of carbohydrate antigen (ca 19-9) as a biochemical marker in the diagnosis of pancreatic cancer. *European Journal of Surgical Oncology (EJSO)*, 33(3):266–270, 2007.
- [119] Erwin Kreyszig. *Advanced engineering mathematics*. John Wiley & Sons, 2010.
- [120] Isaac Jacob Schoenberg. Spline functions and the problem of graduation. *Proceedings of the National Academy of Sciences*, 52(4):947–950, 1964.
- [121] Tibor Antal and PL Krapivsky. Exact solution of a two-type branching process: models of tumor progression. *Journal of Statistical Mechanics: Theory and Experiment*, 2011(08):P08018, 2011.

- [122] Salvador E Luria and Max Delbrück. Mutations of bacteria from virus sensitivity to virus resistance. *Genetics*, 28(6):491, 1943.
- [123] C Bhang Hyo-eun, David A Ruddy, Viveksagar Krishnamurthy Radhakrishna, Justina X Caushi, Rui Zhao, Matthew M Hims, Angad P Singh, Iris Kao, Daniel Rakiec, Pamela Shaw, et al. Studying clonal dynamics in response to cancer therapy using high-complexity barcoding. *Nature medicine*, 21(5):440–448, 2015.
- [124] M Yamasaki, T Makino, T Masuzawa, Y Kurokawa, H Miyata, S Takiguchi, K Nakajima, Y Fujiwara, N Matsuura, M Mori, et al. Role of multidrug resistance protein 2 (mrp2) in chemoresistance and clinical outcome in oesophageal squamous cell carcinoma. *British journal of cancer*, 104(4):707, 2011.
- [125] Jean-Pierre Gillet and Michael M Gottesman. Mechanisms of multidrug resistance in cancer. *Multi-drug resistance in cancer*, pages 47–76, 2010.
- [126] Jing Jin, Feng-Peng Wang, Huailing Wei, and Gengtao Liu. Reversal of multidrug resistance of cancer through inhibition of p-glycoprotein by 5-bromotetrandrine. *Cancer chemotherapy and pharmacology*, 55(2):179–188, 2005.
- [127] Seiko Ishida, Jaekwon Lee, Dennis J Thiele, and Ira Herskowitz. Uptake of the anticancer drug cisplatin mediated by the copper transporter ctr1 in yeast and mammals. *Proceedings of the National Academy of Sciences*, 99(22):14298–14302, 2002.
- [128] Swati S More, Omar Akil, Alexandra G Ianculescu, Ethan G Geier, Lawrence R Lustig, and Kathleen M Giacomini. Role of the copper transporter, ctr1, in platinum-induced ototoxicity. *Journal of Neuroscience*, 30(28):9500–9509, 2010.
- [129] Seiko Ishida, Frank McCormick, Karen Smith-McCune, and Douglas Hanahan. Enhancing tumor-specific uptake of the anticancer drug cisplatin with a copper chelator. *Cancer cell*, 17(6):574–583, 2010.
- [130] Lingjie Bao, Melba C Jaramillo, Zhenbo Zhang, Yunxi Zheng, Ming Yao, Donna D Zhang, and Xiaofang Yi. Induction of autophagy contributes to cisplatin resistance in human ovarian cancer cells. *Molecular medicine reports*, 11(1):91–98, 2015.
- [131] Jun Hayakawa, Chantal Depatie, Masahide Ohmichi, and Dan Mercola. The activation of c-jun nh2-terminal kinase (jnk) by dna-damaging agents serves to promote drug resistance via activating transcription factor 2 (atf2)-dependent enhanced dna repair. *Journal of Biological Chemistry*, 278(23):20582–20592, 2003.
- [132] Mohammad Fallahi-Sichani, Nathan J Moerke, Mario Niepel, Tinghu Zhang, Nathanael S Gray, and Peter K Sorger. Systematic analysis of braf v 600e melanomas reveals a role for jnk/c-jun pathway in adaptive resistance to drug-induced apoptosis. *Molecular systems biology*, 11(3):797, 2015.
- [133] XY Liu, SP Liu, J Jiang, X Zhang, and T Zhang. Inhibition of the jnk signaling pathway increases sensitivity of hepatocellular carcinoma cells to cisplatin by downregulating expression of p-glycoprotein. *Eur Rev Med Pharmacol Sci*, 20(6):1098–1108, 2016.
- [134] ED Lagadinou, PG Ziros, OA Tsopra, K Dimas, D Kokkinou, E Thanopoulou, M Karakantza, P Pantazis, A Spyridonidis, and NC Zoumbos. c-jun n-terminal kinase activation failure is a new mechanism of anthracycline resistance in acute myeloid leukemia. *Leukemia*, 22(10):1899, 2008.
- [135] Xiaoping Ao and Julie A Stenken. Microdialysis sampling of cytokines. *Methods*, 38(4):331–341, 2006.
- [136] Raymond Cheong, Adriel Bergmann, Shannon L Werner, Joshua Regal, Alexander Hoffmann, and Andre Levchenko. Transient  $\text{ikb}$  kinase activity mediates temporal  $\text{nf-}\kappa\text{b}$  dynamics in response to a wide range of tumor necrosis factor- $\alpha$  doses. *Journal of Biological Chemistry*, 281(5):2945–2950, 2006.

- [137] Valerie Sloane Jones, Ren-Yu Huang, Li-Pai Chen, Zhe-Sheng Chen, Liwu Fu, and Ruo-Pan Huang. Cytokines in cancer drug resistance: cues to new therapeutic strategies. *Biochimica et Biophysica Acta (BBA)-Reviews on Cancer*, 1865(2):255–265, 2016.
- [138] John C Gilkey, Lionel F Jaffe, Ellis B Ridgway, and George T Reynolds. A free calcium wave traverses the activating egg of the medaka, *oryzias latipes*. *The Journal of Cell Biology*, 76(2):448–466, 1978.
- [139] Raz Kupferman, Partha P Mitra, PC Hohenberg, and SS Wang. Analytical calculation of intracellular calcium wave characteristics. *Biophysical journal*, 72(6):2430–2444, 1997.
- [140] Torben R Uhrenholt, Timothy L Domeier, and Steven S Segal. Propagation of calcium waves along endothelium of hamster feed arteries. *American Journal of Physiology-Heart and Circulatory Physiology*, 292(3):H1634–H1640, 2007.
- [141] Yutaka Yoshida and Shoichi Imai. Structure and function of inositol 1, 4, 5-trisphosphate receptor. *The Japanese Journal of Pharmacology*, 74(2):125–137, 1997.